Development and Testing of High / Ultra-High Early Strength Concrete for durable Bridge Components and Connections

Final Report
October 2022

Principal Investigator: Kay Wille, Ph.D., Associate Professor

Co-PI: Ramesh Malla, Ph.D., F. ASCE, Professor

Authors
Bijaya Rai, Ph.D. Student
Kay Wille, Ph.D., Associate Professor
Ramesh Malla, Ph.D., F. ASCE, Professor

TIDC Research Thrust: Thrust # 2: New materials for longevity and constructability

Institution: University of Connecticut, Department of Civil & Environmental Engineering, Storrs, CT
PI/Co-PI Emails: kay.wille@uconn.edu / Ramesh.Malla@uconn.edu
Phone: - PI (860) 486-2074 / Co-PI (860) 486-3683

Sponsored By
Transportation Infrastructure Durability Center

A report from
University of Connecticut
Department of Civil and Environmental Engineering
261 Glenbrook Road Unit, 3037
Storrs, CT 06269-3037
Phone: 860-486-2992
Website: https://cee.engr.uconn.edu/

About the Transportation Infrastructure Durability Center

The Transportation Infrastructure Durability Center (TIDC) is the 2018 US DOT Region 1 (New England) University Transportation Center (UTC) located at the University of Maine Advanced Structures and Composites Center. TIDC's research focuses on efforts to improve the durability and extend the life of transportation infrastructure in New England and beyond through an integrated collaboration of universities, state DOTs, and industry. The TIDC is comprised of six New England universities, the University of Maine (lead), the University of Connecticut, the University of Massachusetts Lowell, the University of Rhode Island, the University of Vermont, and Western New England University.

U.S. Department of Transportation (US DOT) Disclaimer

Acknowledgements

Technical Report Documentation Page

1. Report No.	2. Government Accession No.	3. Recipient Catalog No.
4 Title and Subtitle Development and Testing of High / Ultra-High Early Strength Concrete for durable Bridge Components and Connections		**5 Report Date** 10/30/2022
		6 Performing Organization Code
7. Author(s) Bijaya Rai Kay Wille - https://orcid.org/0000-0001-2345-6789 Ramesh Malla - https://orcid.org/0000-0002-8035-8402		**8 Performing Organization Report No.**
9 Performing Organization Name and Address University of Connecticut 261 Glenbrook Rd Storrs, CT 06269-3037		**10 Work Unit No. (TRAIS)**
		11 Contract or Grant No.
12 Sponsoring Agency Name and Address		**13 Type of Report and Period Covered** Final Report 01/01/2019 to 09/30/2022
		14 Sponsoring Agency Code
15 Supplementary Notes		

16 Abstract

The main goal of this project was the development of non-proprietary concrete mixtures with high and ultra-high mechanical and durability performance. The mixture designs considered the constraints of local available materials in the New England area and the interests of state departments of transportation. Mix design solutions were tailored towards workability, mechanical and durability performance as well as cost. Several mixture designs are provided which might address the specific needs of contractors in the future. Upon success in mixing the designed ultra-high performance concretes at larger scale, it is envisioned that this type of concrete will be used more extensively for construction projects. This project aims at directly impacting the construction industry towards a more sustainable infrastructure with enhanced service life.

17 Key Words High / Ultra-High Early Strength Concrete, Ultra-high performance concrete, UHPC	**18 Distribution Statement** No restrictions.

19 Security Classification (of this report) Unclassified	**20 Security Classification (of this page)** Unclassified	**21 No. of pages** XX	**22 Price**

Form DOT F 1700.7 (8-72)

Contents

List of Figures

List of Tables

List of Key Terms

Abbreviation	Definition
A/C	Aggregate to Cement Ratio
A/P	Aggregate to Paste Ratio
A/P_o	Aggregate to Powder Ratio
ASCE	American Society of Civil Engineers
CH	Calcium Hydroxide
C-S-H	Calcium-Silicate-Hydrate
CSA	Calcium Sulphoaluminate
CFP	Carbon Footprint
CTDOT	Connecticut Department of Transportation
EDC	Everyday Counts
FHWA	Federal Highway Administration
FA	Fly Ash
FB	Fine Basalt
GDP	Gross Domestic Product
GGBS	Ground Granulated Blast Furnace Slag
HES	High Early-Strength
HRWR	High Range Water Reducers
MK	Metakaolin
NS	Nano-silica
NETC	New England Transportation Consortium
PC	Portland Cement
PBES	Prefabricated Bridge Elements and Systems
RGP	Recycled Glass Powder
RAM	Resonance Acoustic Mixer
SF	Silica Fume
SCM	Supplementary Cementitious Materials
C_3A	Tricalcium Aluminate
UHPC	Ultra-high performance concrete
W/B	Water to Binder Ratio
W/C	Water to Cement Ratio
W/F	Water to Fines Ratio

Abstract

The functionality of the U.S. highway transportation network mainly relies on the integrity and performance of bridges. The average age of existing bridges in the United States heads towards the design life of 50 years including an increasing number of bridges being classified as structurally deficient. Advancements in construction materials opens opportunities to repair, build and construct bridge structures with enhanced service life, reduced maintenance cost, lower environmental footprint, and thus improved sustainability. Therefore, in pursue to improve the sustainability of bridge structures, the main goal of this project was the development of performance-cost-efficient non-proprietary concrete mixtures with high and ultra-high mechanical and durability performance. The mixture designs considered the constraints of local available materials in the New England area and the interests of state departments of transportation. Mix design solutions were tailored towards workability, compressive strength, cost, and carbon footprint. A resource-efficiency factor was defined to evaluate their performances. Several mixture designs are provided which might address the specific needs of contractors in the future. The minimum strength requirement of 150 MPa (22ksi) were exceeded at material costs of the matrix of about $500/m^3 using local available materials. This included igneous basalt as fine aggregate, un-densified silica fume, recycled glass powder, locally available fly ash and suitable Portland cements. Adding fiber reinforcement was necessary to achieve desired tensile strength and material ductility. The addition of 1% by volume of fibers used here added about $350 per m^3 of composite in cost. Upon success in mixing the designed ultra-high performance concretes at larger scale, it is envisioned that this type of concrete will be used more extensively for construction projects.

Chapter 1: Introduction and Background

1.1 Project Motivations and Main Research Goal

The functionality of the U.S. highway transportation network mainly relies on the integrity and performance of bridges. The average age of existing bridges in the United States was 45 years in 2013 according to the U.S. Department of Transportation National Bridge Inventory [1]. As per American Society of Civil Engineers (ASCE) report card 2021, almost 25% of the 614,387 bridges in the U.S. are at their design life span of 50 years or even older. 56,007 or 9.1% of the nation's existing bridges already fall in the category of "structurally deficient," requiring major maintenance, rehabilitation, or even replacement which puts the nation's backlog of bridge rehabilitation at $123 billion [2]. The American Society of Civil Engineers (ASCE) rated the infrastructure in the United States with a C- in 2021 [2], slightly upgraded from D+, existed for many years [3]. ASCE estimated about $3.3 trillion for the remedy of infrastructure which includes a $1.4 trillion investment-funding gap. If none of these infrastructure gaps is addressed, the U.S. is expected to lose nearly $4 trillion in Gross Domestic Product (GDP) by 2025 [2].

To remedy this situation, the Federal Highway Administration (FHWA) has, as one of a series of initiatives under its "Accelerating Innovation" program, designed an "Everyday Counts" (EDC) program to shorten project delivery, in part by speeding the deployment of proven, underused technologies in the repair and building of bridges. One technology-based initiative promoted through the EDC program is Prefabricated Bridge Elements and Systems (PBES), in which the bridge components or the entire bridge are built offsite and then transported to their final location for quick installation, enabling the state departments of transportation to complete the onsite aspects of construction more safely and efficiently in shorter period. Essential to utilizing PBES technology properly is the use of additional technologies, among which is high early-strength (HES) concrete for closure pour connections of precast bridge elements. Research by *Brena et al*. [4], funded by the New England Transportation Consortium under NETC 13-1, shows that a non-proprietary HES can be developed satisfying the current performance requirements in the New England area. Further research is needed in a threefold manner a) to investigate further performance potential of HES concrete mixtures based on the developed mixture specification, b) to develop the next generation of non-proprietary HES concrete mixture design specifications based on current advances in concrete science and technology to push current performance limits and thus further increase the life span of our future infrastructure, this emphasizes the development of cost efficient non-proprietary ultra-high performance concrete mixture designs, and c) to expand the applicability of high / ultra-high performance concrete to other critical bridge elements such as parapets.

1.2 Research Objectives

The overall goal of this research is to contribute to the enhancement of the life span and resiliency of our current and future infrastructure. Emphasis was placed on the development of products with enhanced applicability.

- The main problem we tried to solve was enhancing the performance versus cost ratio of non-proprietary ultra-high performance concrete using local available materials in the New England area. This will facilitate the wide-spread use of this material to promote more durable, sustainable, and economical efficient bridge structure tailored to current and future conditions.

The problem was important to solve because it tied into the FHWA's EDC program and directly addressed one of the nation's major concerns – aging of the bridge infrastructure.

Based on this, the following three objectives were defined:
1) Investigate further performance potential of HES concrete mixtures

2) Develop mixture design specifications for non-proprietary ultra-high performance concretes with enhanced performance versus cost ratio

3) Expand the applicability of high / ultra-high-performance concrete to other critical bridge elements such as parapets.

In pursuit of *Objective 1* this research built up on the research results by Brena et al. [4] (NETC 13-1) and furthered the investigation and characterization.

In pursuit of *Objective 2* a quadruple methodology was used in this research as shown in **Figure 1.**
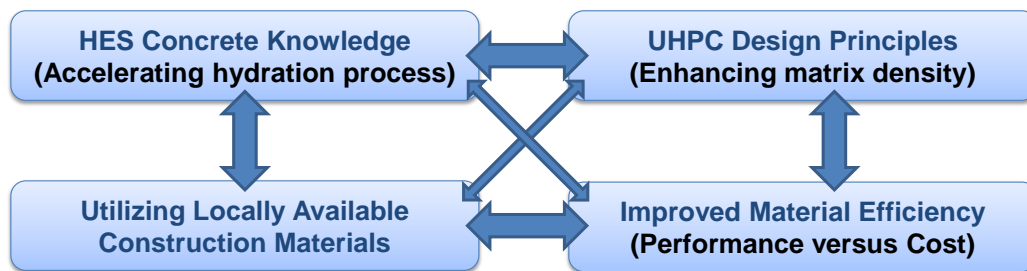
Figure 1: Quadruple scientific methodology

The quadruple approach combines a) current HES concrete knowledge, b) application of ultra-high-performance concrete (UHPC) mixture design principles, c) use of locally available materials, and d) optimization of the design towards enhancing the UHPC performance-to-cost ratio.

1.3 Research Tasks

The following tasks were aligned with the research objectives mentioned listed above:

Task 1: *Testing and Investigating the Performance of HES concrete.* In this task we performed an investigation of early strength performance of HES concrete. This included the use of nano-silica particle, calcium sulphoaluminate (CSA) cement and accelerators.

Task 2: *Developing mixture design specifications for non-proprietary ultra-high performance concretes with enhanced performance versus cost ratio.* In this task, the overall goal was to develop HES concrete mixture design specifications that pushed the limits of current performance requirements. Since the material design of UHPCs is a major contributing factor towards high performance HES, main emphasis of this research was placed on developing cost-efficient UHPC. This included enhancing the particle packing density of

the binding matrix, tailoring the accelerated hydration kinetics of the binding material, and characterizing the mechanical performance under laboratory conditions.

Task 3: *Expanding the applicability of UHPC towards Parapets.* Analysis was conducted to test and investigate the design requirements of parapets constructed with reinforced concrete and UHPC.

Task 4: *Knowledge transfer and practical application.* In this task we will transfer the knowledge of mixture designs obtained in this research to interested people in the construction industry. This is being accomplished by this report, upcoming journal publications as well as several presentations. The transfer of mixture designs under laboratory conditions to mixture designs at larger scale is out of the scope of this research and will be covered in current research which builds upon this research done here.

Task 5: *Documentation and utilization.* In this task we documented material specifications, casting, and curing requirements to enhance the use of the information and products.

1.4 Report Overview

The report is subdivided into 5 chapter. Chapter 1 provides an overview of the research including motivations, goals, objectives and research tasks. Chapter 2 encompasses the research methodology, approaches and material selections. In Chapter 3 all test procedures used in this research will be discussed. This includes workability tests, tests for compression and direct tension. I also includes sample preparation as well. In Chapter 4 test results are discussed and analyzed leading to Chapter 5 which summarizes the main conclusions and provides mixture recommendations. In the appendix, the applicability of UHPC towards parapets are investigated.
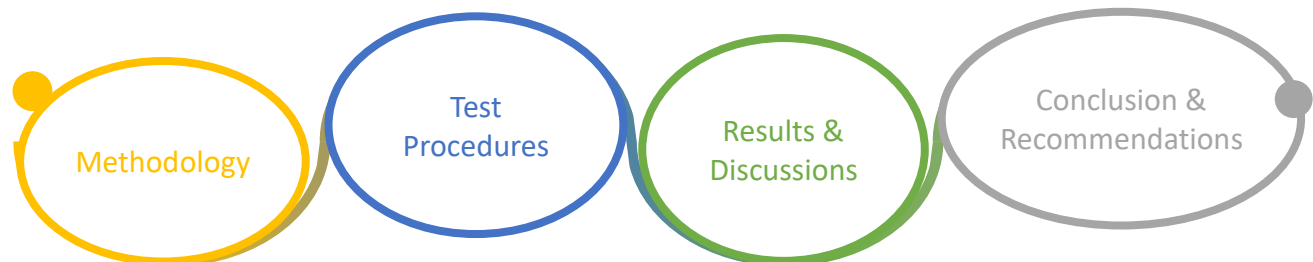
Figure 2: Report overview

Chapter 2: Methodology

This chapter encompasses the research approach and material selection. In 2019 the research started with the development of conventional high early strength concrete and exploring other avenues for developing higher early strength. Considering the interest of the Connecticut Department of Transportation (CTDOT) the research emphasis was shifted towards the development of cost-efficient non-proprietary ultra-high-performance concrete (UHPC). The UHPC exceeds all requirements of high early strength concrete while providing excellent mechanical and durability properties. One major application success of UHPC in bridge construction is its use for closure pour connections between deck and girder or any two girder elements as it has high bond strength and durability properties due to its very high packing density, relatively high binder ratio and low water to cementitious (w/c) ratio [5].

UHPC is a cementitious composite with a relatively high amount of binder in comparison to conventional concrete, is designed to use a water to binder ratio of less than 0.2, achieves compressive strengths of more than 150 MPa or 22 ksi, and the addition of tailored discontinuous fiber reinforcement leads to significantly higher ductility and durability of the cracked composite. The very high packing density of the matrix is the key for the strength and durability properties. **Figure 3** shows the visual difference between regular concrete and UHPC.
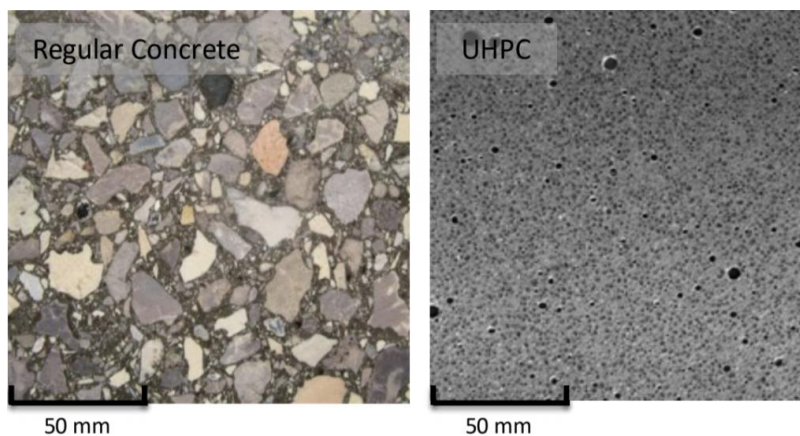
Figure 3: Comparison between a) regular concrete and b) UHPC [6]

2.1 Research Approach

This research started with identifying suitable material suppliers in the New England area, followed by selecting suitable materials. In the first phase of the research, conventional HES concrete was developed, and further early age strength enhancement was investigated by adding nano-silica (NS), using calcium sulphoaluminate (CSA) cement or adding accelerating admixtures. After adjusting the research direction, the development of non-proprietary UHPC became the main research focus.

Based on prior research in the field of UHPC, the development of UHPC mixtures was guided by applying UHPC principles in the mix design and mixing process with the goal to enhance matrix

density. Experimental investigation and material characterization using suitable materials were performed and further tailored based on a resource efficiency factor R – considering compressive strength, workability, cost, and carbon footprint. This led to optimized UHPC pastes and matrices.

As a next step suitable fibers were selected as discontinuous short fiber reinforcement. Emphasis was placed on fiber efficiency, workability, and performance of the composite. This was critical for the development of cost efficient UHPCs since fibers are the most expensive ingredients of this material.

Figure 4 provides a detailed overview of the UHPC development. As it can be seen the development was divided into three parts: a) UHPC paste, b) UHPC matrix, and c) UHPC (fiber reinforced).

```
┌─────────────────────────────────────┐
│            UHPC Paste                │
│  Selecting locally available         │
│  materials                           │
└─────────────────────────────────────┘
                 │
                 ▼
┌──────────────────────────────┐     ┌──────────────────────┐
│ Mix UHPC Paste in Resonance  │ ◄── │ Modify mixture by    │
│ Frequency mixer (starting     │     │ replacing            │
│ with reference mix)           │     │ constituents         │
└──────────────────────────────┘     └──────────────────────┘
                 │                              ▲
                 ▼                              │
┌──────────────────┐    No  ◇ Spread > 110 mm ◇  Yes  ┌──────────────────────┐
│ Modify mix design│ ◄──────│  w/ mini cone?  │──────► │ Cast cubic specimen  │
│ by increase w/c  │        ◇                 ◇        │ for compression      │
│ ratio            │         ◇               ◇         │ strength             │
└──────────────────┘                 │                 └──────────────────────┘
                                      ▼
                    ┌──────────────────────────────┐
                    │ Resource efficiency analysis  │
                    │ based on relative workability,│
                    │ strength, carbon footprint,   │
                    └──────────────────────────────┘
                                      │
                                      ▼
                    ┌──────────────────────────────┐
                    │ Selecting promising paste     │
                    │ components based on R-factor   │
                    └──────────────────────────────┘
                                      │
                                      ▼
┌──────────────────────────────────────────────────────┐
│                  UHPC Matrix                          │
│  Evaluate the matrices resource efficiency with       │
│  different A/C                                        │
└──────────────────────────────────────────────────────┘
                                      │
                                      ▼
┌──────────────────────────────────────────────────────┐
│                     UHPC                              │
│  Test and evaluate UHPC matrices with different V_f   │
└──────────────────────────────────────────────────────┘
                                      │
                                      ▼
                    ┌──────────────────────────────┐
                    │ Cost analysis and             │
                    │ recommendations               │
                    └──────────────────────────────┘
```

Figure 4: Flowchart of UHPC development

Preliminary material selection was based on the recommendation in [7], followed by mixing the UHPC paste using a resonance frequency mixer for enhanced mixing consistency. Due to the limited mixing volume, a mini flow cone of only 172 ml of volume, 1/8 th of the regular flow cone

according to ASTM C230/230M [8], was used to obtain the spread. Based on the spread, the mixture was either modified or one 2" cubic specimen was prepared for compression testing. The mixture was modified by replacing one material constituent at a time or by adjusting the w/c ratio. After all suitable material constituents were tested, the resource efficiency factor, *R*, was calculated for each mixture based on their relative fresh properties, compressive strength, cost, and carbon footprint. This led to UHPC pastes with enhanced performance to cost ratios. As a next step the resource efficiency of UHPC matrices with different aggregate to cement (A/C) ratios was evaluated. As a final step fiber reinforcement was added to the UHPC matrices leading to the UHPC mixture design.

Developing UHPC with compressive strength exceeding 150 MPa or 22 ksi, based on enhanced matrix density leads to enhanced durability properties as well. The investigation of durability properties of selected UHPC in terms of freeze-thaw resistance, shrinkage, permeability, absorption, and air void analysis is out of the scope of this research and is currently investigated in a separate follow up research.

2.2 Material Selection

2.2.1. Overview

Reference HES concrete design:

Table 1 shows the reference mixture of the conventional HES concrete consisting of ordinary Portland cement type III, fly ash class C, natural aggregates, water, and superplasticizer.

Table 1: Reference Conventional HES concrete

Material	Amount (kg/m³)	Mass (%)	Cost $/m³
Cement III	706	39.5	102
Fly ash	125	7.0	8
Aggregates	619	34.6	20
HRWR	236	13.2	0.0
Water	101	5.7	14
Total cost			145

The use of higher finely ground cement such as Portland Cement Type III as per ASTM C 150 [9,10] accelerates the hydration due to the proportionally increased surface area. Concrete with the use of tailored supplementary cementitious materials such as class C fly ash has shown higher rate of reaction at early ages resulting in concrete with higher early strength than concrete containing class F fly ash [9].

To further enhance early age strength the effects of the following three approached were investigated: a) incorporating nano-silica (NS) into the mixture design, b) partially replacing Portland Cement by calcium sulpho aluminate (CSA) cement, and c) using accelerating admixtures. Due to the high surface area of nano-sized pozzolanic material like nano silica (NS) [11–13] pozzolanic reactions are accelerated which forms large amount of C-S-H resulting in potential higher early strength. In addition, the filler effect of NS can potentially increase the matrix density resulting in higher strength and enhanced durability properties of the concrete

[11]. Accelerating admixture, such as calcium chloride was used to accelerate the rate of hydration and strength development in the concrete at an early age [13].

Reference UHPC Paste Design:

Based on suitability and availability, the following material constituents were considered in this research: 5 different types of Portland Cement (PC), 1 type of un-densified silica fume (SF), 5 different supplementary cementitious materials (SCM) (FA class C and F, 1 type of metakaolin (MK), 1 type of recycled glass powder (RGP), 1 type of ground granulated blast furnace slag (GGBS), 3 different types of aggregates, 2 different high range water reducers (HRWR), and 1 type of fiber were mixed and tested at constant mixture proportion to observe the isolated effect of each material. Building up on the recommendation in [7] the mix proportions of the reference UHPC paste in this research are shown in **Table 2** using a weight ratio of PC:SF:SCM=1:0.25:0.25, aggregate to cement ratio by weight (A/C) of 0.8 and aggregate to powder ratio (A/P) of 0.53 (taking into account the higher density of basalt in comparison to silica sand), solid content of HRWR to cement ratio of 0.011, and using materials available in the New England area. The w/c ratio was adjusted to 0.24 to achieve a target standard spread, S_{Stnd} , of 313 mm.

Table 2 – Reference UHPC paste design and its cost analysis

Material	ID	Amount (kg/m³)	Mass (%)	Cost $/m³
Cement	C1	936	39.2	258
Silica fume	SF	234	9.8	158
Fly ash	SCM1	234	9.8	15
Basalt sand	FB	747	31.3	28
HRWR	HRWR1	35	1.5	174
Water		200	8.4	0.0
Total cost				633

The reference mix has w/c=0.24, A/P = 0.53, A/C=0.8, spread S_{Stnd} = 313 mm.

Table 3 provides an overview of the UHPC paste investigation, starting with the reference mix shown in **Table 2** and changing individual constituents while keeping the mixture proportion of PC:SF:SCM constant at 1:0.25:0.25. Initially, several families of paste mixes such as cements, supplementary cementitious materials, superplasticizers were investigated, followed by evaluating their resource-efficiency based on the *R – factor* (see Chapter 3). Furthermore, the pastes were optimized using **SF** reduction, use of **RGP** and use of different amount of **GGBS**.

Table 3: UHPC paste investigation overview

Reference mix (**Table 2**)		Changes		Optimized paste (Based on *R*-factor)
White PC Type I (**C1**) Un-densified SF (**SF1**) Fly ash (**SCM1**) Basalt sand (**FB**) HRWR (**HRWR1**)	→	PC (**C1-C5**) SCM (**SCM1-SCM5**) HRWR (**HRWR1-HRWR2**) SF reduction (1:0.25:0.25-1:0.10:0.25) PC by GGBS replacement (0%-50%)	→	PC Type II/V (**C5**) Un-densified SF (**SF**) Class C Fly ash (**SCM2**) Basalt Sand (**FB**) HRWR (**HRWR1**)

2.2.2 UHPC Paste Constituents

The paste constituents: PC, SF, SCM and HRWR are described below:

Portland Cement (PC)

Five different cement types were used in this study with an emphasis of a tricalcium aluminate (C_3A) content of less than 8% (see **Table 4**). Although the reference mix, as shown in **Table 2**, used white PC I (**C1**) which provided good workability (313 mm) and strength, it is costlier compared to the other four cements. The use of grey PC (**C3**) made the mix more difficult to turn over and provided unsatisfying workability (118 mm). Other types of grey PC type I/II (**C2 and C4**) demanded less water than the UHPC mix with C3 and thus resulted in better workability. Mixes with **C5** used a PC type II/V. As expected the lower C_3A content of only 4% resulted in a suitable workability with a spread of 288 mm. **Table 4** summarizes the clinker phase proportions, Blaine fineness, costs and carbon foot print (CFP) of all five different cements. The costs, CFP, spread and compressive strength of UHPCs without fibers using the different cements is summarized in **Table 5**. All mixes contained the same type of aggregate (**FB**), un-densified **SF**, **SCM1** and **HRWR1**.

Table 4– PC properties and cost

Type	ID	C_3S %	C_2S %	C_3A %	C_4AF %	Blaine (m²/kg)	Cost ($/kg)	CFP_P (kg/kg)
White PC I	C1	75	12	5	1	405	0.276	1.179
PC I/II	C2	54	15	7	10	377	0.165	0.661
PC I/II	C3	59	13	7	11	396	0.145	1.075
PC I/II	C4	55	16	7	11	392	0.154	0.654
PC II/V	C5	57	14	4	11	401	0.154	0.654

Table 5– UHPC paste performance in dependency of different cements only

Type	ID	Cost ($/m³)	CFP_P (kg/m³)	W/C	¹Spread (mm)	²f'_{c-28} (MPa)(ksi)
White PC I	UHPCp C1	633	1112	0.24	313	207 (30.0)
PC I/II	UHPCp C2	523	620	0.25	250	115 (17.0)
PC I/II	UHPCp C3	503	1002	0.25	118	103 (15.0)
PC I/II	UHPCp C4	513	613	0.25	210	135 (19.6)
PC II/V	UHPCp C5	513	613	0.25	288	164 (23.8)

Spread from mini cone converted to standard spread ¹Compressive strength based on one 2" cube

Silica Fume (SF)

Un-densified grey **SF** was chosen in the mixture design, as it is more capable to fill the voids between the cement particles than densified silica fume [14]. Only one type of **SF** was used in this research. It was selected based on median particle size, low carbon content, local availability and based on previous research [7]. Lower carbon content means lower water demand, thus, better flow ability. **Table 6** shows the properties of silica fume used in this research.

Table 6 – SF properties and cost

Type	ID	SiO$_2$ %	Carbon %	Na$_2$O %	K$_2$O %	D$_{50}$ (μm)	Cost ($/kg)	CFP_P (kg/kg)
Grey	SF	>85	0.3<0.7	0.1	0.07	0.4	0.675	0.017

*Loss of ignition (LOI), # Percent retained on 45μm diameter sieve

Supplementary Cementitious Materials (SCMs)

All mixes described in **Table 7** consisted of C1, SF1, FB, and HRWR1 (see **Table 2**).

Table 7 – SCM properties and cost

Type	ID	D$_{50}$ (μm)	Cost ($/kg)	CFP_P (kg/kg)	ID	UHPCp Cost ($/m³)	UHPCp CFP_P (kg/m³)	W/C	Spread (mm)	^{1}f'$_{c-28}$ (MPa)(ksi)
FA F	SCM1	11.3	0.066	0.000007	UHPCp SCM1	633	1112	0.24	313	207 (30.0)
FA C	SCM2	11.3	0.066	0.000007	UHPCp SCM2	633	1112	0.24	303	233 (33.8)
RGP	SCM3	9.4	0.154	0.062	UHPCp SCM3	618	1113	0.25	305	165 (24.0)
GGBS	SCM4		0.154	0.229	UHPCp SCM4	589	610	0.25	293	185 (26.8)
MK	SCM5		0.551	0.079	UHPCp SCM5	744	1127	0.25	118	118 (17.1)

Percent retained on 45μm diameter sieve, *Values of the reference paste using the type of supplementary material, ^{1}Compressive strength based on one 2" cube

High Range Water Reducer (HRWRs)

For the investigations of superplasticizers, reference mix with different FA class was used. Two different types of HRWRs were selected based on previous research [7]. All mixes are described in **Table 8** which consisted of C1, SF1, SCM2, and FB (like the mix as shown in **Table 2**).

Table 8 – High Range Water Reducer costs and performance

ID	Cost $ /gal	UHPC Paste Cost ($/m³)	UHPC Paste CFP_P (kg/m3)	W/C*	Spread* (mm)	^{1}f'$_{c-28}$ (MPa)(ksi)
HRWR1	20	631	770	0.24	303	233 (33.8)
HRWR2	12	560	770	0.24	200	166 (24)

* One paste mix with two different HRWRs were used. This is not the reference mix. ^{1}Compressive strength based on one 2" cube

2.2.3. UHPC Matrix

Aggregates

Aggregates were primarily selected based on locality, type of material, size, and cost. Only one type of fine basalt (**FB**) was included in this research. Basalt was selected because of its higher modulus of elasticity of around 50 GPa and compressive strength of more than 200 MPa. More importantly, it is readily available in the New England area at low cost in comparison to quartz sand (**Table 9**).

Aggregates were first cleaned, and oven dried for a day before performing sieve analysis. All the aggregates above 1.2 mm and below #200 sieve size were sieved out. The modified Andreasen-Andersen curve with q-value = 0.37 was found to provide optimum particle packing density [15],

thus, aggregates were sieved to fit this curve. The particle size distribution of the aggregates is shown below in **Figure 5**. Cost and CFP is included in **Table 9**.

Table 9 – Fine aggregate nomenclature, size and costs

Type	ID	Size (mm)	Cost $/kg	CFP_P (kg/kg)
Basalt	FB	< 0.475	0.037	0.007
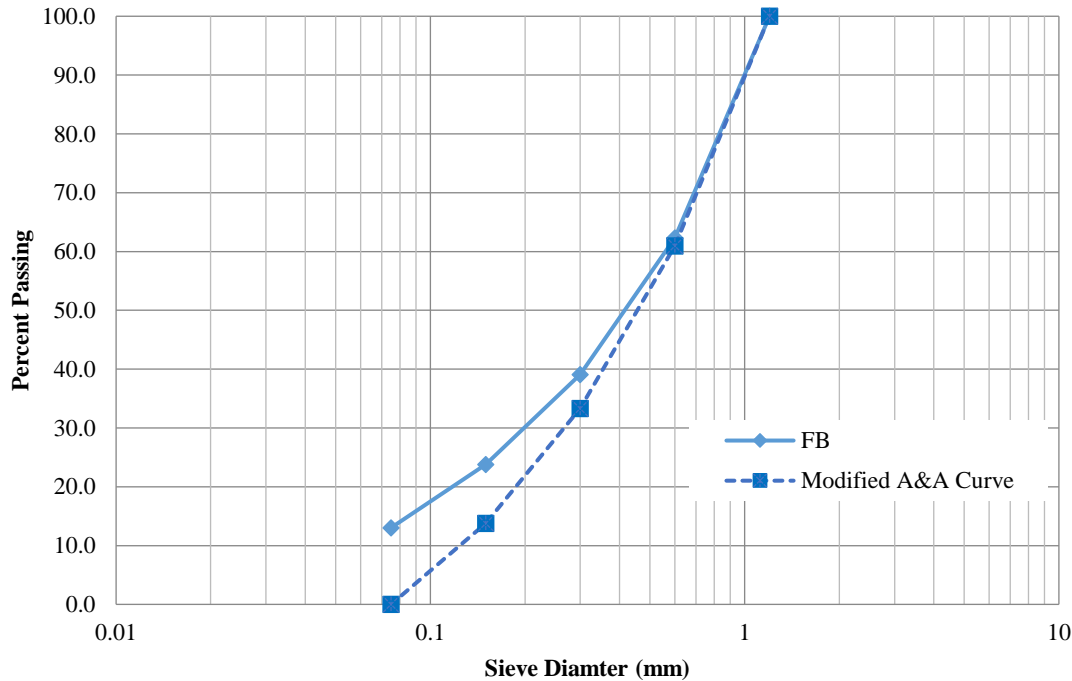
Figure 5: Sieve analysis for basalt sand and their Andreasen and Andersen curve

Fibers

Since detailed investigation of different fiber types is out of scope of this research, only one type of fiber, 13 mm long and 0.2 mm in diameter, smooth and straight, was selected for this research (**Figure 6**). Each fiber volume fraction (V_f = 1%, 1.5% and 2%) was combined with three different aggregate-cement ratios (A/C = 1.2, 1.5 and 1.8) to investigate their interaction on the flow ability of the composite. As the fiber volume and A/C ratio both increased, the spread generally decreased due to the interaction and interference between aggregates and fibers. This relationship was developed and plotted later. A lower fiber volume fraction also significantly decreased the cost of the composite since fibers are the most expensive constituent. Therefore, the limits of the highest A/C ratio and lowest fiber volume fraction allowable are required to optimize cost-efficiency while maintaining acceptable performance. **Table 10** summarizes the description of the steel fiber used in this research.
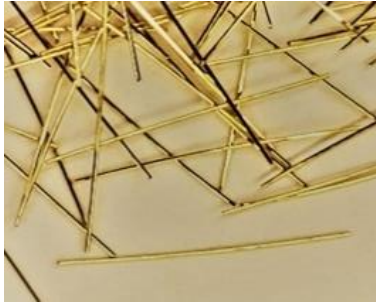
Figure 6: Smooth Steel Fibers

Table 10 – Fiber nomenclature, dimensions and cost

ID	Geometry	Surface Texture	Material	Diameter (mm)	Length (mm)	Cost $/ton
F	Round - straight	Smooth	Steel	0.2	13	4,400

Chapter 3: Test Procedures and Sample Preparation

3.1 Mixing and Workability Testing

3.1.1 Preliminary Paste Mixes in Lab RAM

UHPC pastes were mixed in small batches of 0.16 liters using the resonance acoustic mixer (RAM) shown in **Figure 7 (a)**. RAM consists of a three-mass system, spring assembly, and a loaded mixing vessel without any other mixing tools. This technology allowed mixing the material through a non-contact method of propagating acoustic pressure waves. Using this mixer enabled enhanced mixing quality and consistency in comparison to traditional shear mixers, especially when small mixing volumes were investigated. Additionally, the closed containers prevented any loss of material or moisture during mixing.

| a) | b) |

Figure 7: Mixing in a) Lab RAM   b) Rotary Hobart Mixer

First, all dry materials were mixed at an intensity of 90% for 2.5 minutes. The less dense material (i.e., un-densified SF) was placed at the bottom, followed by SCM and then by PC and aggregate. Some aggregates were already added to each paste in the ratio to the cement of 0.8 to aid in deagglomeration of powdered material during dry mixing. Then, water with HRWR was added to the mix and mixed for another 2.5 minutes at an intensity of 50%. A mixing break of 1.5 minutes was used to release heat and to scrape excess materials off the sides of the vessel. Then mixing was continued until the mix turned over which usually took five to seven minutes. Once it turned over, mixing was continued for two more minutes following the procedure in [16].

The mixing volume was limited by the allowable mass of 500g including the mixing vessel. Therefore, the volume of mixed material was sufficient to only perform a spread test using a self-fabricated mini cone (**Figure 8 a)**).

3.1.2 Testing Workability

The workability was tested using a spread cone in accordance with ASTM C 230/C 230M [8]. The standard flow cone (**Figure 8b**) was used to measure the spread of UHPC. However, to accommodate the small mixing volume of the RAM, a mini flow cone was fabricated and used to measure the spread. The dimensions of this miniature cone (upper diameter, lower diameter, and height) were exactly half that of a standard spread cone. Both the miniature and standard spread cones are shown in **Figure 8 a, b** and their dimensions are summarized in **Table 11**.

Special emphasis was placed on keeping the spread cone and the base plate at a similar humidity for each test. To achieve this, the spread cone and baseplate were both wiped with a slightly dampened cloth immediately prior to testing. After the spread cone was filled, any excess material was scraped from the top of the cone with a metal spatula to ensure the proper volume of material was evaluated. The cone was then lifted in an upward, and rotational motion at a similar pace. Any leftover material sticking to the inside wall of the cone was scraped off and left to fall into the remainder of the spreading material. The material was allowed to spread on the

base plate until no further expansion was measured. The diameter of the spread was measured in two directions. The average of these two measurements was recorded as the overall spread and used for further analysis.

(a)

(b)

(c)

(d)
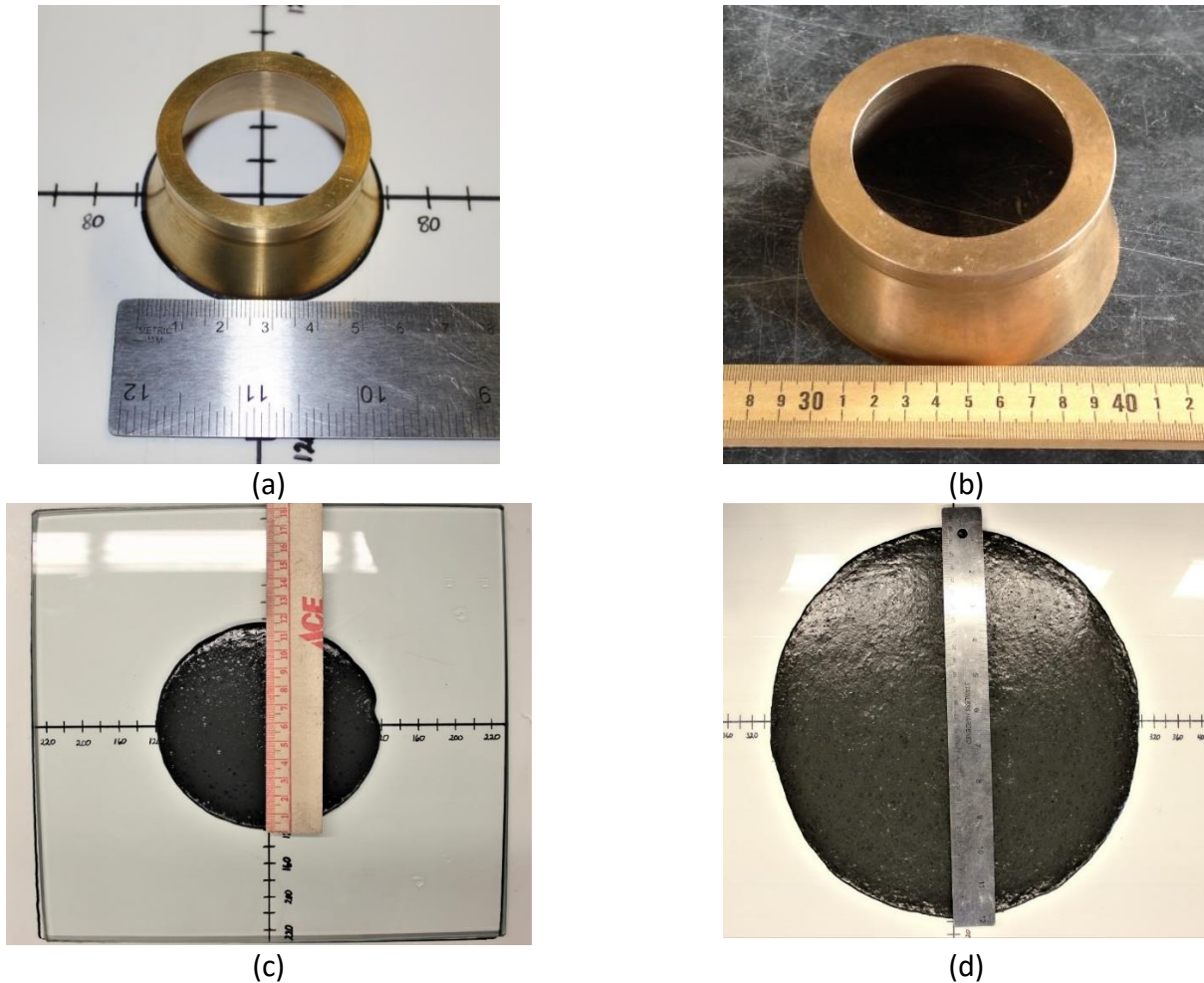
Figure 8: a) miniature spread cone, b) standard spread cone, c) miniature spread test example, d) standard spread test example

Table 11: Spread cone size comparison

Spread Cone Size	Upper Diameter (mm)	Lower Diameter (mm)	Height (mm)	Volume (mL)
Miniature	35	50	30	43
Standard	70	100	60	344

To compare the spread from the mini-flow cone S_{mini} to the standard spread S_{Stnd} of regular cone size according to ASTM C 230/230M [16] the following **Equation 1** was used.

$$S_{Stnd} = 2.5 \times S_{mini} - 7.2 \qquad (1)$$

The standard targeted workability of the UHPC paste was in the range of 280-340 mm [7] which becomes 110-133 mm with using the mini flow cone.

3.1.3 Preliminary Paste Mixes in Hobart Mixer

All the UHPCs and UHPC matrices were mixed using Hobart – rotary mixer (**Figure 7b**). This mixer provides a bi-rotary mixing technology at three different mixing speeds. All the mixes followed the standard UHPC mixing procedure [17]. The concrete mixing emphasized breaking particle agglomerations and keeping particles well dispersed.

First, the silica fume and aggregates were mixed for five minutes at speed one (at 136 rpm) to break down the agglomerations, then followed by adding fly ash or glass powder as pozzolans, then cement and mixed for five more minutes at same speed. Water with one third of superplasticizer was added to the premixed dry powders. Then, left over superplasticizer was added to the mix. During adding water and superplasticizer, the speed of the rotating blade was maintained at speed one. Then, speed of the mixer was raised to two and let it mix until it started to turn over. Once it started to turn over, the speed was lowered to one.

Once the mix was fluid, the speed was increased to two and allowed to mix for five more minutes. For fiber reinforced UHPCs, fibers were added to the mix at half speed. Once adding fibers was completed, the speed was raised to one for two more minutes to make sure the fibers were sufficiently dispersed.

The best performing matrices were selected from the paste mix series based on the R factor and continued with investigation of mechanical properties using straight smooth fibers.

3.2 Resource-Efficiency Factor R

The resource-efficiency factor R in **Equation 2** is used in this research to evaluate the performance of each material constituent in the UHPC paste. Inspired by the material performance efficiency E from Wille and Boisvert-Cotulio [7] R is a dimensionless efficiency parameter which comprises the relative compressive strength ($\frac{f'_{c,N}}{f'_{c,N,\emptyset}}$), the relative workability ($\frac{spread_N}{spread_{N,\emptyset}}$), the relative cost ($\frac{cost_P}{cost_{P,\emptyset}}$) and the relative carbon footprint of each paste ($\frac{CFP_P}{CFP_{P,\emptyset}}$).

$$R = \frac{0.7 \times \dfrac{f'_{c,N}}{f'_{c,N,\emptyset}} + 0.3 \times \dfrac{spread_N}{spread_{N,\emptyset}}}{0.6 \times \dfrac{cost_P}{cost_{P,\emptyset}} + 0.4 \times \dfrac{CFP_P}{CFP_{P,\emptyset}}} \qquad (2)$$

, where $f'_{c,N}$ is the 28-day compressive strength normalized at w/c = 0.25, $f'_{c,N,\emptyset}$ is the average normalized 28-day compressive strength over all pastes of one series, $spread_N$ is the spread value normalized at w/c = 0.25, $spread_{N,\emptyset}$ is the average normalized spread value over all pastes of one series, $cost_P$ is the cost of the paste per m³, and $cost_{P,\emptyset}$ is the average cost over all pastes of one series, CFP_P is the carbon footprint of the paste per m³, and $CFP_{P,\emptyset}$ is the average carbon footprint over all pastes of one series.

The weight factors were defined by the author to consider strength with higher priority over workability in the nominator and cost with slightly higher priority than carbon footprint in the denominator.

The effect of each material component on the paste's relative strength, spread, cost and carbon footprint were evaluated. Then the material component with the best efficiency out of each series was chosen to form the optimized paste.

3.3 Sample Preparation and Curing

Immediately after the spread test, samples were cast for the compression test, and direct tension test. Three 2 in × 2 in cube specimens were prepared for the compression test using 2 in brass cube molds. Five full dog bone shaped specimens were prepared for direct tension test. Dog bone samples were made by pouring the freshly mixed concrete in the dog bone shaped molds in layers. All the cube molds and dog bone molds were vibrated for consolidation for 5 minutes at a frequency of 3.5 Hz. About 30 minutes after pouring the concrete, the molds were covered with plastics to avoid excessive evaporation of water from the specimen. The samples were demolded after 24 hours and stored in the curing room at 20 degrees Celsius and 95% of relative humidity until testing.

3.4 Compression Test

Three 2" x 2" concrete cubes were used for the compression test. The cubes were polished before testing to minimize stress concentrations due to irregular load surfaces. Once the cubes were ground, they were inspected for planeness using a metal straight edge with dimensions of 0.25" x 1" x 4" (6.3 mm x 25.4 mm x 101.6 mm) and a precision feeler gauge with a thickness of 0.0015" (0.038 mm) (**Figure 9**).

Figure 9: a) Loading face preparation of cube on rotary grinder/polisher b) Planeness inspection

The straight edge was placed on the prepared loading face of the cube and attempted to push the very thin feeler gauge underneath the straight edge. If the gauge was allowed under the straight edge, the cube was not sufficiently plane and must be ground/polished until the gauge cannot fit between the loading face of the specimen and the straight edge. Both loading faces were prepared this way.

Once the cube specimens reached 28 days of casting and their loading faces were prepared to acceptable planeness, they were centrically loaded in a hydraulic load frame for the compression testing following ASTM C109/C109M-16a [18]. The specimens were tested at the rate of loading of 30,000 lb/min. The used test machine has a capacity of 250,000 pounds. **Figure 10** shows the test setup for the compression test. The cubes were placed between the 2.8" (71 mm) diameter load platens, one of which was spring-loaded and free to rotate about a ball-bearing. This spring and ball-bearing mechanism ensured perfect contact with the loading faces during testing. Test duration was typically 3-5 minutes. In comparison, the composite specimen (with fibers) generally kept its cubic form due to the fibers, unlike cone-failure mode, which is caused by friction-induced confinement at the top and bottom of the specimen from the loading platens and showed very brittle and explosive failure in case of UHPC without fibers (**Figure 11**).

(a)   (b)
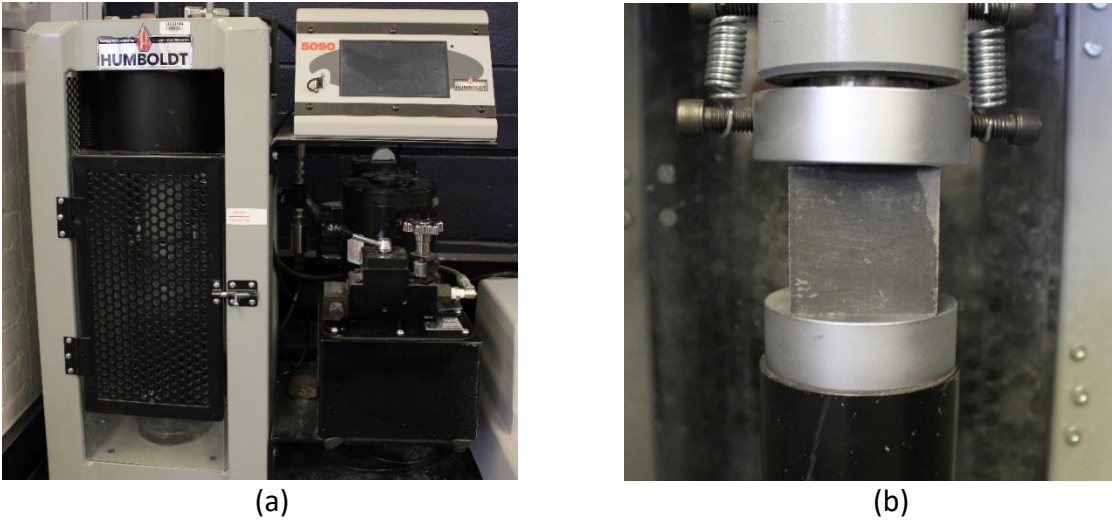
Figure 10: a) Compression test load frame b) test-set up

(a) Brittle failure (no steel fibers)   (b) Ductile failure (with steel fibers)

Figure 11: Failure of compressive specimens with and without steel fibers

3.5 Direct Tension Test

Five to six dog bone specimens were prepared for direct tension testing. A 400 kips hydraulic test machine was used to carry out the tests. **Figure 12 (a)** shows the test setup located in the Structural Lab (FLC 115) at the University of Connecticut. Dog bone shaped specimen were prepared and tested at 28 days. These samples were reinforced with the steel mesh on edges, both on the top and bottom to ensure tensile failure at the middle. Each specimen had a constant cross-sectional area of 1 in^2 (25 mm^2) and a gauge length of 3.14 in (80 mm).

The top surface of the specimens was slightly polished to facilitate the attachments of LVDTs.

The direct tension test set up was designed to provide rotational freedom at the top and bottom of the specimens (**Figure 12 (a)**). This resulted in more consistent stress versus strain curves of specimens from the same concrete mixture. Two LVDTs were attached on both sides of the specimen to measure the extension precisely.

(a)   (b)
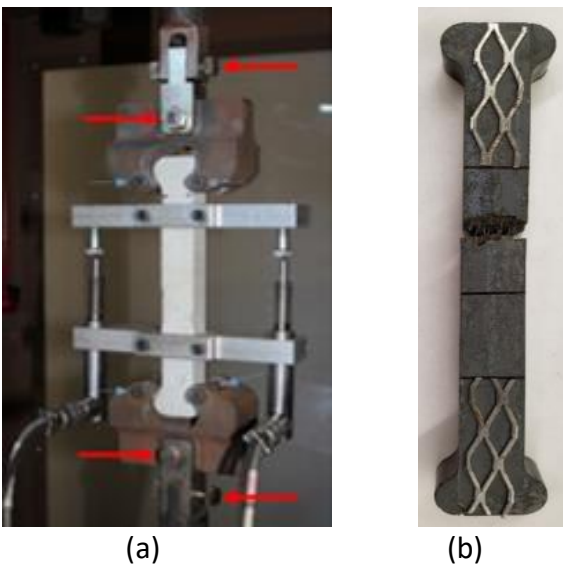
Figure 12: a) direct tension test setup b) dog bone specimen

3.6 Early Age Compression Strength Test

Some of the best performing mixes were remixed and cured with steam of 90 degrees Celsius for up to 24 hours. Several 2 inch cubes were prepared. The specimens were demolded after 12 hours and then exposed to steam curing for 6 hours, 12 hours, and 24 hours. After steam curing the cubes were tested for their compression strengths. The investigation of early age properties is used to correlate with the hardened concrete properties of normal cured specimens.

Chapter 4: Results and Discussion

4.1 Investigation of High Early Strength (HES) Conventional Concrete

4.1.1 HES using Nano-silica (NS)

In the first step of this research mortar cubes were cast, using 0.5%, 2%, and 3% of NS in replacement for cementitious material. The average compressive strengths at 24h using different amounts of NS are summarized in **Figure 14 a** (Mix6 refers to the mixture provided in Table 1). The results show that the addition of 0.5% of NS already slightly decreased the compressive strength. The reduction of the compressive strength at this and higher amounts of NS might have been caused by particle agglomerations and has not been further investigated.

4.1.2 HES using Calcium Sulpho-Aluminate (CSA)

The replacement of Portland cement with calcium sulphonate aluminate (CSA) cement at 10%, 15%, 20% by weight of Portland cement of Mix 6 led to difficulties in material consolidation. The effect on the compressive strength at 24h is summarized in **Figure 14 b**.

4.1.3 HES using Accelerating Admixtures

Figure 13 c shows the results of average compressive strength with 2%, 2.5%, and 3% accelerating admixture. The addition of 2% of accelerator resulted in an increase of strength of about 20%.

(a)   (b)
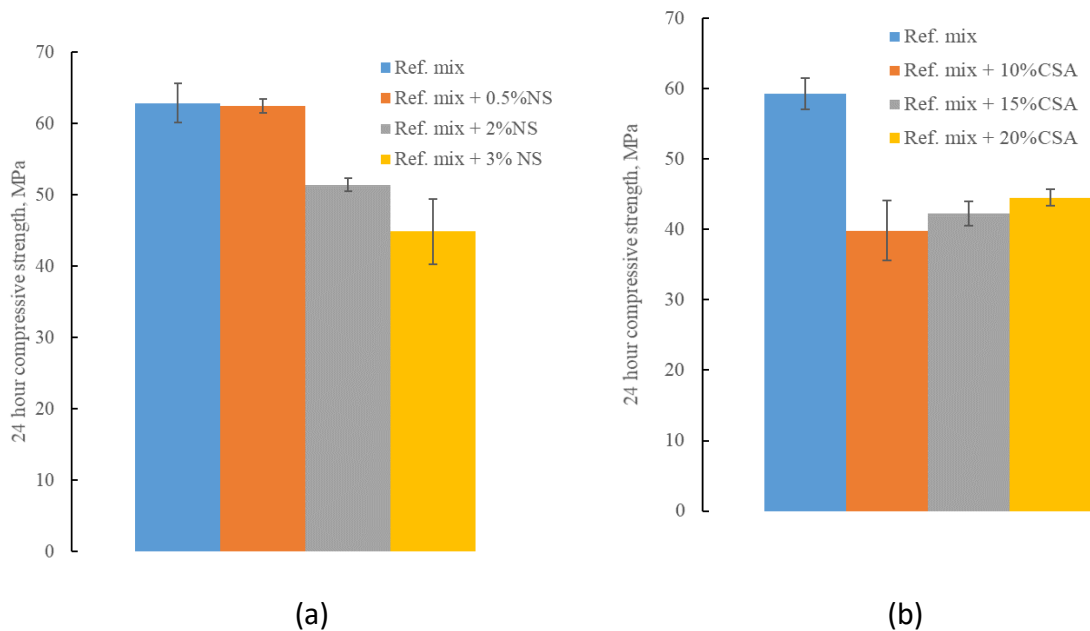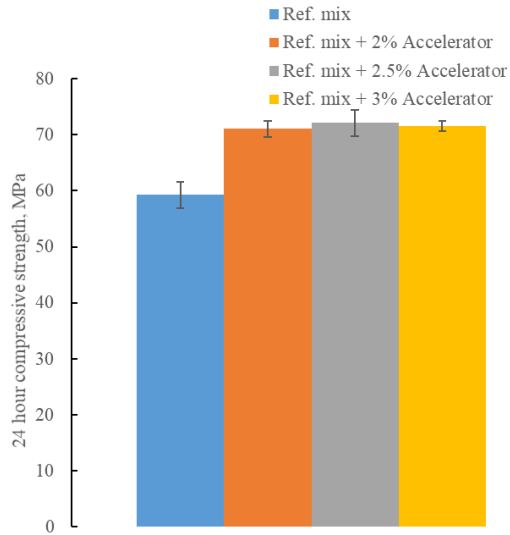
(c)

Figure 13: 24-hour compressive strength of conventional HES using (a) nano-silica, (b) calcium sulpho-aluminate cement, and (c) accelerating admixture
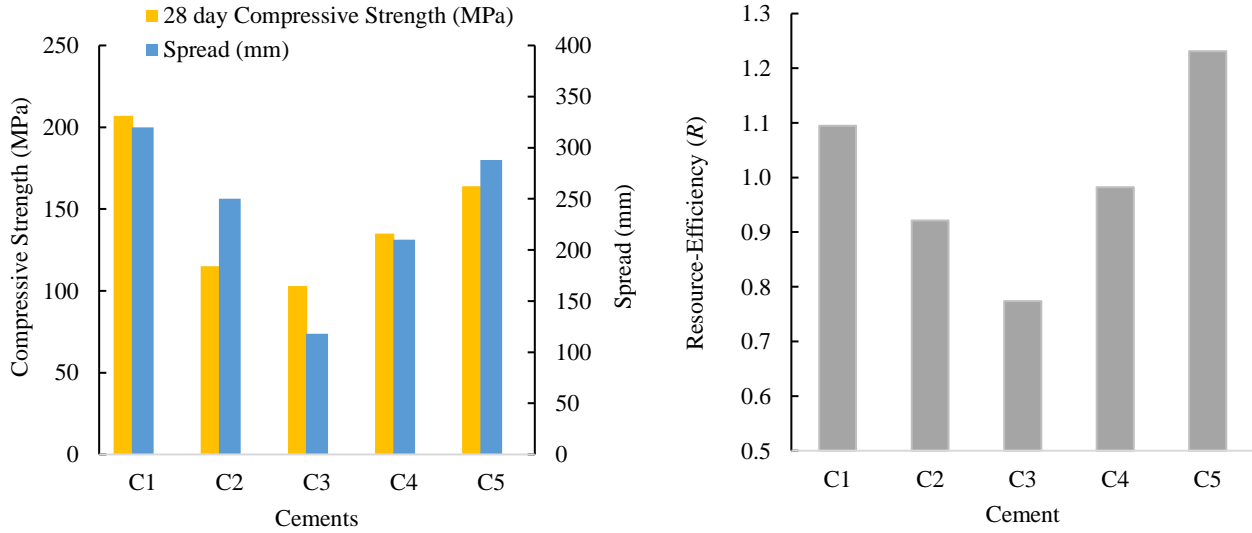
Figure 14: Performance of different cement types

From **Figure 14**, it can be seen that the UHPC with **C5** had the highest resource efficiency factor, *R*, while UHPC with **C1** led to the highest compressive strength and best workability. For further investigation **C5** was selected.
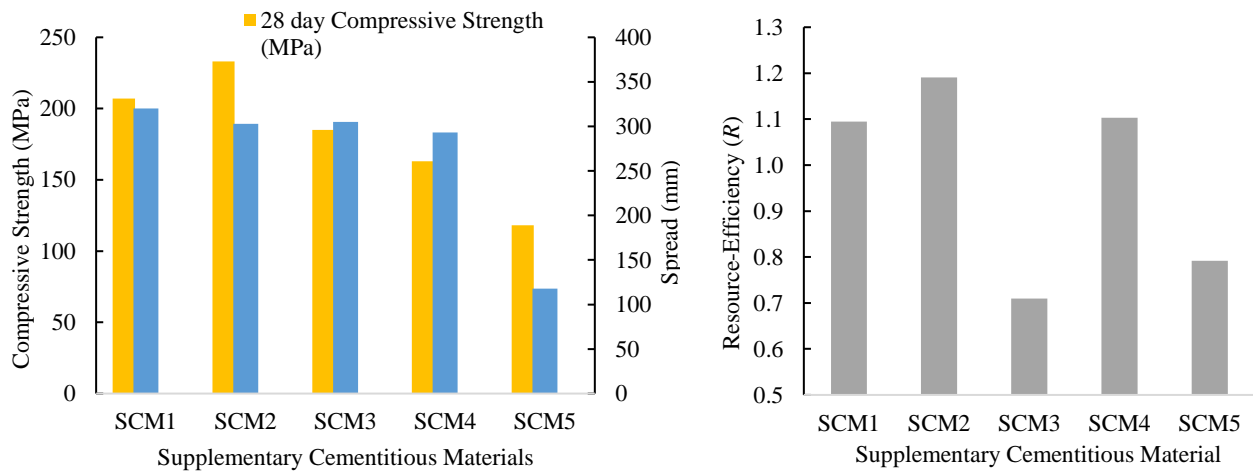
Figure 15: Performance of different supplementary cementitious materials

From **Figure 15**, it can be seen that **SCM2** had the highest resource efficiency factor, *R*, and thus was selected for further investigation.
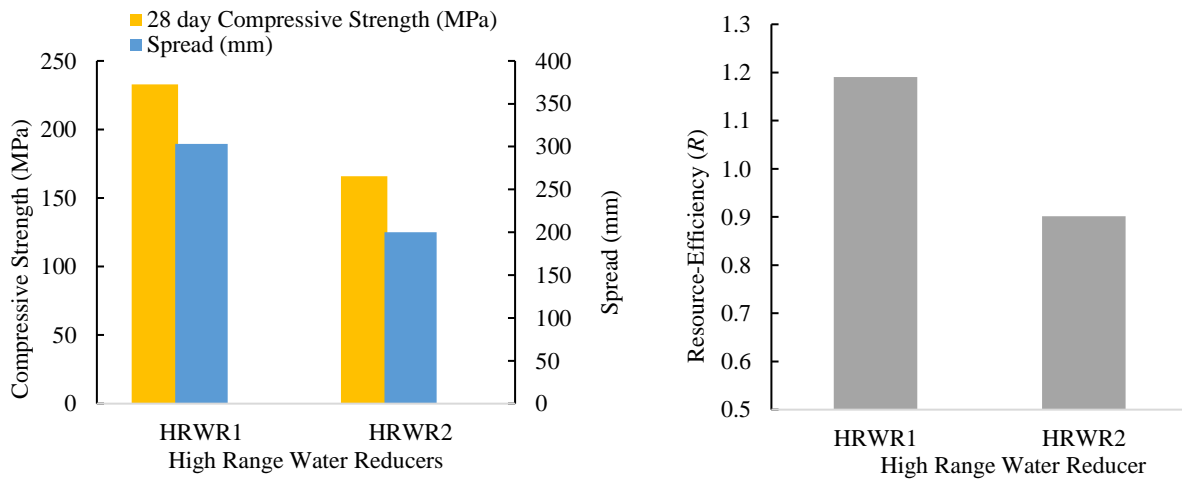
Figure 16: Performance of different superplasticizers

From **Figure 16**, it can be seen that **HRWR1** had the highest resource efficiency factor, *R*, and thus was selected for further investigation.

4.3 Further Optimization of UHPC Pastes

4.3.1 Alternative Paste

As per recommendation from previous research [7], an alternative paste was investigated in this research using type II/V cement (**C5**). The standard size spread achieved was 288 mm (above the preferable 280 mm) at a w/c ratio at or below 0.25 and attained a compressive strength of 164 MPa (23.8 ksi), which was above the minimum requirement of 150 MPa (22 ksi). This confirmed the alternative paste as a viable alternate option to the chosen paste at a significantly reduced cost by $120 per m^3 in comparison to reference paste.

Table 12– Performance of alternative paste

W/C (by mass)	W/F (by vol.)	A/C (by mass)	A/P (by vol.)	Mini Spread (observed) (mm)	Standard Spread (converted) (mm)	28-day compressive strength (MPa)(ksi)
0.25	0.42	0.81	0.33	118	288	164 (23.8)

However, since type II/V cements (**C5**) are not readily available everywhere in large quantities, an alternate option would be type I/II cements (**C4**). **Table 13** summarizes the performance of the UHPC using **C4**, instead of **C5** while all other alternative paste constituents were used. The mix design for this paste was the same as the alternative paste presented in **Table 12** since the specific gravities of cements (**C4**) and (**C5**) were identical.

Table 13 – Performance of C4 with alternative paste

W/C (by mass)	W/F (by vol.)	A/C (by mass)	A/P (by vol.)	Mini Spread (observed) (mm)	Standard Spread (converted) (mm)	28-day compressive strength (MPa)(ksi)
0.25	0.42	0.81	0.33	86	208	153 (22.2)

From these results it can be observed that the achieved standard size spread was not preferable (below 280 mm). Still, this paste was workable.

4.3.2 Silica Fume Reduction with Fly Ash (FA)

As silica fume is the most expensive fine powder constituent, its proportion to the cement was reduced from 25% to 10% to decrease the cost of the paste. The effects on workability and compressive strength are discussed below. **Table 14** and **Figure 17** summarize the performance of the UHPC with each silica fume proportion while their mix designs for each proportion and associated costs per volume for each of these proportions are presented in **Table 15-16**.

The water to fines ratio (W/F) and aggregate to powder ratio (A/P) ratios were kept constant throughout to isolate the influence of the silica fume reduction. Since the volume of the fines was decreased with each reduction of the silica fume mass, the w/c ratio must also be decreased to keep the water to fines ratio constant. Decrease in amount of silica fume increased the amount of cement. **Table 14** and **Figure 17** show that the UHPC with the proportion of 1:0.**20**:0.25 performed best regarding spread and compressive strength.

Table 14 – Performance of alternative paste with silica fume/cement mass ratios (10%, 15%, 20%, and 25%)

Proportion (C:SF:SCM)	W/C (by mass)	W/F (by vol.)	A/P (by vol.)	Mini Spread (observed) (mm)	Standard Spread (converted) (mm)	28 day compressive strength (MPa)(ksi)	R
1:0.10:0.25	0.22	0.42	0.33	117	285	156 (22.7)	1.08
1:0.15:0.25	0.23	0.42	0.33	117	285	164 (23.8)	1.12
1:0.20:0.25	0.24	0.42	0.33	121	295	175 (25.4)	1.19
1:0.25:0.25	0.25	0.42	0.33	118	288	164 (23.8)	1.13

Table 15 – Mix designs and cost analysis of alternative paste with varying silica-fume proportions (10% and 15%)

C:**SF**:SCM	10% (1:**0.10**:0.25)				15% (1:**0.15**:0.25)			
ID	Amount (kg/m³)	Mass (%)	Cost ($US/m³)	CFP$_P$/m³	Amount (kg/m³)	Mass (%)	Cost ($US/m³)	CFP$_P$/m³
C5	1060	43.8	164	530	1010	42	156	505
SF	106	4.4	72	1.4	152	6.3	102	1.97
SCM2	265	10.9	18	0.0	252	10.5	17	0.0
HRWR1	40	1.6	197	0.0	38	1.6	187	0.0
FB	747	30.8	28	4.0	747	31.1	28	4.0
Water	205	8.5	0	0.0	206	8.6	0	0.0
Cost			477	535			490	511

Table 16 – Mix designs and cost analysis of alternative paste with varying silica-fume proportions (20% and 25%)

C: **SF**: SCM	20% (1:**0.20**:0.25)				25% (1:**0.25**:0.25)			
ID	Amount (kg/m³)	Mass (%)	Cost ($US/m³)	CFP$_P$/m³	Amount (kg/m³)	Mass (%)	Cost ($US/m³)	CFP$_P$/m³
C5	965	40.4	149	483	924	38.9	143	462
SF	193	8.1	130	2.51	231	9.7	156	3.0
SCM2	241	10.1	16	0.0	231	9.7	15	0.0
HRWR1	36	1.5	179	0.0	34	1.4	171	0.0
FB	746	31.3	28	4.0	747	31.5	28	4.0
Water	206	8.6	0	0.0	207	8.7	0	0.0
Cost			502	489			513	469

The results in **Table 14-16** are summarized and plotted in **Figure 17** below.
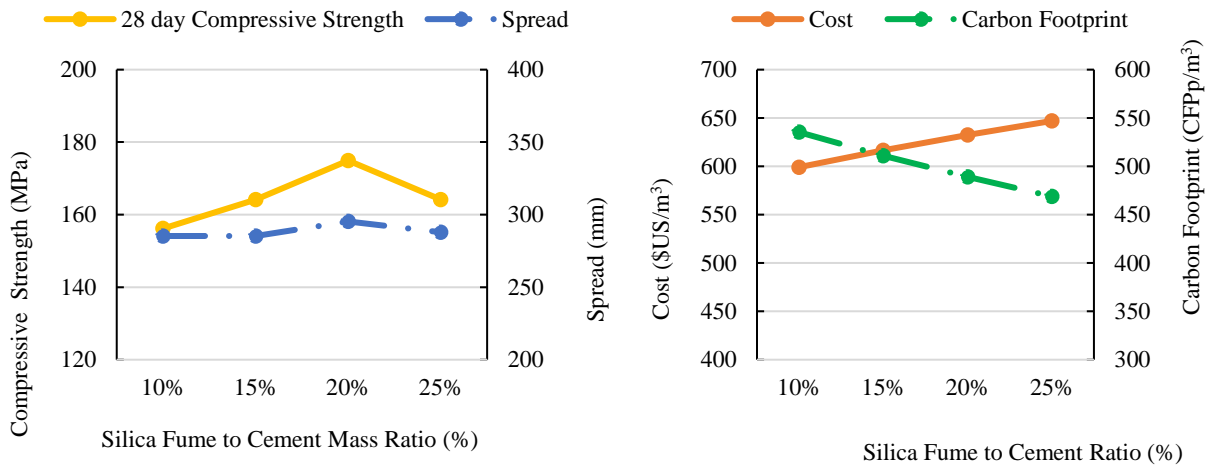
Figure 17: Influence of silica fume reduction on workability, strength and overall efficiency

From the graph of **Figure 17** it can be observed that the pastes exhibited a steady increase in compressive strength from a 10% to 20% silica fume to cement proportion. This rate of increase was approximately linear at roughly 10 MPa gained for every 5% increase in silica fume. This supports the concept that as the silica fume proportion increases from 10-20%, more SiO_2 is made available for pozzolanic reaction with CH to produce more C-S-H structures. Thereby increasing compressive strength. Based on the data, a 20% silica fume proportion resulted in the highest particle packing during mixing and densest matrix after hardening, leading to highest values in workability and compressive strength, respectively. At 25%, the paste demonstrated a significant decrease in spread and strength.

The proportion of 1:**0.25**:0.25 (C:**SF**:SCM) was used in this research as the proportion of reference based on the recommendations of Wille et al [17]. In comparison to the white cements, which had a C_3S compositions of more than 70%, **C5** had a relatively low C_3S content of 57%. In addition, **SF** had a very high SiO_2 composition of more than 95%. With the relatively low C_3S of **C5** which produced CH, and the very high SiO_2 content of **SF** which reacted with CH, it is quite possible that the majority of the CH already reacted at a silica fume proportion of 20%. If this were the case, any silica fume added beyond 20% would not contribute to C-S-H formation and would only serve as unreacted filler.

Based on these findings, a proportion of 1:**0.20**:0.25 (PC:SF:SCM) is recommended for optimal performance of the alternative paste in both workability and strength.

Although a silica fume proportion of 20% achieved the highest performance, all pastes with varying proportions performed suitably for UHPC, achieving spread values greater than 280 mm and compressive strengths above 150 MPa (22 ksi). For this reason, all proportions can be recommended to produce viable UHPC pastes. Discretion can be applied by field users as to what parameters are of higher significance to their specific needs.

If cost is of the highest priority, a 10% silica fume proportion (1:**0.10**:0.25) is recommended since it has the lowest associated cost and achieved adequate workability and strength. If performance

is most valued, a 20% (1:**0.20**:0.25) silica fume proportion is recommended. It is also worth noting that the proportions of 15% and 25% silica fume demonstrated almost identical performance. They exhibited identical compressive strengths of 164 MPa (23.8 ksi) and had a difference in spread of only 3 mm: 285 mm and 288 mm for 15% and 25%, respectively. For this reason, a proportion of 15% silica fume (1:**0.15**:0.25) is recommended as the best balance between performance and cost.

Each of these proportions provided cost savings relative to the alternative paste (with a 25% silica fume proportion) of $37, $23, and $11 per cubic yard, respectively. **Table 14** shows the performance vs. resource-efficiency *R* of each of these pastes, where a silica fume proportion of 20% obtained the highest *R* value of 1.19. Since all three of these reduced proportions provide suitable performance for UHPC, if greater cost savings are desired over slightly improved performance, 10% and 15% silica fume proportions are also recommended.

4.3.3 Silica Fume Reduction with Recycled Glass Powder (RGP)

During months of high construction volume the limited availability of fly ash might become a more pressing issue. Recycled ground glass powder (RGP) could be a viable alternative SCM option. Therefore, RGP (**SCM3**) was further investigated in combination with various silica fume to cement ratios (12.5%, 15%, 17.5%, 20%, and 25%). SCM3 used here had a median particle size of 9.5 μm, a SiO_2 content of 71.7% (indicative of the potential of pozzolanic reactivity), a reasonable cost, and a favorable environmental footprint as it is composed of 100% post-consumer recycled glass. The mixture designs and performances are summarized in **Tables 17-19,** respectively, and graphically summarized in **Figure 18**.

Table 17– Performance of alternative paste with RGP and silica fume/cement mass ratios (12.5%, 15%, 17.5%, 20%, and 25%)

(C:**SF**:SM)	W/C (by mass)	W/F	A/P	Mini spread (observed) (mm)	Standard spread (converted) (mm)	[1]f'_{c-28} (MPa)(ksi)	*R*
1:**0.125**:0.25	0.22	0.45	0.33	105	255.3	159.2 (23.1)	1.06
1:**0.15**:0.25	0.22	0.45	0.33	99	240.3	158.9(23.5)	1.04
1:**0.175**:0.25	0.23	0.45	0.33	120	292.8	165.9(24.1)	1.13
1:**0.20**:0.25	0.23	0.45	0.33	109	265.3	168.8(24.5)	1.12
1:**0.25**:0.25	0.25	0.45	0.33	105	255	153.0(22.2)	1.01

Table 18 - Mix designs and the cost analysis of alternative paste with RGP and silica fume/cement mass ratios (12.5%, 15%, and 17.5%)

| C: **SF**:SM	12.5% (1:**0.125**:0.25)				15% (1:**0.15**:0.25)				17.5% (1:**0.175**:0.25)			
ID	Amount (kg/m³)	Mass (%)	Cost $US /m³	CFP_P/m³	Amount (kg/m³)	Mass (%)	Cost $US /m³	CFP_P/m³	Amount (kg/m³)	Mass (%)	Cost $US /m³	CFP_P/m³
C5	999	42.1	154	500	976	41.2	151	488	954	40.4	147	477
SF	125	5.3	84	1.60	146	6.2	99	1.90	167	7.1	113	2.2
SCM3	250	10.5	39	12	244	10.3	38	12	238	10.1	37	11
HRWR1	37	1.6	185	0.0	36	1.5	181	0.0	36	1.5	177	0.0
FB	747	31.5	28	4.0	747	31.6	28	4.0	747	31.7	28	4.0
Water	216	9.1	0.0	0.0	217	9.2	0.0	0.0	217	9.2	0.0	0.0
Total			490	517			496	505			501	494

Table 19 - Mix designs and the cost analysis of alternative paste with glass powder with RGP and silica fume/cement mass ratios (20 % and 25%)

C: **SF**:SM	20% (1:**0.20**:0.25)				25% (1:**0.25**:0.25)			
ID	**Amount (kg/m³)**	**Mass (%)**	**Cost $US /m³**	CFP_P/m^3	**Amount (kg/m³)**	**Mass (%)**	**Cost $US /m³**	CFP_P/m^3
C5	933	39.7	144	466	924.6	39.2	143	462
SF	187	7.9	126	2.42	231.1	9.8	156	3.0
SCM3	233	9.9	15	11.0	231.1	9.8	36	11
HRWR1	35	1.5	173	0.0	34.4	1.5	172	0.0
FB	747	31.8	28	4.0	718.9	30.5	27	4.0
Water	217	9.2	0.0	0.0	215.9	9.2	0.0	0.0
Total			507	484			533	480

Table 20 – Comparative performance of alternative pastes (RGP vs FA)

Material	W/C (by mass)	W/F (by vol.)	A/P (by vol.)	Mini Spread (observed) (mm)	Standard Spread (converted) (mm)	28-day compr. strength (MPa)(ksi)	*R*
SCM3 (RGP)	0.26	0.44	0.32	110	268	161 (23.3)	1.01
SCM1 (FA)	0.25	0.42	0.33	118	288	164 (23.8)	1.13

As demonstrated by these results, the RGP (**SCM3**) is a viable substitute for FA in the case of limited availability and for increased environmental sustainability. Comparing the UHPC using RCP (**SCM3**) with UHPC using FA (**SCM1**) the following conclusions can be drawn (**Table 20**): The mix with RGP required slightly more water (w/c ratio of 0.26 instead of 0.25) and still had a slightly reduced mini spread of 110 mm (268 mm standard spread) in comparison to 118 mm (288 mm standard spread). The compressive strengths of the UHPCs using RGP or FA showed a very small difference of only 3 MPa (0.5 ksi) and was above the minimum requirement of 150 MPa (22 ksi). RGP is significantly more expensive than FA at a cost of $154 per ton compared to only $66 per ton (**Table 7**). However, the supplementary material only constituted less than 10% of the paste mix design by mass. Therefore, this cost difference does not have a significant impact on the overall cost of the paste when mixed to proportion as the cost per ton of these materials might imply. Additionally, the reduced environmental impact of the RGP compensates for a small increase in cost.
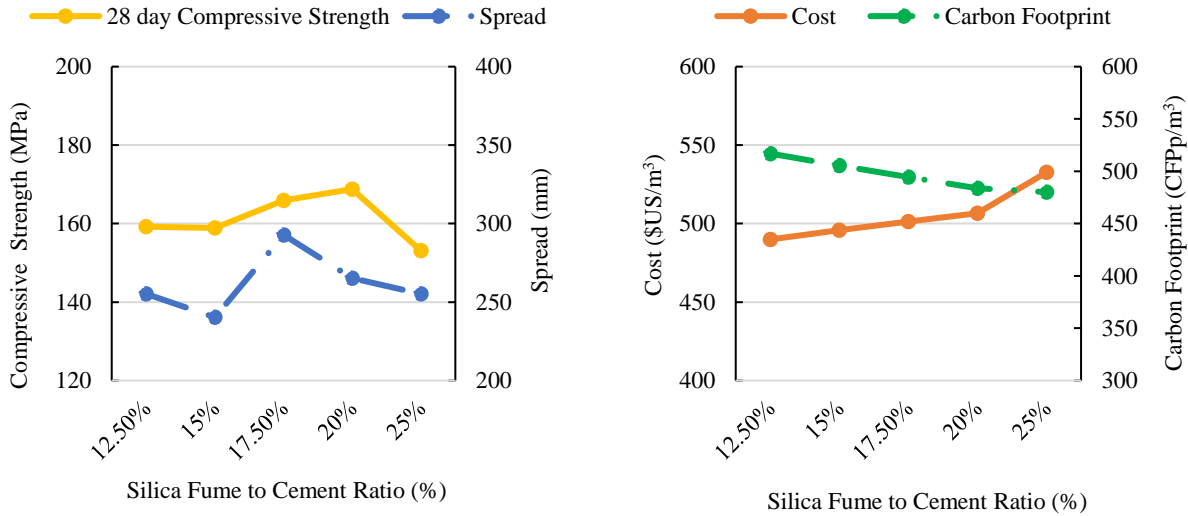
Figure 18: Influence of reduction of silica fume on performance in combination with glass powder

From **Figure 18**, it can be seen that mixtures with RGP (SM3) and 17.5% of silica fume to cement by weight performed best.

4.3.4 Cement Replacement by GGBS

The objective of this research part was to investigate the effect on workability and strength of partial cement replacement by GGBS (**SCM4**) at ratios of 30%, 40% and 50%. The W/F ratio and A/P ratios were held constant at 0.42 and 0.33, respectively. By maintaining these ratios, a better spread value suggests better particle packing and the isolated effect of the cement replacement by GGBS can be observed. It is worth noting that the w/c ratio for these pastes was the mass of the water divided by the combined mass of cement and GGBS. This is because the GGBS has cementitious and pozzolanic properties. By considering the w/c ratio in this way, it remained constant at 0.25. The performances of pastes with varying percentages of cement replacement are summarized by **Table 21-23** and displayed in **Figure 19**.

Table 21 – Performance of alternative paste with 30%, 40% and 50% replacement of cement by GGBS (SCM4) by volume

Paste	W/C (by mass)	W/F (by vol.)	A/P (by vol.)	Mini spread (observed) (mm)	Standard spread (converted) (mm)	[1]$f'_{c\text{-}28}$ (MPa)(ksi)	R
0 % GGBS	0.25	0.42	0.33	118	288	164 (23.8)	1.13
30 % GGBS	0.25	0.42	0.33	123	300	164 (23.7)	1.15
40% GGBS	0.25	0.42	0.33	125	305	161 (23.4)	1.16
50% GGBS	0.25	0.42	0.33	127	310	153 (22.2)	1.13

Table 22 – Mix designs and the cost analysis with varying GGBS proportions (0% and 30%)

Cement replacement	0%				30%			
ID	Amount (kg/m³)	Mass (%)	Cost $US /m³	CFP_P/m^3	Amount (kg/m³)	Mass (%)	Cost $US /m³	CFP_P/m^3
C5	924	38.9	143	462	660	28.0	102	344
SCM4	0.0	0.0	0.0	0.0	257	10.9	40	40
SF	231	9.7	156	0.0	229	9.7	155	0.0
SCM2	231	9.7	15	3.0	229	9.7	15	3.0
HRWR1	34	1.4	172	0.0	34	1.4	170	0.0
FB	747	31.5	28	4.0	746	31.6	28	4.0
Water	207	8.7	0.0	0.0	205	8.7	0.0	0.0
Cost			513	469			509	391

Table 23 – Mix designs and the cost analysis with varying GGBS proportions (40%, and 50%)

Cement replacement	40%				50%			
ID	Amount (kg/m³)	Mass (%)	Cost $US /m³	CFP_P/m^3	Amount (kg/m³)	Mass (%)	Cost $US /m³	CFP_P/m^3
C5	572	24.3	88	286	485	20.6	75	243
SCM4	342	14.5	53	159	427	18.2	66	198
SF	229	9.7	154	0.0	228	9.7	153	0.0
SCM2	229	9.7	15	3.0	228	9.7	15	3.0
HRWR1	34	1.4	170	0.0	34	1.4	169	0.0
FB	747	31.7	28	4.0	747	31.7	28	4.0
Water	204	8.7	0.0	0.0	204	8.7	0.0	0.0
Cost			508	452			507	447
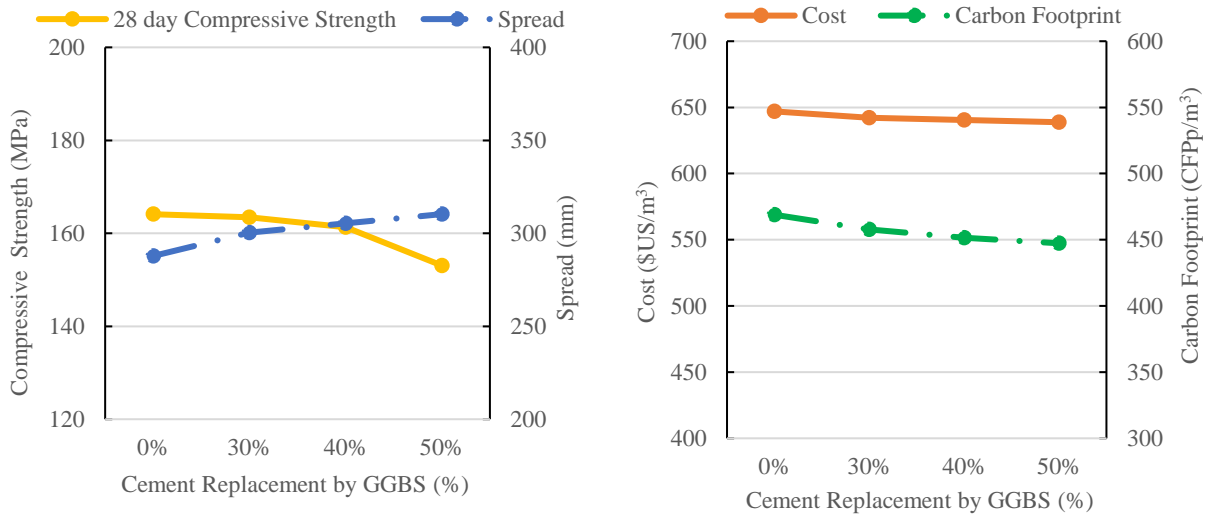
Figure 19: Influence of cement replacement by GGBS on workability, compressive strength, cost and carbon footprint

From the graph in **Figure 19** it can be observed that the cement replacement percentage by GGBS (SCM4) was proportional to workability and inversely related to the 28-day compressive strength. As the percentage of cement replacement increased, the spread value also increased, confirming this proportional relationship reported by Liu et al. [21]. For cement replacement percentages between 30-50%, the spread increased linearly by 5 mm for every 10% of cement replacement. All three GGBS-based pastes achieved higher spread values than the alternative paste. This improvement in workability without influence from the W/F or A/P ratios suggested that for up to 50% cement replacement by cement, better particle packing of the paste was achieved.

Converse to workability, the 28-day compressive strength remained the same or decreased as the percentage of cement replacement increased as reported by Yazici, 2008 [22]. However, the strength of the alternative paste and the paste with 30% GGBS both achieved the same strength of 164 MPa (23.8 ksi). With the same strength, same cost, and better workability than the alternative paste, the paste with 30% GGBS is preferable. The paste with 40% GGBS achieved a strength of 161 MPa (23.4 ksi), which was also very close to 164 MPa (23.8 ksi) reached by the alternative paste. Although the strength of the paste with 50% GGBS was slightly lower at 153 MPa (22.2 ksi), it was still very comparable to the strength of the alternative paste and surpassed the minimum requirement of 150 MPa (22 ksi).

In addition, Liu et al. [21] highlights that GGBS suppresses early age strength and increases later age strength gains due to its semi-adiabatic heat of evolution. GGBS decreases the maximum temperature rise of the early age hydration reaction (which hinders early formation of C-S-H) but can sustain hydration beyond 28 days better than Portland cement alone, increasing later age strength. It is hypothesized that UHPC pastes utilizing GGBS would surpass the compressive strength of the alternative paste at 56 days and beyond. More research is needed to generate a strength development curve for GGBS based UHPCs with ages of 56 days and greater to convey its benefits more effectively.

Within the perspective of this research and its objectives, all three GGBS-based pastes achieved the goal of improving workability relative to the alternative paste. They also achieved the same or similar 28-day strength in comparison to the alternative paste. All three GGBS-based pastes achieved spread values in the preferred range of 280-340 mm and exhibited 28-day compressive strengths greater than the minimum requirement of 150 MPa (22 ksi). For this reason, all three pastes can be recommended, which also decreases the environmental impact of UHPC.

The pastes incorporating GGBS demonstrated a very slight reduction in cost when compared to the alternative paste with savings of $3.74, $5.00, and $6.23 per cubic yard for cement replacement of 30%, 40% and 50%, respectively.

Since GGBS reduces the comprehensive environmental impact in comparison to Portland cement, the higher the cement replacement by GGBS, the lower the environmental impact [23]. The performance vs. resource-efficiency factor R of **Equation 2** does not take into consideration the late-age strength gain and the reduced environmental impact of GGBS-based pastes. Therefore, due to all GGBS-based pastes having a lower cost, better workability, comparable strength, and lower environmental impact in comparison to the alternative paste, all GGBS-based pastes are recommended over the alternative paste.

## 4.4 Investigation of Early Age Properties of Optimized UHPC Matrices

One of the goals of this research project was to develop ultra/high early strength concrete that can be used in the bridge closure pour connections. Steam curing of concrete specimen helps to attain desired properties just in 24 hours. For example, 28-day compressive strength can be achieved in 12 to 24 hours of steam curing.

Table 24 shows the mixture design details of the promising mixes. These mixes were evaluated based on the resource efficiency factor, *R*, whichever mixes obtained the highest R factor in that series were considered here. The mixture designs without fibers were tabulated in the **Table 24**. The reference mixture is identified here as **M**, mixture with 20% of silica fume reduction as **M-0.2SF**, mixture with recycled glass powder as **M-RGP** and mixture with GGBS as **M-0.3GGBS**.

Table 24 - Mix Details of Optimized UHPC Matrices

Material	M Amount (kg/m³)	M Mass (%)	M-0.2SF Amount (kg/m³)	M-0.2SF Mass (%)	M-RGP Amount (kg/m³)	M-RGP Mass (%)	M-0.3GGBS Amount (kg/m³)	M-0.3GGBS Mass (%)
Cement	924	38.9	965	40.4	925	39.6	660	28.0
GGBS	0.0	0.0	0.0	0.0	0.0	0.0	257	10.9
Silica fume	231	9.7	193	8.1	231	9.9	229	9.7
Fly ash or RGP	231	9.7	241	10.1	231	9.9	229	9.7
Aggregate	747	31.5	747	31.3	689	29.5	747	31.6
Superplasticizer	34	1.4	36	1.5	38	1.6	34	1.4
Water	207	8.7	206	8.6	223	9.5	205	8.7
Cost in $/ m³	513		502		533		509	

The early age compression strengths of these promising newly developed UHPC mixes are illustrated in **Figure 20**. **Figure 20** shows the strength values after being exposed to various times of steam curing at 90 degrees Celcius. At 0 hours of steam curing the specimens were 12h old. All the mixes surpassed the criteria of UHPC of more than 150 MPa after 6h of steam curing.
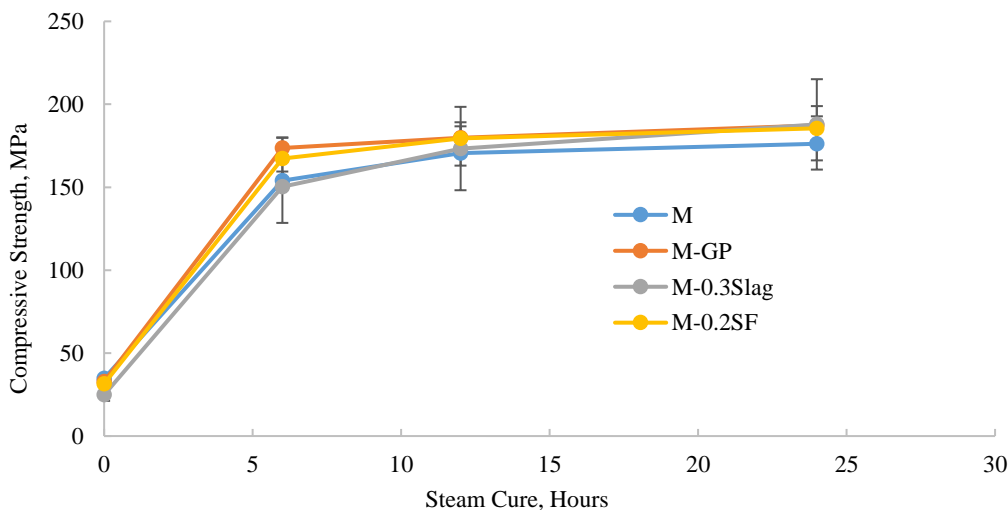
Figure 20: Compressive strength development of steam cured UHPC matrices

4.5 Investigation of UHPCs (with fibers)

All UHPCs consisted of alternative cement **C5**, un-densified **SF**, **FA** class C at a proportion of 1:0.25:0.25 (PC:SF:SCM), a W/C ratio of 0.31, fine basalt (**FB**), HRWR, and fibers at different volume fractions. Aggregate to cement (A/C) ratios were varied to see their effect and interaction with different fiber volume fractions.

4.5.1 Effect of Fiber Volume Fraction and Aggregate to Cement Ratio (A/C) in Workability

As the fiber volume fraction (V_f) and A/C ratio both increased, the interaction and friction between fibers and aggregates reduced the flow-ability of concrete. This can be observed below in **Figure 21-22**. A summary of the data from which this graph was rendered is listed in **Table 25**.

**Table 25 – Spread values at varying V_f and A/C**

V_f	0%			1.0%			1.5%			2.0%		
A/C	1.2	1.5	1.8	1.2	1.5	1.8	1.2	1.5	1.8	1.2	1.5	1.8
Spread (mm)	305	290	258	293	278	237	290	263	228	280	256	219

As seen in the graphs of **Figure 21** and **22**, the UHPC with no steel fibers achieved the largest spread diameter since there was no interaction between aggregates and steel fibers. The addition of both aggregates and fibers affected the workability of the UHPC. The spread decreased with increased in A/C, meaning adding more aggregates decreased the workability of the concrete. A similar trend was observed by adding fibers to the concrete. Therefore, changing the A/C can be used to offset the effect of added fiber reinforcement. To find out the optimum value of A/C and fiber volume fraction, one can use **Figure 21** and **22** to check against the targeted range of the spread.

The fiber factor (χ_f) can be calculated using **Equation 3** as follows:

$$\chi_f = V_f \times L_f / D_f \quad\quad\quad (3)$$

, where V_f is the fiber volume fraction, L_f is the length of fiber, and D_f is the diameter of fiber. The change in spread with respect to the fiber factor χ_f are presented below in the **Figure 21**.
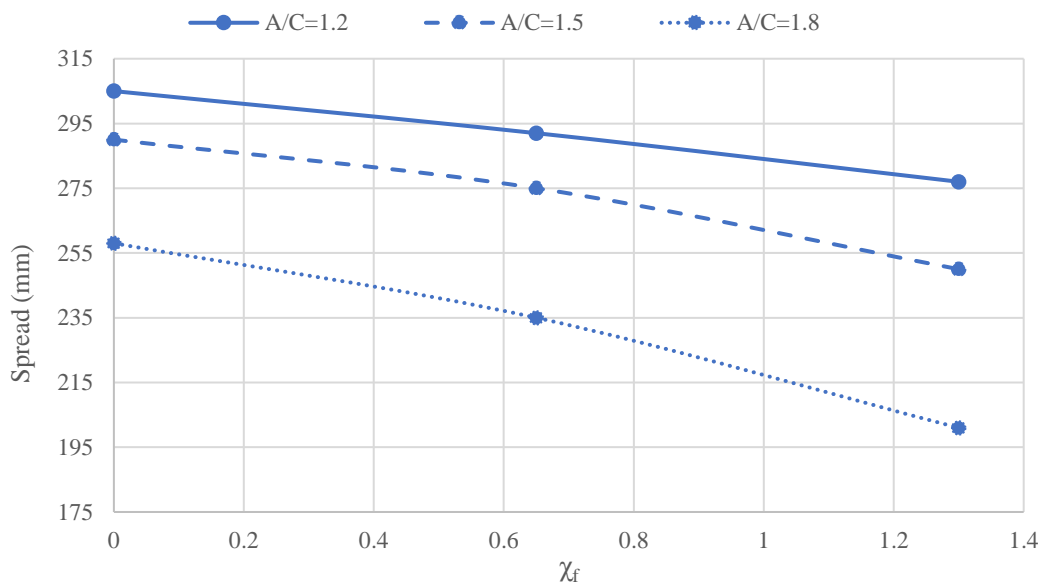
Figure 21: Workability versus fiber factor at different A/C ratios
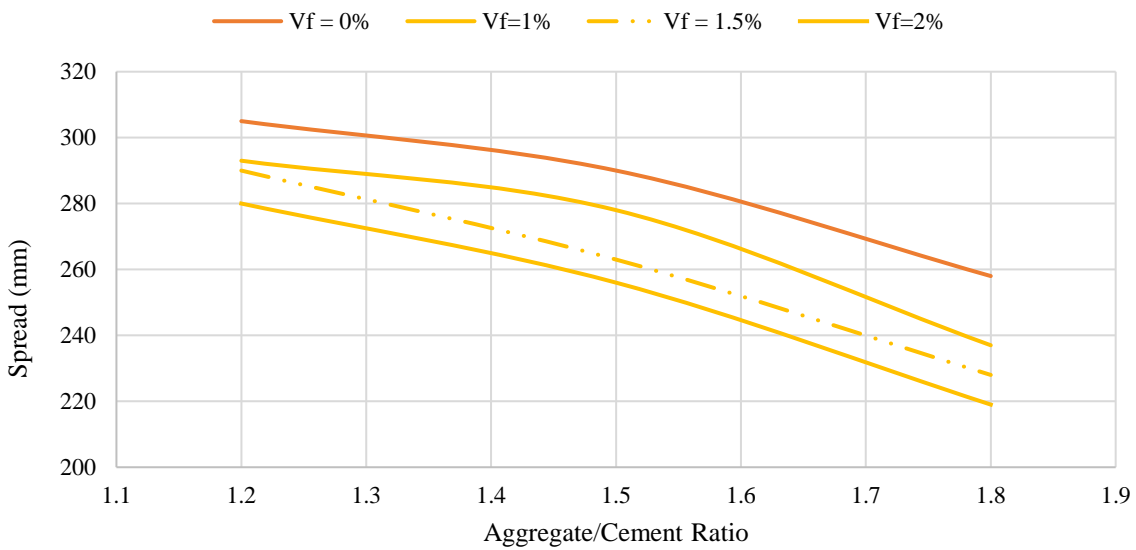
Figure 22: Workability versus different A/C at different V_f in %

Increase in fiber volume and A/C increased the compressive strength as seen in **Figure 23**.

Figure 23: Compressive strength of different UHPC matrices with different A/C and V_f in %
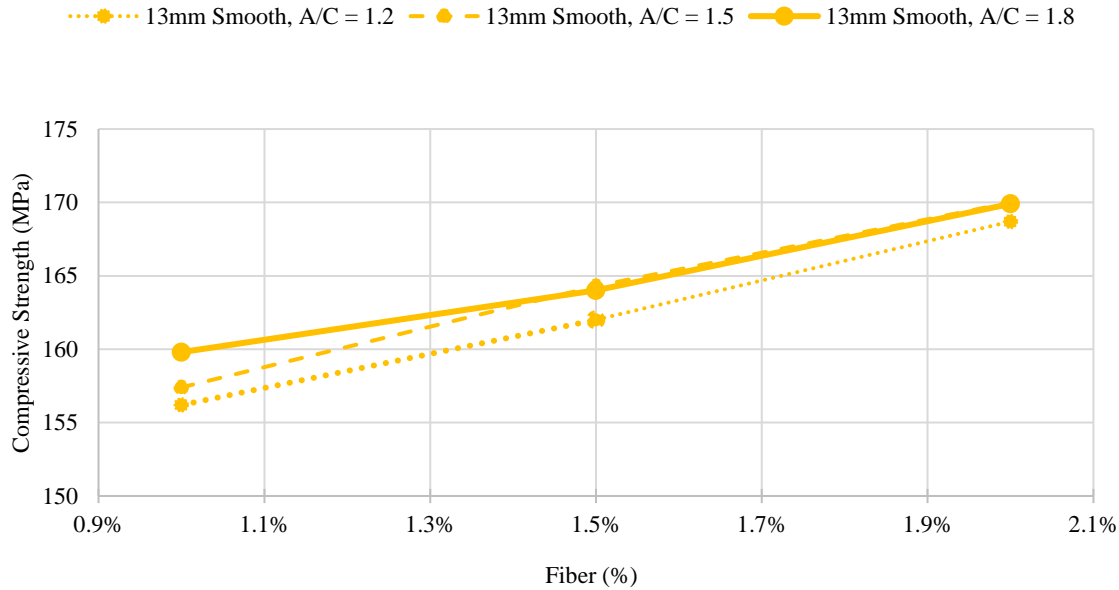
Spread decreased as A/C increased and compressive strength increased as the A/C increased. Increase in fiber content followed the similar trends. To design a UHPC with compressive strength in excess of 150 MPa and spread in the workable range, A/C less than or equal to 1.5 and a fiber volume content greater than or equal to 1.5% is recommended based on the above observations.

4.8 Mechanical Properties of UHPCs (with fibers)

4.8.1 Effect of Fiber Volume Fraction and Aggregate to Cement Ratio (A/C) on the Tensile Behavior of UHPCs

Increase in V_f % increased the maximum post cracking tensile strength and the corresponding strain values in the UHPC. The maximum post cracking tensile strength ranged from 7.8 MPa at V_f = 1.0% to 10.1 MPa at V_f = 2.0% for A/C = 1.2, 8.1 MPa at V_f = 1.0% to 10.2 MPa at V_f = 2.0% for A/C = 1.5 and 8.4 MPa at V_f = 1.0% to 11.6 MPa at V_f = 2.0% for A/C = 1.8. As expected, A/C ratios did not significantly affect the tensile strength of the composite. A summary of the test results are shown in the **Figure 24 (a), (b), and (c)** and **Table 26.**

Table 26 – Effect of V_f % on tensile strength at different A/C

V_f	A/C = 1.2		A/C = 1.5		A/C = 1.8	
	σ_{pc} (MPa)	ϵ_{pc} (%)	σ_{pc} ((MPa)	ϵ_{pc} (%)	σ_{pc} ((MPa)	ϵ_{pc} (%)
1.0%	7.8	0.03	8.1	0.09	8.4	0.12
1.5%	8.6	0.04	8.8	0.12	9.9	0.09
2.0%	10.1	0.25	10.2	0.12	11.6	0.21
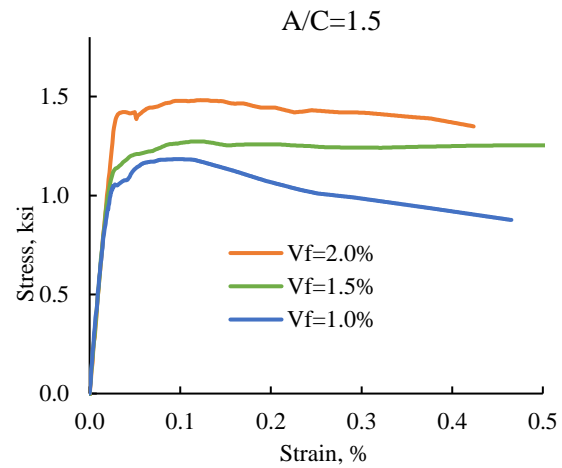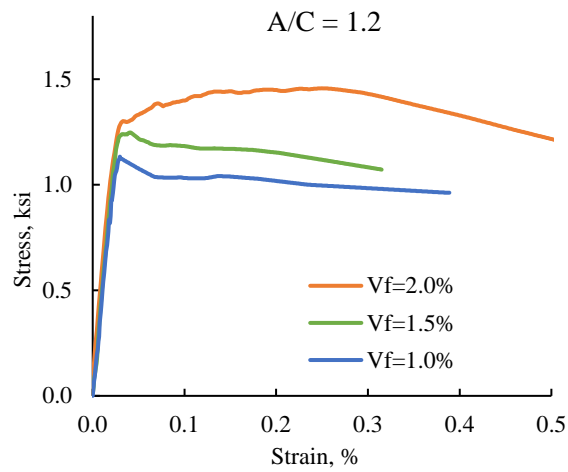
a)

b)
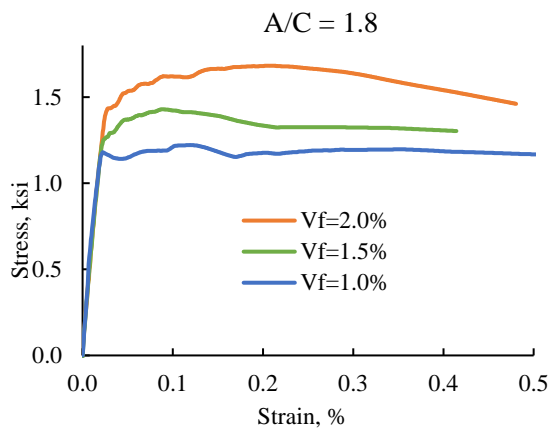
c)

Figure 24: Stress – strain curves for UHPCs withdifferent fiber volume fractions at a) A/C = 1.2, b) A/C = 1.5 and A/C = 1.8

4.8.2 Cost Analysis of Fiber Reinforced UHPC Matrix

Figure 25 shows the effect of A/C ratio and fiber volume fraction on the cost in $US per cubic meter. It can be seen that the A/C ratio had a minor effect on cost whereas the amount of fibers significantly affected the composite cost.

Figure 25: Cost of UHPC matrices having different fibers with different A/C and V$_f$%

Further detailed cost breakdowns are tabulated in the **Table 27-29.**

Table 27 - Cost of UHPC with smooth fiber with V$_f$ =1% at different A/C ratios

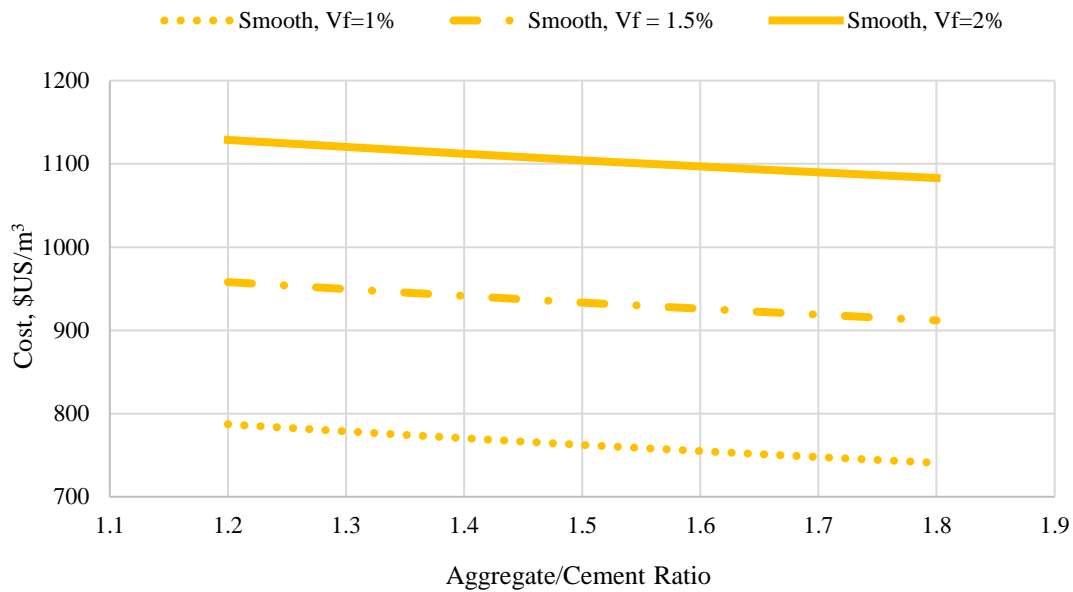| ID	A/C = 1.2		A/C = 1.5		A/C = 1.8	
	Amount (kg/m³)	Cost $US/m³	Amount (kg/m³)	Cost $US/m³	Amount (kg/m³)	Cost $US/m³
C5	771	120	717	111	668	103
SF	193	131	179	121	167	113
SCM1	1923	13	179	12	167	11
HRWR1	29	144	27	133	25	124
F	118	346	79	346	79	346
FB	925	34	1076	39	1202	44
Cost		787		762		741

Table 28 - Cost of UHPC with smooth fiber with V$_f$ = 1.5% at different A/C ratios

ID	A/C = 1.2		A/C = 1.5		A/C = 1.8	
	Amount (kg/m³)	Cost $US/m³	Amount (kg/m³)	Cost $US/m³	Amount (kg/m³)	Cost $US/m³
C5	771	119	714	110	664	103
SF	193	130	178	120.	166	112
SCM1	193	13	178	12	166	11
HRWR1	29	143	27	132	25	123
F	118	519	118	519	118	519
FB	925	34	1070	39	1195	44
Cost		958		933		912

Table 29 - Cost of UHPC with smooth fiber with V_f = 2% at different A/C ratios

ID	A/C = 1.2 Amount (kg/m³)	Cost $US/m³	A/C = 1.5 Amount (kg/m³)	Cost $US/m³	A/C = 1.8 Amount (kg/m³)	Cost $US/m³
C5	767	118	710	110	661	102
SF	192	129	178	120	165	112
SCM1	192	13	178	12	165	11
HRWR1	29	142	26	132	25	123
F	157	692	157	692	157	692
FB	920	34	1065	39	1189	44
Cost		1129		1104		1083

Chapter 5: Conclusions and Recommendations

The main goal of this research was to enhance the performance versus cost ratio of non-proprietary ultra-high performance concrete. A resource-efficiency parameter R was defined and used to evaluate the performance mixtures which were affected by different material constituents and proportions. A systematic approach facilitated the development of performance effective UHPC composites using the materials available in the New England area. The following conclusions can be derived from this research:

1. Several UHPC matrices were developed exceeding the minimum strength requirements of 150 MPa (22ksi) at material costs of about $500/m³ using local available materials. This included igneous basalt as fine aggregate, un-densified silica fume, recycled glass powder, locally available fly ash and suitable Portland cement.

2. The defined resource-efficiency factor R has been used successfully to evaluate the suitability of mixture components and proportions.

3. A resonance frequency mixer has successfully been used to mix small quantities of UHPC paste effectively, efficiently and consistently.

4. The spread test was successfully used as an indicator of enhanced particle packing.

5. Test results showed that fly ash, recycled ground glass powder and ground granulated blast furnace slag are very suitable sources for a desired UHPC matrix.

6. Cement replacement up to 50% by ground granulated blast furnace slag still produced suitable UHPC matrices. In terms of performance an optimum value lays at 30% cement replacement.

7. Silica fume to cement ratios of 10% to 25% produced suitable UHPC matrices. The optimum ratio depends on the type of cement used. In combination with a Portland cement type II/V the optimum ratio was determined to be 20%.

8. Adding fiber reinforcement was necessary to achieve desired tensile strength and material ductility. The addition of 1% by volume of fibers used here added about $350 per m^3 of composite in cost.
9. Test results show that an ultimate tensile strength can be obtained in the range of 7.5 MPa – 12.0 MPa and peak strain values of 0.03% - 0.25% at V_f = 1.0 – 2.0% using 13mm long – 0.2mm diameter straight smooth fibers.

Further recommendation:
- This research was limited to using fine basalt. Increasing the maximum size of aggregates might allow to increase the A/C and thus reducing the amount of paste at comparable workability. However, there might be an adverse effect in combination with fiber reinforcement.
- All mixtures were mixed in small batches. Testing the mixture performance at larger volume will be necessary for evaluating their suitability in practical applications.
- To reduce the cost of UHPC further studies related to fiber efficiency will be necessary.
- More research is needed to generate a strength development curve for GGBS based UHPCs with ages of 56 days and greater.
- The durability performance and long-term stability of the UHPC mixtures need to be investigated.

References

[1]   FHWA Bridge and Structures: Bridge Counts by Year, 2021.

[2]   2021 Report Card for America's Infrastructures, 2021.

[3]   Infrastructure Report Card: A Comprehensive Assessment of America's Infrastructure, 2017.

[4]   S.F. Breña, S.A. Civjan, S. Castine, S. Assistant, G. Ramos, Development of High Early-Strength Concrete for Accelerated Bridge Construction Closure Pour Connections, 2018.

[5]   FHWA Report: Properties and Behavior of UHPC-Class Materials. FHWA Publication No: FHWA-HRT-18-036., 2018.

[6]   S. El-Tawil, Y.-S. Tai, J.A.B. Ii, D. Rogers, Open-Recipe Ultra-High-Performance Concrete Busting the cost myth, n.d. www.concreteinternational.com|.

[7]   K. Wille, C. Boisvert-Cotulio, Material efficiency in the design of ultra-high performance concrete, Constr Build Mater. 86 (2015) 33–43. https://doi.org/10.1016/j.conbuildmat.2015.03.087.

[8]   ASTM C143/C143M-03: Standard Test Method for Slump of Hydraulic-Cement Concrete, Annual Book of ASTM Standards, 2003.

[9]   Adam M. Neville, Properties of Concrete, 5th, Illustrated ed., Pearson, 2011, 2011.

[10]   S.H. Kosmatka, M.L. (Architectural engineer) Wilson, Design and control of concrete mixtures : the guide to applications, methods, and materials, Portland Cement Association, 2011.

[11]   H. Du, S. Du, X. Liu, Durability performances of concrete with nano-silica 1 2, n.d.

[12]   M. Liu, H. Tan, X. He, Effects of nano-SiO2 on early strength and microstructure of steam-cured high volume fly ash cement system, Constr Build Mater. 194 (2019) 350–359. https://doi.org/10.1016/j.conbuildmat.2018.10.214.

[13]   R. Palla, S.R. Karade, G. Mishra, U. Sharma, L.P. Singh, High strength sustainable concrete using silica nanoparticles, Constr Build Mater. 138 (2017) 285–295. https://doi.org/10.1016/j.conbuildmat.2017.01.129.

[14]   J. van der Putten, J. Dils, P. Minne, V. Boel, G. de Schutter, Determination of packing profiles for the verification of the compressible packing model in case of UHPC pastes, Materials and Structures/Materiaux et Constructions. 50 (2017). https://doi.org/10.1617/s11527-016-0986-2.

[15]   H.J.H. Brouwers, H.J. Radix, Self-compacting concrete: the role of the particle size distribution, in: Springer Nature, 2005: pp. 109–118. https://doi.org/10.1617/2912143624.010.

[16]   A. Vandenberg, K. Wille, A. Professor, Evaluation of Resonance Acoustic Mixing Technology using Ultra High Performance Concrete, 2018.

[17]   K. Wille, A.E. Naaman, G.J. Parra-Montesinos, Ultra-High Performance Concrete with Compressive Strength Exceeding 150 MPa (22 ksi): A Simpler Way, ACI Mater J. 108 (2011) 34–46.

[18]   ASTM C109/C109M-02: Standard Test Method for Compressive Strength of Hydraulic Cement Mortars (Using 2-in. or [50-mm] Cube Specimens), 2002.

[19] Z. Liu, S. El-Tawil, W. Hansen, F. Wang, Effect of slag cement on the properties of ultra-high performance concrete, Constr Build Mater. 190 (2018) 830–837. https://doi.org/10.1016/j.conbuildmat.2018.09.173.

[20] H. Yazici, M.Y. Yardimci, H. Yiğiter, S. Aydin, S. Türkel, Mechanical properties of reactive powder concrete containing high volumes of ground granulated blast furnace slag, Cem Concr Compos. 32 (2010) 639–648. https://doi.org/10.1016/j.cemconcomp.2010.07.005.

[21] Y. Li, Y. Liu, X. Gong, Z. Nie, S. Cui, Z. Wang, W. Chen, Environmental impact analysis of blast furnace slag applied to ordinary Portland cement production, J Clean Prod. 120 (2016) 221–230. https://doi.org/10.1016/j.jclepro.2015.12.071.

Appendices

I. Independent Study Final Report - Ultra-High Performance Concrete for Highway Bridge Parapets by Raymond Basar - May 2019

35 Flagstaff Road
Orono, Maine 04469
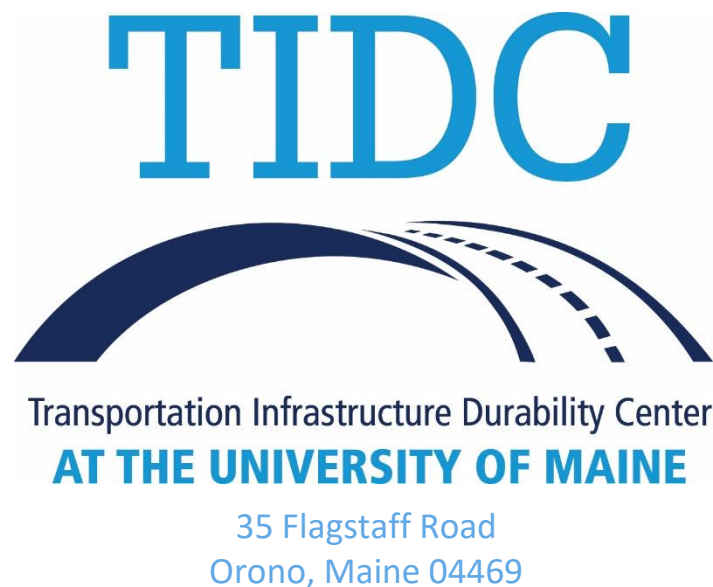
Appendix

Ultra-High Performance Concrete for Highway Bridge Parapets

by

Raymond I. Basar

for

CE 5020

Department of Civil and Environmental Engineering

at

the University of Connecticut

May 10, 2019

TABLE OF CONTENTS   **Page No.**

Ultra-High Performance Concrete for Highway Bridge Parapets

1. Introduction

Ultra – High Performance Concrete (UHPC) has been considered as the next generation of concrete to be used for the construction of highway infrastructures. UHPC has been available in the market since the early 2000s and its performance has been closely monitored by State and Federal level agencies since then. Federal Highway Administration (FHWA) started considering the use of UHPC for highway infrastructures such as highway bridges in the early 2000s. The observed benefits of UHPC not only motivated FHWA closely scrutinize this new class of cementitious composites but also encouraged the State DOTs to implement UHPC for the highway bridges that are in poor condition requiring either replacement or rehabilitation.

UHPC is a steel fiber reinforced cementitious based composite that is castable and preferably designed to be self-consolidating and strain hardening with superior mechanical properties and high durability. A typical UHPC mix in North America consists of Portland cement, superplasticizers, particle packing, fiber reinforcement, and supplementary cementitious materials. Since there is not a universally accepted specific definition of UHPC, FHWA and ACI 239 have adopted the following definitions for UHPC respectively:

> *"UHPC is a cementitious composite material composed of an optimized gradation of granular constituents, a water-to-cementitious materials ratio less than 0.25, and a high percentage of discontinuous internal fiber reinforcement. The mechanical properties of UHPC include compressive strength greater than 21.7 ksi (150 MPa) and sustained post-cracking tensile strength greater than 0.72 ksi (5 MPa)."* [FHWA]

> *"Concrete, ultra – high performance – concrete that has a minimum specified compressive strength of 150 MPA (22,000 psi) with specified durability, tensile ductility and toughness requirements; fibers are generally included to achieve specified requirements."* [ACI]

UHPC, which is a class of concrete product developed after utilizing many recent advancements in concrete material science allows engineers to design bridges that are not only constructible but also more durable and resilient. According to FHWA publication FHWA-HRT-18-036, UHPC tensile strength is at least twice as high as that of conventional concrete and its compressive strength can be up to four times higher than the compressive strength of conventional concrete. The performance of UHPC includes:

- High compressive strength and stiffness

    f_c' = 18 to 35 ksi; E = 6000 to 8000 ksi

- Considerable tensile strength

    Tensile capacity = 0.9 to 1.5 ksi

- Low permeability and high durability

    RCT = 20 to 360 Coulombs; F/T RDME > 95%

- Strain-hardening behavior allows keep gaining strength with aging

Unlike conventional concrete, the steel fiber micro reinforcement allows UHPC to sustain tensile loads even after tensile cracking by providing post – cracking tensile ductility. In addition to its superior mechanical properties, UHPC is highly durable. Its discontinuous pore structure significantly reduces permeability compared to conventional concrete helping the concrete resist freeze and thaw damage and chloride penetration. FHWA and the State DOTs

have been in need of finding innovative solutions to design and construct bridges in better ways to increase longevity. The goal has been to have bridges that are easy to construct to diminish disruptions to the community so does the cost but also bridges that are sustainable and durable to minimize maintenance cost. Concrete bridge components exposed to aggressive environments such as bridge deck and parapet are susceptible to salts and de-icing chemical solutions splashed from roadways typically begin falling apart within 15 to 20 years. UHPC's high durability over conventional concrete may be considered as a viable option to implement constructing highway bridge parapets in order to attain more longevity and to reduce maintenance efforts and repair cost. In North America, UHPC has been utilized in a variety of bridge construction projects and the demand has been increasing as the State DOTs experience the benefits of UHPC. As the demand increases for UHPC, the need for design guidance grows as well. Highway bridge parapets are one of the bridge components experience deterioration due to concrete cover delamination and reinforcement corrosion when subjected to salts and de-icing materials thus UHPC-class concrete may be suitable to eliminate early degradation of bridge parapets. This report will provide a detailed design guidance for UHPC bridge parapets to be used for highway bridge projects.

2. Objective

The main objective of this study is to develop and provide a novel design guidance for parapets made of UHPC in highway bridge design to help bridge design engineers familiarize themselves with UHPC parapet design. In order to provide a UHPC parapet design guidance, the followings will be investigated:

- UHPC mechanical properties
- Safety evaluation of highway bridge railings
- AASHTO provisions for the analysis of concrete railing resistance

3. Literature Review on Mechanical Properties and Durability

In order to evaluate the mechanical properties and durability of commercially-available UHPC-class concrete materials, FHWA executed a study[5], which was later included in *FHWA-HRT-18-036* FHWA publication in 2018. The investigated mechanical properties under this study included but not limited to compressive strength and tensile strength of the aforementioned UHPC-class materials. Five different commercially-available materials identified as U-A through U-E by FHWA were tested under this study.

U-A UHPC-class concrete mix was developed in the United States, and its constituents included cement, silica sand, ground quartz, silica fume, superplasticizer, water, and 3 percent steel fibers by volume.

U-B UHPC-class concrete mix was produced in Europe and the product included pre-blended and pre-bagged powder, liquid admixtures, 2 percent combined short and long steel fibers by volume, and water.

U-C UHPC-class concrete mix was also advanced in Europe and its ingredients included pre-blended and pre-bagged powder, 2 percent (4.5 percent supplier recommended) steel fibers by volume, and water.

U-D UHPC-class was a proprietary concrete mix supplied by a U.S. based subsidiary of an International Corporation and its ingredients included pre-blended and pre-bagged powder, plasticizer, superplasticizer, accelerator, 2 percent steel fibers by volume, and water.

U-E UHPC-class was a proprietary concrete mix developed in Canada, and its constituents included pre-blended and pre-bagged powder, liquid admixtures, 2 percent steel fibers by volume, and water.

3.1 Compressive Strength

The compressive strength gain of the five commercially-available UHPC-class concrete mixes exhibited both similarities and differences. All the concrete mixes attained higher than a 14 ksi (96.5 MPa) of compressive strength within 7 days without applying any heat

treatment during curing. Figure 1 depicts the concrete compressive strength gain with respect to age. As shown on Figure 1, UHPC-class concrete mix U-D showed the most rapid compressive strength gain due to its accelerator constituent and attained a 16.9 ksi (117 MPa) of compressive strength within 3 days.
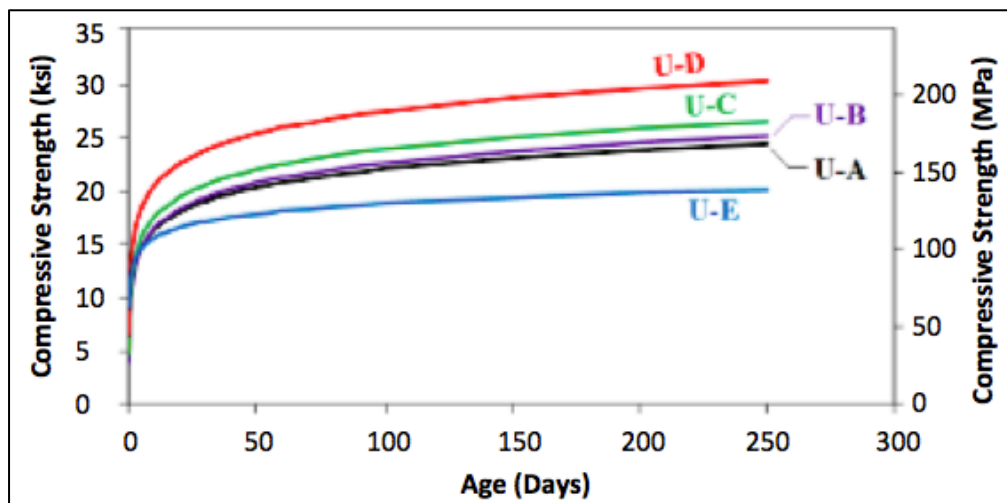

Figure 1. Graph of Compressive Strength Gain for UHPC-class concrete mixes with 2 percent steel fiber. *Adapted from FHWA-HRT-18-036 FHWA* [5].

U-C was the next UHPC-class concrete mix with the most rapid compressive strength gain rate and achieved a 15.2 ksi (105MPa) of compressive strength within 3 days. U-A and U-B mixes exhibited similar compressive strength gain rates and attained approximately a 9 ksi (69 MPa) of compressive strength within 2 days. The measured strengths for U-A and U-B within 7 days were 17.4 ksi (120 MPa) and 15.8 ksi (109 MPa) respectively. U-E UHPC-class mix showed the slowest compressive strength gain rate and attained a 14.9 ksi (102 MPa) of compressive strength within 7 seven days. After longer curing periods, all the mixes excluding U-E attained compressive strengths ranging from 20 ksi (137 MPa) to 25 ksi (172 MPa) at 28 days. The acquired compressive strength after proper curing of U-E UHPC-class concrete mix was slightly below 20 ksi (137 MPa) at 28 days.

Another study conducted by Michigan DOT[2] showed that the tested UHPC specimens achieved much higher compressive strengths. The air-cured specimens exhibited a 23.9 ksi (165 MPa) of compressive strength and the steam-cured specimens achieved a 30.5 ksi (211 MPa) of compressive strength after 3 days of casting with 2 days of steam curing. Similar to the FHWA study[4], the study[2] showed that the attained compressive strength of the air-cured specimens increased with respect to time and a 14 ksi (97 MPa) and a 19 ksi (131 MPa) of compressive strengths were achieved after 3 and 7 days respectively.

The results of the study[5] also showed that the compressive stress-strain behavior of all the five commercially-available UHPC-class concrete mixes were similar. The tested UHPC-
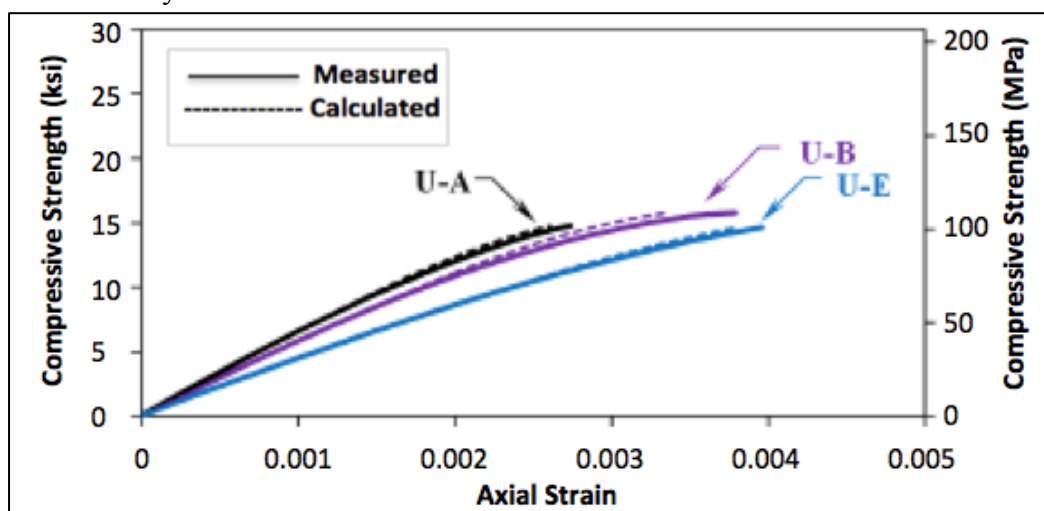

Figure 2. Graph of measured and calculated stress-strain curves with compressive strength near 15 ksi (103 MPa). *Adapted from FHWA-HRT-18-036 FHWA* [5].

class materials gained strength as the materials aged. The materials' stress-strain response was linear until the 50 percent of the corresponding compressive strength and subsequently the behavior was changed to a non-linear response as shown on Figure 2 and Figure 3. The observed and calculated axial strains at early age of each tested material varied from approximately 0.00275 to 0.004 for UHPC-class U-A, U-B, and U-E.

As shown on Figure 2, the U-E concrete mix attained a 0.004 of axial compressive strain and was the highest with a corresponding 15 ksi (103 MPa) of compressive strength. In comparison, the U-A concrete mix achieved a 0.00275 of axial compressive strain at 15 ksi (103 MPa) of compressive strength and was the lowest among the three concrete mixes tested.

Figure 3 below shows the measured and calculated axial compressive strains with respect to the peak compressive strength of UHPC-class U-A, U-C, and U-E mixes. The axial compressive strain for these concrete materials ranged between 0.00375 and 0.0042 at the peak compressive strengths above 18 ksi (122 MPa).
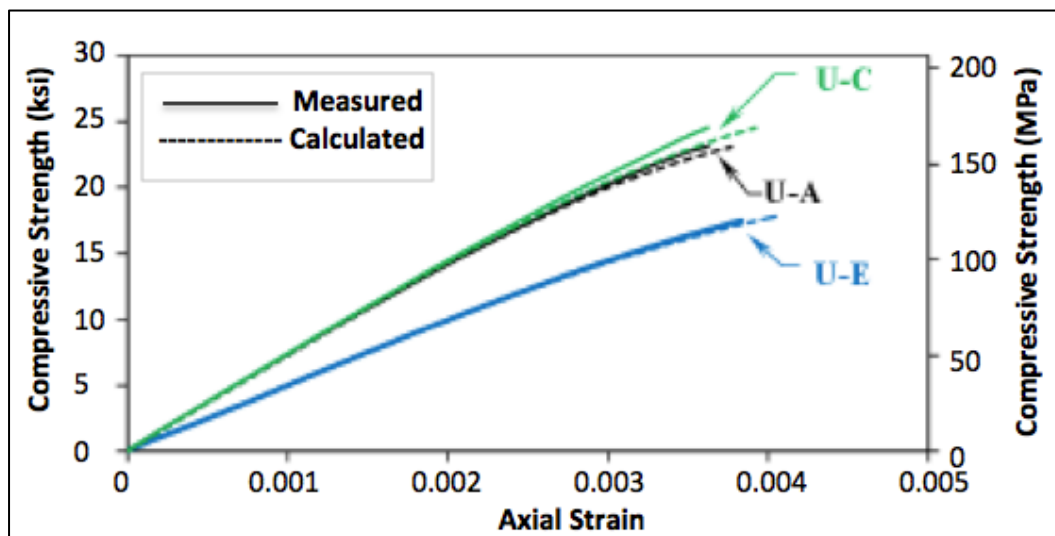

Figure 3. Graph of measured and calculated stress-strain curves with compressive strength above 18 ksi (122 MPa). *Adapted from FHWA-HRT-18-036 FHWA* [5].

Below Chart 1 is the summary of the average axial compressive strains of the five commercially-available UHPC-class concrete mixes at the corresponding peak compressive strengths with the consideration of ± one standard deviation. The bars represent the error margin and the indicated values are the average axial compressive strain for each UHPC-class material at the peak compressive stresses. The measured average strain ranged between 0.0033 and 0.0047 at peak compressive stresses. UHPC-class U-A and U-D materials achieved similar axial strains, 0.0033 and 0.0034 respectively. On the other hand,

Chart 1. Average axial compression strains measured at peak compressive stress. *Adapted from FHWA-HRT-18-036 FHWA* [5].

UHPC-class U-E material attained an axial strain of 0.0047 at its peak compressive stress and measured to be the highest among those five UHPC-class materials. UHPC-class materials U-B and U-C exhibited axial strains of 0.0040 and 0.0042 respectively, which was relatively higher than the axial strains of U-A and U-D mixes.

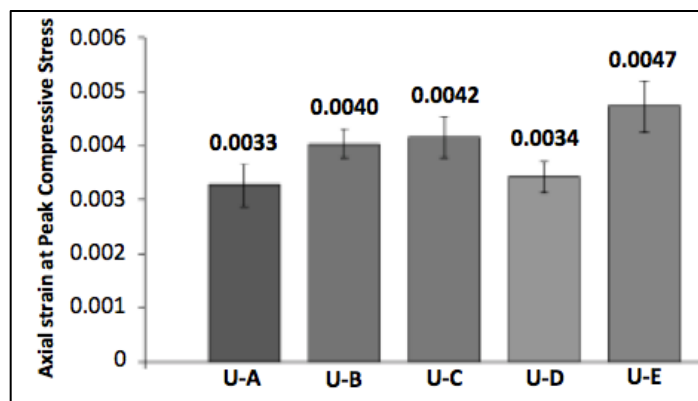Based on the variation of UHPC compressive strength observed in different studies and implemented bridge design projects, *Design Guide for Precast UHPC Waffle Deck Panel System, Including Connections*[10] recommends taking UHPC compressive strength as 24 ksi

(165 MPa) and 18 ksi (124 MPa) for steam-cured and air-cured conditions respectively to design bridge structures. The design guide also recommends limiting the axial compressive strain to 0.0032 in structural design. Below Figure 4 indicates the recommended stress-strain behavior to be used in structural design of UHPC bridge structures.
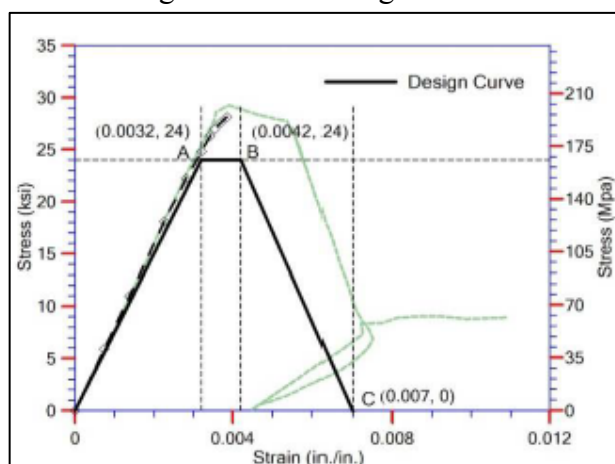

Figure 4. Graph of Stress-strain relationship of a UHPC.
for structural design. Adapted from FHWA-HIF-13-032[10].

3.2 Tensile Strength

The tensile strength of conventional concrete at service and ultimate stages of moment-curvature relation is not considered in design of concrete structures. This is due to the fact that the conventional concrete with mild reinforcement and without prestressing steel cannot sustain tensile loads after tensile crack initiation as it does not provide post – cracking resistance through tensile ductility. The service and ultimate stages are above the initial cracking stage of conventional concrete, which occurs at modulus of rupture of concrete where the entire section of concrete resists bending. Once the section is cracked its tensile strength contribution is neglected. For prestressed members the tensile strength of conventional concrete for transportation infrastructures is often taken as $0.19*\sqrt{fc'}$ as specified by AASHTO 8th, 2017 provisions.[1]

Unlike conventional concrete, tensile strength is a unique mechanical property of UHPC mixes and can be considered in structural design of UHPC members even at ultimate stage. According to ACI Materials Journal Publication[3], the tensile strength of UHPC is considerably higher than that of conventional concrete since the UHPC materials behave differently after the initial crack formation occurs. Figure 5 illustrates the tensile mechanical response of an idealized UHPC-class material. Phase I indicates the elastic behavior of UHPC. Within this phase, UHPC exhibit its global straining and the phase continues until the first crack occurrence

Figure 5. Graph of idealized uniaxial tensile mechanical response of a UHPC. Adapted from ACI Journal [3].

showing linear behavior. Phase II represents the development of simultaneous multi-cracking of UHPC. Due to the presence of steel fibers no significant widening occurs within a particular crack and strain keeps accumulating with no change in tensile stress. Phase III indicates tension hardening of UHPC. The tensile stress and strain start increasing again with the increase of the applied loading showing the post-cracking tension capacity of a UHPC-class material. Phase III continues until a localized individual crack occurrence. At the beginning of Phase IV, the individual crack reaches its ultimate strain and the steel fibers serving as bridging the crack start debonding and pulling out of the concrete matrix. Eventually, the deformation of the UHPC-class material starts and the material looses its tensile capacity.

The study[4] conducted by Graybeal and Baby to investigate the tensile mechanical properties of UHPC-class material shows the idealized stress-strain relation for each response phase described previously. According to Figure 6, the first crack initiation occurs at an approximately 0.00012 axial tensile strain. Multi-cracking formation phase continues until UHPC attains a 0.004 of tensile strain and then begins tensile hardening, which is the indication of post-cracking tensile ductility. At an approximately 0.0075 tensile strain, the localized individual crack forms leading to deformation of the section.
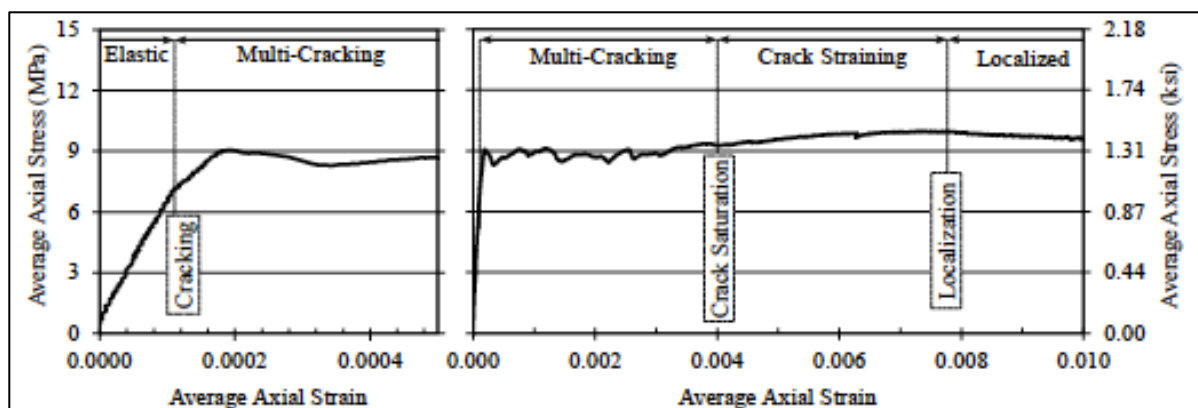

Figure 6. Graph of idealized uniaxial tensile mechanical response of a UHPC. *Adapted from FHWA-HRT-17-053* [4].

The earlier study[6] performed by Graybeal to probe the tensile strength of UHPC-class material exhibited that the first tensile cracking strength of UHPC is approximately 1.3 ksi (9 MPa) and 0.9 ksi (6 MPa) for specimens with steam-cured and air-cured respectively. The tension parameters were measured through the combination of flexural prisms, split cyclinders, mortar briquettes, and direct tension tests in the study.[6] The results of the follow-up study[4] conducted by Graybeal and Baby through series of uniaxial direct tension test method provided similar tension parameters to those measured in the previous studies.[3][6] The study[4] also revealed that UHPC could withstand larger tensile loads since the measured tensile strength in a standard laboratory environment was more than 1.3 ksi (9 MPa) in Phase III as shown on Figure 6.

According to FHWA-HIF-13-032[10], the investigated tensile stress-strain behavior in the previous studies shown on Figure 7a have been effectively utilized to predict the flexural response of H-piles, I-girders, and waffle deck panels. As indicated in the report[7], Graybeal proposed a more conservative stress-strain behavior shown on Figure 7b to be used in the structural design of UHPC as a result of flexural and shear testing of a large-scale bridge I-Girder. FHWA-HIF-13-032[10] report also advocates this conservative approach and recommends limiting the tensile strength and strain to 1.2 ksi (8 MPa) and 0.007 respectively to characterize the flexural response of UHPC for structural design.
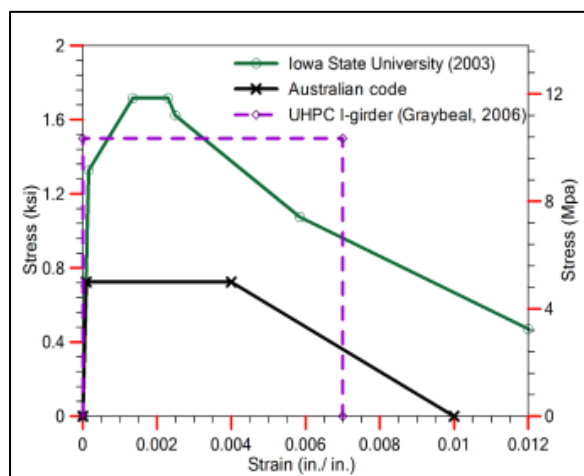

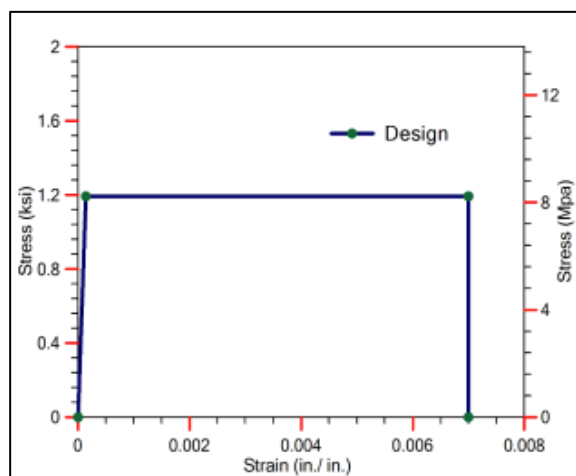Figure 7a. Experimental stress-strain behavior. *Adapted from FHWA-HIF-13-032* [10].

Figure 7b. Proposed stress-strain behavior. *Adapted from FHWA-HIF-13-032* [10].

3.3 Durability

Permeability:

UHPC's discontinuous pore structure significantly reduces its permeability thus helping the concrete resist freeze and thaw damage and chloride penetration. The tested UHPC specimens in Graybeal's study exhibited very minimal chloride penetration nearly negligible.[6] Similar to Graybeal's study, Michigan DOT also reported a negligible chloride penetration based on the testing for deep foundation characterization.[12] Graybeal's study showed that all the properly steam-cured specimens achieved values less than 100 coulombs at 28 days exhibiting a negligible chloride ion penetrability. The untreated specimens resulted in values of 360 coulombs, which was considerably lower than that of conventional concrete. Besides providing resistance to chloride penetration, the test results indicated negligible freeze-thaw damage showing extremely high freeze-thaw resistance. Presence of large contents of cementations and other filler materials such as silica flour prohibits the penetration of detrimental compounds. Below Chart 2 provides durability comparison between UHPC, High-Performance Concrete (HPC), and conventional (normal) concrete.
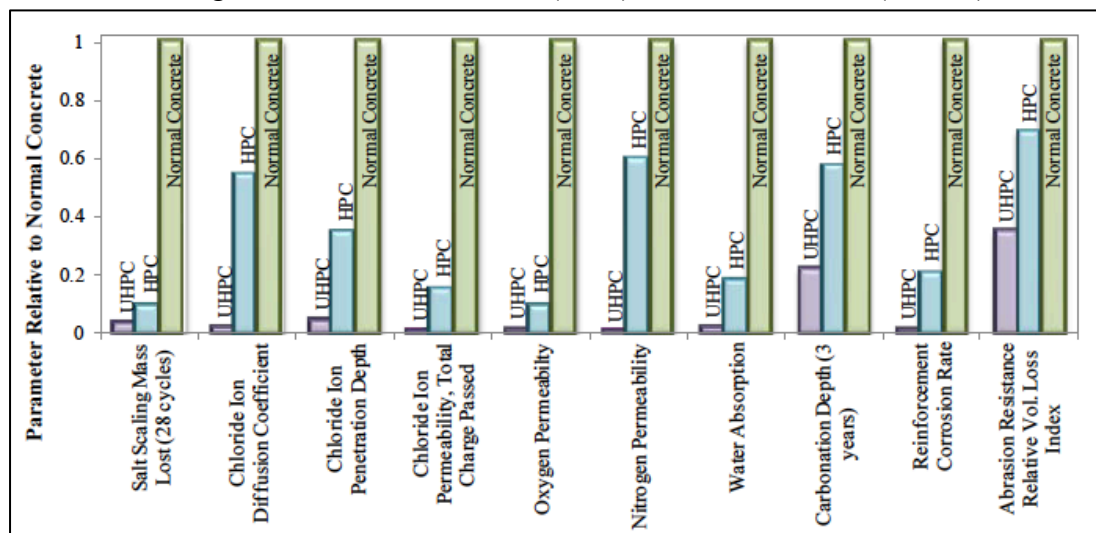
Chart 2. Durability properties of UHPC and HPC relative to conventional concrete. *Adapted from IHRB Project TR 558[12].*

Shrinkage:

Unlike conventional concrete, UHPC experiences more early-age shrinkage within short amount of time after casting.[5] The susceptibility of UHPC to early-age shrinkage is due to the fact that its high cementations material content and the low water to binder ratio in the mixture design. The early-age shrinkage may result in large internal stress within the section resulting in shrinkage cracks. However, the presence of steel fibers helps redistributing the shrinkage strain resulting in mitigation of shrinkage cracks since the fibers bridge shrinkage cracks. On the other hand, the drying shrinkage for UHPC is not more than it is for conventional concrete because of the lack of free water and low permeability although high cementations material content is present. In fact, the low water to binder ratio prevents the formation of the dry shrinkage cracks.

One of the possible solutions mitigating the shrinkage cracks is a heat treatment. UHPC with heat treatment exhibits almost no shrinkage. If no treatment is performed, the ultimate shrinkage cracks will typically form within 2 months after casting for UHPC.[6] Penetrating Sealer Protective Compound can then be applied to all the exposed UHPC surfaces to seal the shrinkage cracks when no heat treatment is performed. Another possible solution would be increasing the steel fiber content. The large amount of fibers disperses shrinkage cracks and serves as a bridge across the cracks causing redistribution of shrinkage strain. Lastly, expensive additives and/or shrinkage reducing agents can significantly bring the shrinkage amount down to that of conventional concrete.[9]

4. Highway Bridge Railing Design Review

4.1 General

The primary function of highway bridge railings including open railings and concrete parapets is to provide protection at the edges of bridge deck for vehicles and pedestrians traveling on the deck. In order to provide satisfactory protection, the railings should provide adequate structural strength to withstand vehicular impact loads and the geometry to safely redirect the vehicles in collision with railing back to the roadway without causing a serious damage to neither the vehicle nor the occupant. AASHTO requires all new bridge railings proven to be structurally and geometrically crashworthy; therefore, all bridge railings need to be physically crash tested prior to its implementation. The crash test should prove that the proposed railing when in collision with a vehicle ensures the safety of the occupants of a vehicle, protection of other vehicles in the vicinity, and the protection of pedestrians and properties near roadways.

For the safety evaluation of highway bridge railings AASHTO required full compliance with National Cooperative Highway Research Program Report 350 (NCHRP-350) from 1998 to 2011. Starting from 2011, all new bridge railing hardware needed to be in compliance with Manual for Assessing Safety Hardware (MASH) requirements as per the requirement of AASHTO provisions. The hardware tested meeting NCHRP-350 requirements prior to the publication of MASH 2009 by AASHTO need not to be re-tested. However, as per the policy change of FHWA, all new bridge parapets and open railings should meet the safety requirements of MASH 2016 starting from December of 2019. A crashworthy railing or parapet system requires no further structural analysis as long as all the crash tested features of the system, which are in compliance with the aforementioned safety tests requirements are implemented in construction. Should any minor change made to the tested and approved system, the railing or parapet system's adequacy in terms of structurally and geometrically should be determined through an analysis and/or an engineering judgment.

4.2 Bridge Railing Test Levels

AASHTO MASH and NCHRP-350 includes six different test levels to ensure the principle performance factors including sufficient structural capacity, occupant safety and vehicle post-impact safety are warranted after the collision with bridge railings. Below Table 1 lists the test levels with the corresponding vehicle characteristics and test speeds.

	Vehicle Characteristics	Small Automobiles		Pickup Truck	Single-Unit Van Truck	Van-Type Tractor-Trailer		Tractor-Tanker Trailer
NCHRP Report 350	W (kips)	1.55	1.8	4.5	18.0	50.0	80.0	80.0
	B (ft.)	5.5	5.5	6.5	7.5	8.0	8.0	8.0
	G (in.)	22	22	27	49	64	73	81
	Crash angle, θ	20°	20°	25°	15°	15°	15°	15°
	Test Level	Test Speeds (mph)						
	TL-1	30	30	30	N/A	N/A	N/A	N/A
	TL-2	45	45	45	N/A	N/A	N/A	N/A
	TL-3	60	60	60	N/A	N/A	N/A	N/A
	TL-4	60	60	60	50	N/A	N/A	N/A
	TL-5	60	60	60	N/A	N/A	50	N/A
	TL-6	60	60	60	N/A	N/A	N/A	50
AASHTO MASH	W (kips)	2.42	3.3	5.0	22.0	N/A	79.3	79.3
	B (ft.)	5.5	5.5	6.5	7.5	N/A	8.0	8.0
	G (in.)	N/A	N/A	28	63	N/A	73	81
	Crash angle, θ	25°	N/A	25°	15°	N/A	15°	15°
	Test Level	Test Speeds (mph)						
	TL-1	30	N/A	30	N/A	N/A	N/A	N/A
	TL-2	45	N/A	45	N/A	N/A	N/A	N/A
	TL-3	60	N/A	60	N/A	N/A	N/A	N/A
	TL-4	60	N/A	60	55	N/A	N/A	N/A
	TL-5	60	N/A	60	N/A	N/A	50	N/A
	TL-6	60	N/A	60	N/A	N/A	N/A	50

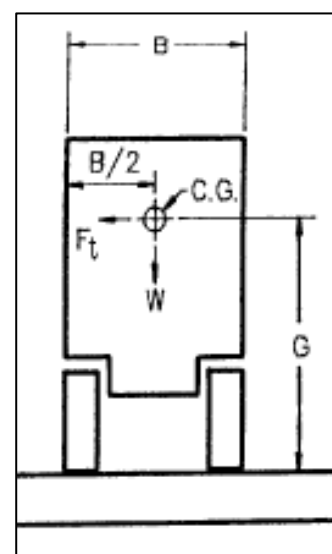**Table 1. Bridge railing test levels.** *Adapted from AASHTO[1].*

Figure 8. Vehicle Geometry. *Adapted from AASHTO[1].*

Test Level 1 (TL-1) is typically chosen for low-volume local roads with low-speed limits. The test level can also be chosen for construction zones.

Test Level 2 (TL-2) is taken for local and collector roads with reduced speed where a small percentage of heavy vehicles occupy the Average Daily Traffic (ADT).

Test Level 3 (TL-3) is selected for high-speed arterial highways with very low volume of heavy vehicles.

Test Level 4 (TL-4) is applicable to interstate highways, freeways, and expressways where considerable amount of heavy vehicles and trucks occupy the traffic volume.

Test Level 5 (TL-5) is pertinent to interstate highways, freeways, and expressways where the traffic volume includes significant amount of large trucks.

Test Level 6 (TL-6) is chosen for highways and freeways where the presence of large vehicles such as tankers and high gravity vehicles are expected.

4.3 Bridge Railing Design Forces

Bridge railings satisfying the test requirements and levels indicated earlier are approved to resist a set of design forces. AASHTO Appendix A13 Article lists these forces and the forces are as shown in the below Table 2. The Article also indicates the railing geometric variables pertaining to the minimum height of railing and the minimum height required for the application of the design force for each test level.

Design Forces and Designations	Railing Test Levels					
	TL-1	TL-2	TL-3	TL-4	TL-5	TL-6
F_t Transverse (kips)	13.5	27.0	54.0	54.0	124.0	175.0
F_L Longitudinal (kips)	4.5	9.0	18.0	18.0	41.0	58.0
F_v Vertical (kips) Down	4.5	4.5	4.5	18.0	80.0	80.0
L_t and L_L (ft)	4.0	4.0	4.0	3.5	8.0	8.0
L_v (ft)	18.0	18.0	18.0	18.0	40.0	40.0
H_e (min) (in.)	18.0	20.0	24.0	32.0	42.0	56.0
Minimum H Height of Rail (in.)	27.0	27.0	27.0	32.0	42.0	90.0

Table 2. Bridge railing design forces for each test levels. *Adapted from AASHTO[1].*

As shown in Table 1, higher test levels can provide resistance to a greater impact speed. The chart also shows that heavier vehicles can be resisted with higher test level tested and approved bridge railings. Similar to Table 1, Table 2 also shows that a greater impact force should be resisted by railings tested and approved for higher test levels. Additionally, the minimum height requirement for railings at higher test levels should be higher than that of lower test levels. As the minimum required railing height increase with higher test levels, the minimum height of the required transverse design load application from the bridge deck increases as well.

Figure 9. Railing design forces, location of load application, and distribution length. *Adapted from AASHTO[1].*

AASHTO bridge railing test levels, design forces, and the minimum required railing geometry and force distribution for each test level shown in this report are applicable to any type of bridge railings including but not limited to open railings and concrete parapets and shows no variations from a type of railing to another.
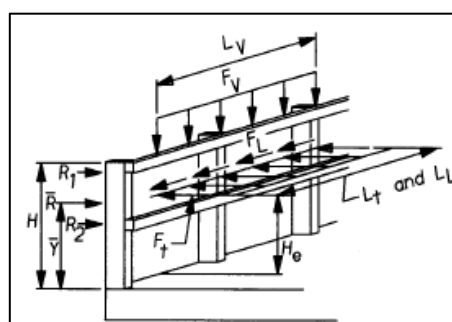
4.4 Bridge Parapet Resistance

AASHTO Appendix A13 Article provides design guidance for concrete parapets. The design guidance has been developed through a yield line analysis to compute the nominal parapet resistance to a transverse impact force, F_t shown on Figure 9. The resistance is a function of flexural resistance about a vertical and a longitudinal axis, the force distribution, and the length of yield line pattern the resistance distributed over. The analysis assumes that the failure pattern determined from yield line analysis does not extend to the bridge deck and the failure occurs within the parapet alone.

The yield line patterns shown on Figure 10 and Figure 11 have been specified by AASHTO Appendix A13 to determine the nominal parapet resistance at failure due to a vehicular impact load. AASHTO considers two different failure mechanisms: failure within a parapet segment and a failure at a near parapet end. The shown yield line failure patterns are valid when the failure remains within the parapet. If the failure extends down to the bridge deck, the yield line failure mechanism predicted to calculate the parapet capacity cannot be utilized and an appropriate analysis should be performed to determine the parapet resistance.
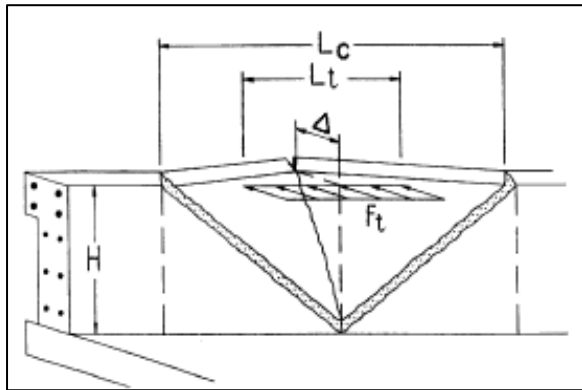

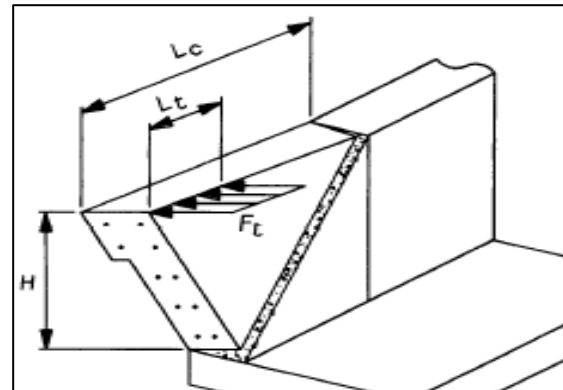**Figure 10. Yield line pattern for impact failure within parapet segment.** *Adapted from AASHTO[1].*

Figure 11. Yield line pattern for impact failure near parapet end. *Adapted from AASHTO[1].*

Parapet resistance for Impact within Internal Segment

The yield line has been determined based on the assumption that a sufficient longitudinal parapet length exists that allows the critical length of yield line pattern, L_c, so that the yield line failure pattern forms within a parapet segment.

Parapet Resistance for impacts within a parapet segment:

$$R_w = \left(\frac{2}{2L_c - L_t}\right)\left(8M_b + 8M_w + \frac{M_c L_c^2}{H}\right) \quad \textit{(AASHTO A13.3.1-1)}$$

The critical length of yield line pattern within a parapet segment:

$$L_c = \frac{L_t}{2} + \sqrt{\left(\frac{L_t}{2}\right)^2 + \frac{8H(M_b + M_w)}{M_c}} \quad \textit{(AASHTO A13.3.1-2)}$$

Parapet resistance for Impact near End

The predetermined yield line analysis is valid as long as a single yield line is formed near a parapet end. A sufficient parapet length should exist to provide the critical length of yield line pattern, L_c, so that the yield line failure pattern forms near parapet end.

Parapet Resistance for impacts at near parapet end:

$$R_w = \left(\frac{2}{2L_c - L_t}\right)\left(M_b + M_w + \frac{M_c L_c^2}{H}\right) \quad \textit{(AASHTO A13.3.1-3)}$$

The critical length of yield line pattern occurs at near parapet end:

$$L_c = \frac{L_t}{2} + \sqrt{\left(\frac{L_t}{2}\right)^2 + H\left(\frac{M_b + M_w}{M_c}\right)} \quad \textit{(AASHTO A13.3.1-4)}$$

10

5. UHPC Highway Bridge Parapet Design Guidance

5.1 Parapet Yield Line Analysis Review

AASHTO required parapet resistance depends on the flexural resistance of the parapet. The flexure resistances, M_b, M_w, and M_c are related to the total transverse parapet resistance determined from yield line analysis as shown on the below Figure 12 and 13.
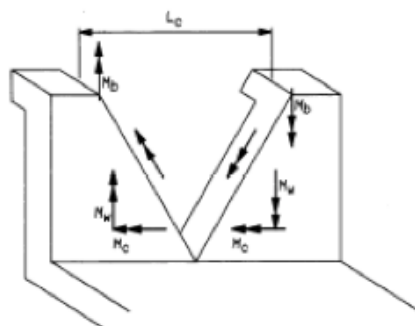

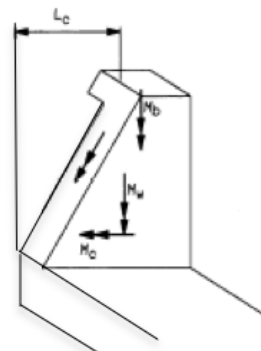**Figure 12. Yield line pattern and flexural resistance within parapet segment.** *Adapted from AASHTO[1].*   **Figure 13. Yield line pattern and flexural resistance near parapet end.** *Adapted from AASHTO[1].*

The plastic moment develop along the yield line at failure consists of three flexural resistances. The followings are the flexural resistances to be considered to determine the transverse parapet resistance:

> Mc: The flexural resistance of cantilevered parapet section about an axis parallel to the longitudinal axis of the bridge.

> Mw: The flexural resistance of the parapet section about its vertical axis.

> Mb: The additional flexural resistance of parapets with cap beams located at the top of parapet stem, which are typically wider than the parapet stem width if present. Otherwise, should be taken as zero.

The yield line analysis has been developed based on the assumption that all the negative and positive parapet resisting moments provided about different axes are equal.

It should be noted that AASHTO Commentary, CA13.3.1, recommends that the average value of Mc determined at different locations along the parapet height should be used to calculate the transverse parapet resistance for parapets whose stem width varies along its height.

AASHTO Commentary, CA13.3.1, also recommends that stirrups or ties should be provided if needed in order to resist shear and diagonal tension forces.

5.2 Flexural Capacity of UHPC Members

Similar to conventional concrete, the flexural capacity of concrete members with mild reinforcement serving as primary tension reinforcement can be determined through equilibrium equations and strain compatibility method at the member design section according to FHWA design guidance[10].

The guidance indicates that there are two different states of stress-strain distribution of UHPC members: Cracking Limit State and Ultimate Limit State. The compressive and tensile strain and stress are linearly distributed along the full height of the design section within Cracking Limit State. The state continuous until the initial crack formation occurs. Based on the proposed conservative stress-strain behavior as a result of flexural and shear testing of a large-scale bridge I-Girder, Graybeal[7] suggests that the initial crack formation occurs at a tensile strain of 0.000144 where the tensile stress is 1.2 ksi.

Rectangular Section   Cracking Limit State
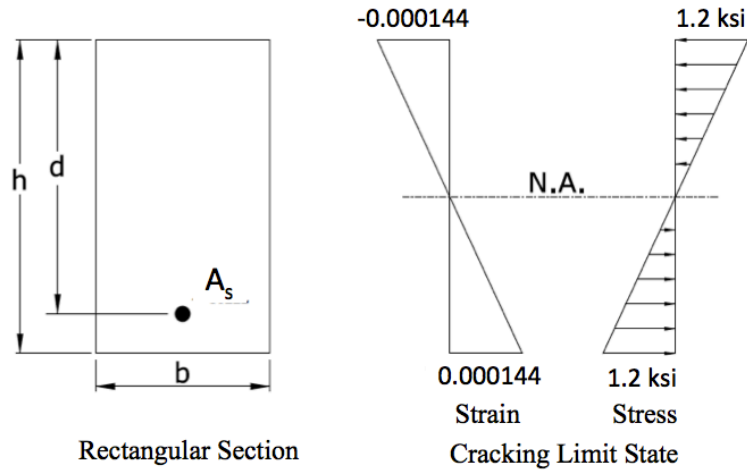
The below equation can be used for the estimation of the cracking moment of a rectangular section.

$$M_{CR} = f_{TU} * S \qquad\qquad \text{Eq. (1)}$$

$$M_{CR} = (1.2\text{ksi}) * \frac{bh^2}{6} \qquad\qquad \text{Eq. (2)}$$

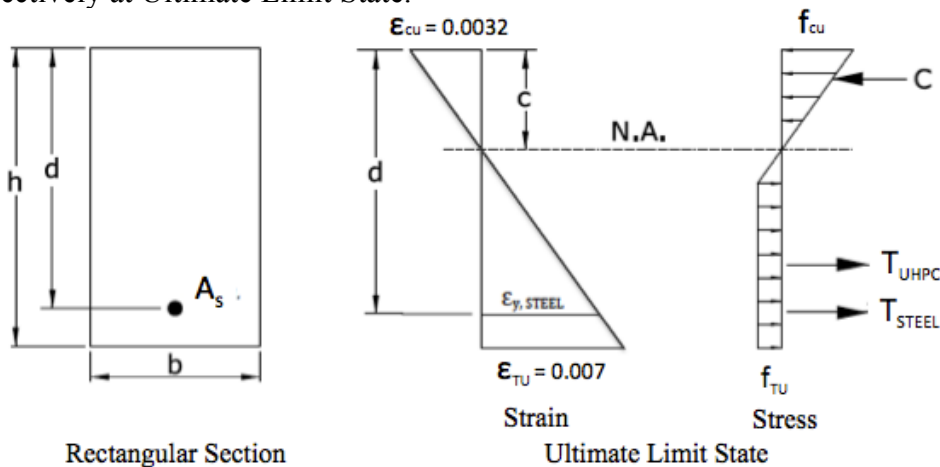The linear tensile strain distribution continues until the design section experience fiber pullout. It should be noted that the fiber pullout occurs well beyond the initial crack formation due to the provided post-cracking tensile ductility as discussed in section 3.2 and as shown on Figure 6. The fiber pullout occurs at a tensile strain, ε_{TU}, of 0.007 with a corresponding tensile stress, f_{TU}, of 1.2 ksi. As discussed in section 3.2, FHWA-HIF-13-032[10] report recommends limiting the tensile strength and strain to 1.2 ksi (8 MPa) and 0.007 respectively at Ultimate Limit State.

Rectangular Section   Ultimate Limit State

On the compression side, the linear distribution of compressive strain continuous until a 0.0032 of compressive strain is attained at failure. The design guidance included in FHWA-HIF-13-032[10] report also recommends limiting the compressive strain, ε_{CU}, to 0.0032 in structural design. The compressive stress varies from zero at the Neutral Axis (N.A.) to a maximum value at the extreme fiber where concrete crushes at a strain of 0.0032. The maximum recommended compressive stress, f_{CU}, to be used in structural design is as followings:

- $f_{CU} = 24$ ksi (165 MPa) for steam-cured condition

- $f_{CU} = 18$ ksi (124 MPa) for air-cured condition

The area of the compressive and tensile stress distribution can be used to determine the horizontal compressive force, C, and the tensile force, T respectively. Once the compressive and tensile forces are determined, the resulting internal force couple serving as the resisting moment of the section can be computed through internal equilibrium.

Horizontal compressive force:

$$C = \frac{1}{2}f_{CU}cb \qquad \text{Eq. (3)}$$

Horizontal tensile forces:

$$T_{UHPC} = f_{TU}(h - c)b \qquad \text{Eq. (4)}$$

$$T_{STEEL} = A_s f_y \qquad \text{Eq. (5)}$$

Equating the compressive and tensile horizontal forces to determine the depth of neutral axis, c, from the compression extreme fiber

$$C = T_{UHPC} + T_{STEEL} \qquad \text{Eq. (6)}$$

Substituting horizontal forces in Eq. (6) with Eq. (3), Eq. (4), and Eq. (5) provides below expression

$$\frac{1}{2}f_{CU}cb = f_{TU}(h - c)b + A_s f_y \qquad \text{Eq. (7)}$$

Substituting A_s with $\rho_{STEEL}bh$ in Eq. (7) gives below expression

$$\frac{1}{2}f_{CU}cb = f_{TU}(h - c)b + \rho_{STEEL}bhf_y \qquad \text{Eq. (8)}$$

Manipulating Eq. (8) provides the depth of neutral axis from the extreme fiber

$$c = \left(\frac{f_{TU} + \rho_{STEEL}f_y}{0.5f_{CU} + f_{TU}}\right)h \qquad \text{Eq. (9)}$$

Prior to calculating the nominal flexural capacity, Mn, the controlling limit state needs to be determined. Depending on whether the section is compression-controlled or tension-controlled the depth of the neutral axis may need to be adjusted. In order to determine the controlling limit state, the following equalities are recommended to be consider in FHWA-HIF-13-032[10] report:

$$\text{If } \left(\frac{f_{TU} + \rho_{STEEL}f_y}{0.5f_{CU} + f_{TU}}\right) > 0.314 \text{ then the section is compression-controlled}$$

$$\text{If } \left(\frac{f_{TU} + \rho_{STEEL}f_y}{0.5f_{CU} + f_{TU}}\right) < 0.314 \text{ then the section is tension-controlled}$$

For compression-controlled sections, Eq. (9) can be used for the depth of neutral axis from the extreme fiber.

$$c = \left(\frac{f_{TU} + \rho_{STEEL}f_y}{0.5f_{CU} + f_{TU}}\right)h$$

For tension-controlled sections, the depth of neutral axis from the extreme fiber should be determined from the stress-strain relationship of UHPC.

From stress-strain relationship $f_{CU} = \varepsilon_{CU}E_{UHPC}$ \qquad Eq. (10)

From linear strain distribution

$$\frac{c}{\varepsilon_{CU}} = \frac{h - c}{\varepsilon_{TU}} \implies \varepsilon_{CU} = \frac{\varepsilon_{TU}c}{h - c}$$

Substitute ε_{CU} with $\frac{\varepsilon_{TU}c}{h - c}$ in Eq. (10)

$$f_{CU} = \varepsilon_{TU}E_{UHPC}\left(\frac{c}{h - c}\right) \qquad \text{Eq. (11)}$$

13

Substituting f_{CU} in Eq. (9) with above Eq. (11) and manipulating Eq. (9) provides the below depth of neutral axis from the extreme fiber for tension-controlled sections

$$c = \left(\frac{f_{TU} + \rho_{STEEL}f_y}{\frac{1}{2}\varepsilon_{TU}E_{UHPC}\left(\frac{c}{h-c}\right) + f_{TU}} \right) h \qquad \text{Eq. (12)}$$

Modulus of Elasticity for UHPC members can be estimated by the below equation as recommended by the Graybeal.[6]

$$E_{UHPC} = 1,460\sqrt{f_{CU}} \ (ksi)$$

Because the tensile capacity is limited to tensile strength at fiber pullout and steel reinforcement yielding well before the concrete reaches its ultimate crushing strength, the product of internal tensile forces and the corresponding lever arm to the compressive force provides the internal resisting moment. The nominal flexural resistance of either tension-controlled or compression-controlled UHPC members with rectangular design section should be calculated by using the below equation.

$$M_n = f_{TU}b(h-c)\left(\frac{3h+c}{6}\right) + \rho_{STEEL}f_ybh\left(d - \frac{c}{3}\right) \qquad \text{Eq. (13)}$$

5.3 UHPC Parapets Resistance

As discussed in section 5.1, three flexural resistance components developing the plastic moment along the yield line at failure should be computed to determine the transverse parapet resistance. Flexural resistance components can be determined by the following recommended procedure:
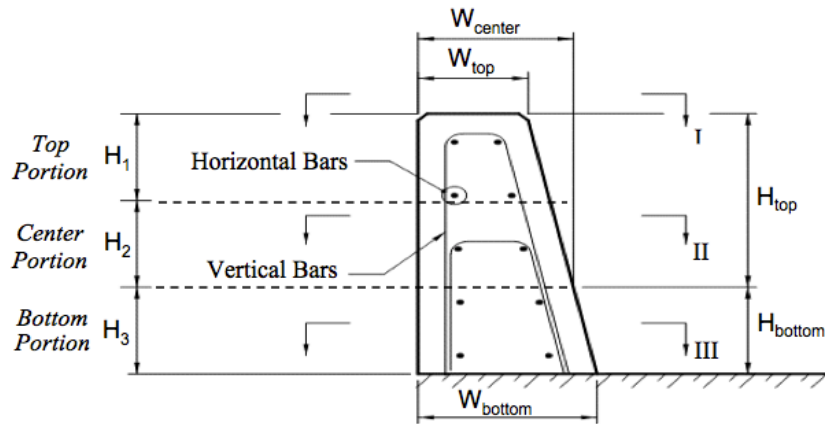
Figure 14. Typical single slope parapet.

Determine M_w

Using the center details of each portion along the height of the parapet, the flexural capacity about a vertical axis is determined. Only the rear reinforcement is effective in tension and should be considered determining the flexural capacity. The parapets with varying thickness along its height may be divided into multiple portions to calculate the flexural resistance. Eventually, the flexural resistance of each portion may be added together to determine the overall moment resistance about a vertical axis. It should be noted that the positive and negative moments should be computed and the average should be used. However, in the case of collision near the end of the parapet, which is the controlling case, the only yield line is caused by a moment causing tension along the front face. Therefore, only the flexural resistance for negative moment should be used. Assume the failure mechanism includes the entire height of the parapet, the ultimate flexural resistance of parapet about its vertical axis, Mw, is computed by adding the flexural resistance of each portions.

Determine the followings for top, center, and bottom portions shown on Figure 14:

14

- As$_{\_HOR.}$ – Total area of horizontal rebars
- ρs$_{\_HOR.}$ – Steel ratio of horizontal rebars

For top portion: $\quad \rho_{STEEL} = \dfrac{As_{HOR}}{H_1\left(\dfrac{\dfrac{W_{top}+W_{center}}{2}+W_{top}}{2}\right)}$

For center portion: $\rho_{STEEL} = \dfrac{As_{HOR}}{H_2\left(\dfrac{\dfrac{W_{top}+W_{center}}{2}+W_{center}}{2}\right)}$

For bottom portion: $\rho_{STEEL} = \dfrac{As_{HOR}}{H_3\left(\dfrac{W_{center}+W_{bottom}}{2}\right)}$

- d – Effective depth of rear horizontal bars from the front face

    For top portion:

$$d = \left(\dfrac{\dfrac{W_{top}+W_{center}}{2}+W_{top}}{2}\right) - cover - Dia_{Vert\,bar} - \frac{1}{2}Dia_{Horz\,bar}$$

    For center portion:

$$d = \left(\dfrac{\dfrac{W_{top}+W_{center}}{2}+W_{center}}{2}\right) - cover - Dia_{Vert\,bar} - \frac{1}{2}Dia_{Horz\,bar}$$

    For bottom portion:

$$d = \left(\dfrac{W_{center}+W_{bottom}}{2}\right) - cover - Dia_{Vert\,bar} - \frac{1}{2}Dia_{Horz\,bar}$$

- Determine the controlling limit state (compression or tension controlled)

    If $\left(\dfrac{f_{TU}+\rho_{STEEL}f_y}{0.5f_{CU}+f_{TU}}\right) > 0.314$ then the section is compression-controlled

    If $\left(\dfrac{f_{TU}+\rho_{STEEL}f_y}{0.5f_{CU}+f_{TU}}\right) < 0.314$ then the section is tension-controlled

- Calculate the depth of neutral axis from the front face

    For compression-controlled section

$$c = \left(\dfrac{f_{TU}+\rho_{STEEL}f_y}{0.5f_{CU}+f_{TU}}\right)t \quad where\ t\ is\ W_{top_{Ave}}, W_{Center_{Ave}}\ or\ W_{Bottom_{Ave}}$$

    For tension-controlled section

$$c = \left(\dfrac{f_{TU}+\rho_{STEEL}f_y}{\frac{1}{2}\varepsilon_{TU}E_{UHPC}\left(\frac{c}{t-c}\right)+f_{TU}}\right)t \quad where\ t\ is\ W_{top_{Ave}}, W_{Center_{Ave}}\ or\ W_{Bottom_{Ave}}$$

- Calculate nominal flexural capacity for each portion: M$_{w1}$, M$_{w2}$, and M$_{w3}$

$$M_n = f_{TU}b(t-c)\left(\dfrac{3t+c}{6}\right) + \rho_{STEEL}f_ybt\left(d-\dfrac{c}{3}\right)$$

- Mw is summation of M$_{w1}$, M$_{w2}$, and M$_{w3}$

$$M_w = M_{w1} + M_{w2} + M_{w2}$$

15

Determine M_c

Using the full height of parapet, the flexural capacity about a longitudinal axis parallel to the bridge is determined. Parapet is acting as a cantilevered beam and only the front vertical reinforcement is effective in tension and should be considered determining the flexural capacity. The parapets with varying thickness along its height results in varying effective depth, d, for the front vertical bars from the rear concrete face. Therefore, Mc, the flexural resistance of each portion shown on Figure 14 may be calculated individually and then a weighted average of the individual flexural resistance is taken to determine the ultimate flexural resistance of the parapet about its longitudinal axis, Mc.

Determine the followings for top, center, and bottom portions shown on Figure 14:

- $As\_{VER.}$ – Area of vertical bars
- fy – Yield strength of vertical bars may need to be adjusted if the rebar embedment into deck required to develop its full tensile strength is not provided due to geometric constraints.
- $\rho s\_{VER.}$ – Steel ratio of vertical bars
  For top portion:
  $$\rho_{STEEL} = \frac{As_{VERT}}{12W_{top}}$$
  For center portion:
  $$\rho_{STEEL} = \frac{As_{VERT}}{12W_{center}}$$
  For bottom portion:
  $$\rho_{STEEL} = \frac{As_{VERT}}{12W_{bottom}}$$

- d – Effective depth of front vertical bars from the rear face
  For top portion:
  $$d = W_{top} - cover - \frac{1}{2}Dia_{Vert_{bar}}$$
  For center portion:
  $$d = W_{center} - cover - \frac{1}{2}Dia_{Vert_{bar}}$$
  For bottom portion:
  $$d = W_{bottom} - cover - \frac{1}{2}Dia_{Vert_{bar}}$$

- Determine the controlling limit state (compression or tension controlled)
  If $\left(\frac{f_{TU} + \rho_{STEEL}f_y}{0.5f_{CU} + f_{TU}}\right) > 0.314$ then the section is compression-controlled

  If $\left(\frac{f_{TU} + \rho_{STEEL}f_y}{0.5f_{CU} + f_{TU}}\right) < 0.314$ then the section is tension-controlled

- Calculate the depth of neutral axis from the rear face

  For compression-controlled section

  $$c = \left(\frac{f_{TU} + \rho_{STEEL}f_y}{0.5f_{CU} + f_{TU}}\right)t \quad where\ t\ is\ W_{top}, W_{Center}\ or\ W_{Bottom}$$

  For tension-controlled section

  $$c = \left(\frac{f_{TU} + \rho_{STEEL}f_y}{\frac{1}{2}\varepsilon_{TU}E_{UHPC}\left(\frac{c}{t-c}\right) + f_{TU}}\right)t \quad where\ t\ is\ W_{top}, W_{Center}\ or\ W_{Bottom}$$

16

- Calculate nominal flexural capacity for each portion: M_{c1}, M_{c2}, and M_{c3}

$$M_n = f_{TU} b(t - c)\left(\frac{3t + c}{6}\right) + \rho_{STEEL} f_y bt \left(d - \frac{c}{3}\right)$$

- Mc is a weighted average of M_{c1}, M_{c2}, and M_{c3}

$$M_c = \frac{\left(\frac{M_{c1} + M_{c2}}{2} H_{Top} + \frac{M_{c2} + M_{c3}}{2} H_{Bottom}\right)}{H_{Overall}}$$

Determine M_b

The additional flexural resistance from cap beams located at the top of parapet stems can be ignored conservatively. Typically, the presence of cap beam on bridge parapets is rare. Consequently, the resisting moment component, Mb, is equal to zero in the parapet transverse resistance computations.

Resistance Factor

The bridge railing resistance should be evaluated at Extreme Event II limit state to comply with AASHTO Provision 3.4. At extreme limits states, the resistance factors should be taken as 1.0 as specified by AASHTO Provision 1.3.2.1. Consequently, no resistance factors should be applied to the parapet flexural resistance.

Parapet Transverse Resistance

With M_w and M_c computed, the parapet transverse resistance can be computed with the equations determined through yield line analysis in AASHTO Appendix A13 as discussed in section 4.4.

Parapet resistance for Impact within Internal Segment

Parapet Resistance for impacts within a parapet segment:

$$R_w = \left(\frac{2}{2L_c - L_t}\right)\left(8M_b + 8M_w + \frac{M_c L_c^2}{H}\right) \quad \textit{(AASHTO A13.3.1-1)}$$

The critical parapet length of yield line pattern occurs within a parapet segment:

$$L_c = \frac{L_t}{2} + \sqrt{\left(\frac{L_t}{2}\right)^2 + \frac{8H(M_b + M_w)}{M_c}} \quad \textit{(AASHTO A13.3.1-2)}$$

Parapet resistance for Impact near End

Parapet Resistance for impacts at near parapet end:

$$R_w = \left(\frac{2}{2L_c - L_t}\right)\left(M_b + M_w + \frac{M_c L_c^2}{H}\right) \quad \textit{(AASHTO A13.3.1-3)}$$

The critical parapet length of yield line pattern occurs at near parapet end:

$$L_c = \frac{L_t}{2} + \sqrt{\left(\frac{L_t}{2}\right)^2 + H\left(\frac{M_b + M_w}{M_c}\right)} \quad \textit{(AASHTO A13.3.1-4)}$$

The above computed parapet resistance, Rw, should be checked against the vehicular impact load based on the test level of interest of the owner to ensure the structural adequacy. The design impact loads for each test level is shown in section 4.3. If any modifications deemed necessary due to insufficient structural capacity, the crash-tested parapet geometry, concrete material strength, and/or reinforcement ratio may be modified with engineering judgment as indicated in AASHTO C13.7.3.1.1.

6. Economy

6.1 General

The unit cost of UHPC surpasses the cost of conventional concrete in the current U.S market. The scarcity of concrete plants pre-qualified to mix UHPC and the commercially-available UHPC mix design being proprietary blend are the major reasons of the high cost of UHPC in the U.S. Pre-bagged UHPC costs about $2,000 per cubic yard in the market currently.[11] The cost includes the development and the delivery of the mix. The cost goes up to nearly $2,500 per cubic yard with the addition of steel fiber reinforcement whose cost ranges between $250 and $500 per cubic yard depending on the volume of fiber reinforcement desired. The such high cost currently limits the usage of UHPC to conventional pre-cast concrete deck panel closure pours in the U.S. Although the initial cost of UHPC is approximately 20 times higher than the cost of conventional concrete, which costs about $125 per cubic yard[8], the life cycle cost of structures with UHPC over 100 years is expected to be less than the life cycle cost of structures with conventional concrete. This is due to the fact that UHPC provides superior durability properties resulting in an increased service life and the reduced maintenance cost.

6.2 Parapet Cost Comparison

In this study, 45" Connecticut Department of Transportation (CTDOT) modified MASH crash-tested conventional (normal) concrete Texas single slope parapet meeting Test Level 5 requirements was evaluated for cost comparison.

Figure 15. Normal Concrete Parapet.   **Figure 16. UHPC Parapet.**   **Figure 17. Hybrid Parapet.**
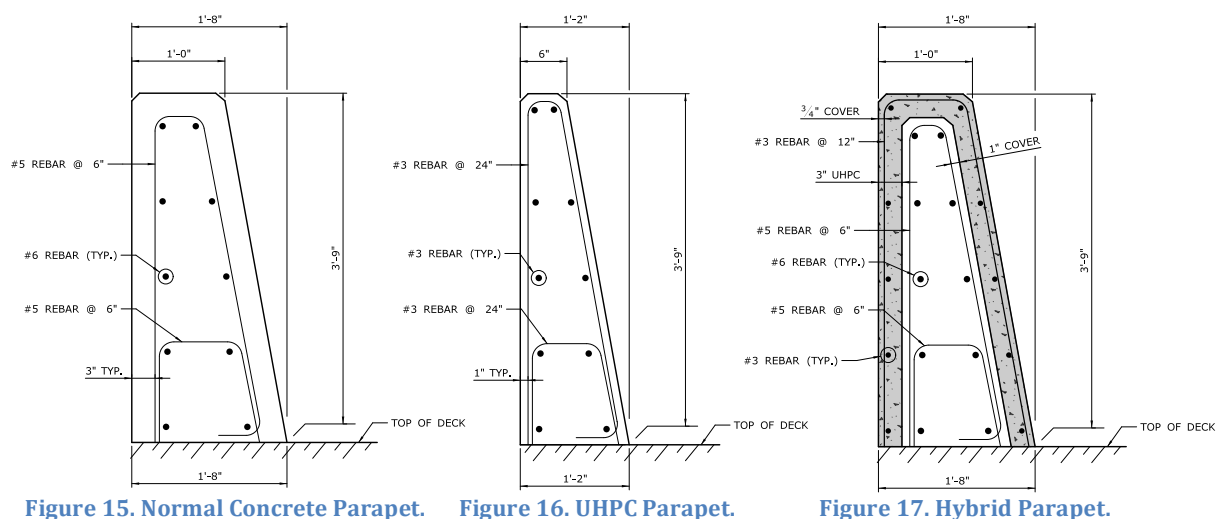
Figure 15 shows a 45-inch single slope parapet. The parapet was crash-tested as 36-inch tall and was modified to 42 inches by Texas Department of Transportation (TXDOT) through structural analysis. The parapet was further modified by CTDOT to 45 inches to account for 3 inches of overlay. Besides the height, the width of the parapet was altered in order to meet the State's parapet geometric requirements for any appurtenance attachment to the top of parapet. The material cost of the parapet including normal strength concrete and reinforcement was estimated as $68 per linear foot.

Under this study, when the 45-inch parapet was redesigned by considering UHPC in lieu of conventional concrete, the parapet details shown on Figure 16 was achieved. The vertical geometry and the font face slope are maintained to ensure the crash-testing compliance. The horizontal geometry and the reinforcement were altered to obtain adequate structural capacity. The material cost of UHPC along with the required reinforcement was estimated as $295 per linear foot.

This study also included consideration of UHPC only for facing (topping) application over the conventional concrete all around its exposed faces to reduce the parapet cost. The overall geometry shown in Figure 15 was maintained and the hybrid parapet with the details shown

on Figure 17 was developed. The hybrid parapet consists of conventional concrete, which occupies 60 percent of the overall volume and UHPC occupying 40 percent of the overall volume. The estimated cost for the hybrid parapet was $244 per linear foot.
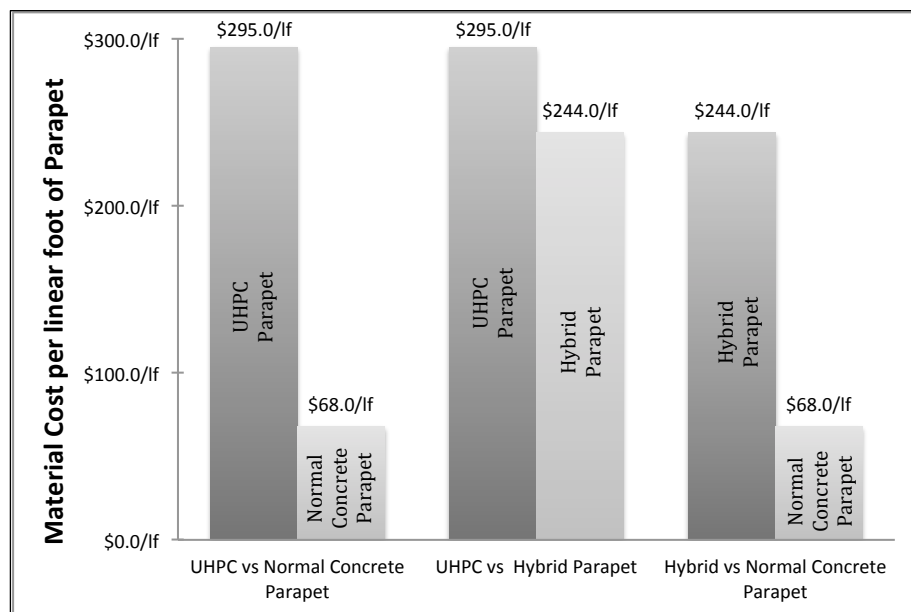
Chart 3. Cost comparison: UHPC Parapet vs Normal Concrete Parapet
UHPC Parapet vs Hybrid Parapet
Hybrid Parapet vs Normal Concrete Parapet

Above Chart 3 provides a cost comparison for the 45-inch single slope parapets with different normal concrete and UHPC quantities described earlier. The cost of 45-inch UHPC Parapet way far exceeds the cost of parapet with normal concrete. The UHPC Parapet cost is almost 4 times higher than that of Normal Concrete Parapet. When the cost of UHPC Parapet is compared to the cost of Hybrid Parapet, $51 per linear foot of difference can be observed. Similar to UHPC parapet, the cost of Hybrid Parapet is much more than the cost of Normal Concrete Parapet.

Graybeal in his research[8] emphasized the development of a non-proprietary UHPC concrete mix. Graybeal claims that a non-proprietary UHPC mix design can be developed for cost efficiency. Using locally available materials in the UHPC mix design may significantly reduce the material cost. Additionally, Graybeal[8] states that the paste, the matrix, and the amount of fiber reinforcement of UHPC may be optimized to reduce material cost while maintaining its mechanical properties and durability characteristics.

7. Summary and Conclusions

7.1 Summary

A novel design guidance for highway bridge parapets with UHPC was developed under this study for the analysis and modification of crash-tested bridge parapets. FHWA Publications and State DOT studies were referenced for the mechanical and durability properties of UHPC, and the properties were incorporated in the design guidance. The guidance was developed in accordance with AASHTO LRFD Bridge Design Specifications 8th Edition provisions for highway bridge railings. The design guidance is applicable to any UHPC parapet geometry and Test Level specified in AASHTO provisions.

The design guidance and the cost comparison provided in this report will help the bridge owners and the design engineers better understand how UHPC structurally behaves and how feasible UHPC application on highway bridge parapets. The guidance provides the technical and material information of UHPC along with the associated cost to allow State DOTs as the bridge owners to consider UHPC for the state bridge projects.

7.2 Conclusions

This study provides a complete design guidance for the bridge design engineers to analyze and/or modify an existing crash-tested bridge parapet system in accordance with MASH 2016 requirements. The study also provides the cost for UHPC applications on the highway bridge parapets for the bridge owners. The following conclusions drawn from the development of the design guide, analysis of 45-inch single slope parapet, and the associated cost:

Design:

AASHTO LRFD Bridge Design Specification for Railings should be used for the desired Test Levels and the corresponding geometric requirements to evaluate bridge parapet performance. The mechanical properties investigated and reported by FHWA publications and FHWA funded State research studies should be referenced for the parapet performance evaluation. Any modification to an existing crash-tested parapet should be performed through either an engineering judgment or a structural analysis to ensure crash-testing compliance is not compromised. For UHPC bridge parapets the following mechanical properties should be considered for the structural analysis:

- The UHPC compressive strength should be considered depending on the curing condition. For steam-cured condition f_{CU} of 24 ksi (165 MPa) should be used and for air-cured condition f_{CU} of 18 ksi (124 MPa) should be considered.

- A linear compressive strength distribution from the extreme compression fiber to the neutral axis should considered.

- The axial compressive strain of UHPC should be limited to 0.0032.

- The UHPC tensile strength should be limited to 1.2 ksi (8MPa) in determining the flexural response from the initial crack formation to steel fiber pulling out of the concrete matrix.

- At Ultimate Limit State, the tensile strength should be limited to 1.2 ksi (8 MPa) and the corresponding tensile strain should be considered as 0.007. A rectangular uniform tensile stress distribution should be considered from the extreme tension fiber to the neutral axis of the section being analyzed.

- Either coated or uncoated mild reinforcement can be provided as needed. The tensile capacity of UHPC and the mild reinforcement should be considered in the analysis. No resistance factors should be applied for UHPC parapet analysis at Extreme Event Limit State.

- The tensile strength of vertical reinforcement should be adjusted when the embedment into a bridge deck slab is less than the required development length allowing the rebar achieve its full tensile strength. The full yield strength should be considered only when the embedment not less than the required development length into the deck is provided.

- The modulus of elasticity can be estimated as $E_{UHPC} = 1,460\sqrt{f_{CU}}\ (ksi)$.

- The need for stirrups or ties within UHPC parapet should be determined by the design engineer.

- The design engineer should also check the interface shear resistance between the UHPC parapet base and the bridge deck or overhang surface.

Analysis Results:

A single slope parapet, which was originally crash-tested by TXDOT was analyzed. The parapet was crash-tested as 36-inch tall and was modified to 42 inches by the DOT through structural analysis. The parapet was further modified by CTDOT to 45 inches to account for

3 inches of overlay. In this study, the parapet was analyzed considering the following concrete materials:

- Conventional (normal) concrete

- UHPC

- Combination of UHPC and normal strength concrete

The overall geometry of the parapet including the height and the slope at front face was maintained in order not to compromise the crash-testing compliance. Depending on the required structural resistance to the transverse impact force at Test Level 5, the width and the reinforcement were modified. The results of the analysis exhibited that the resistance at near end of parapet (barrier) of each parapet type listed in Table 3 was the controlling location of the design at Test Level 5.

The 45-inch single slope parapet with normal concrete was analyzed with the crash-tested width and reinforcement configuration shown on Figure 15. Based on the analysis, the parapet provided an impact resistance of 126.5 kips at near parapet end.

When UHPC alone was considered, the width of the parapet and the reinforcement were significantly decreased. Although the UHPC parapet shown on Figure 16 appears "slim", the parapet provided almost 2.5 times higher impact resistance than that of conventional concrete parapet due to its higher compressive and tensile strength. The calculated resistance near parapet end was 300.6 kips.

Because of the excessive resistance achieved from the UHPC parapet, the UHPC was considered as 3-inch facing only on the exposed faces of conventional concrete to eliminate the excessive use of UHPC. The hybrid parapet consisting of conventional concrete and UHPC, shown on Figure 17, provided 127.5 kips of impact resistance near parapet end. The analysis results showed that more efficient parapet design was achieved by limiting UHPC usage to facing application. Not only the excessive resistance but also the additional cost was eliminated.

SUMMARY OF ANALYSIS RESULTS					
PARAPET TYPE	CRASHWORTHY SYSTEM PER	TEST LEVEL	IMPACT FORCE (KIPS)	RESISTANCE, RW (KIPS) IMPACT WITHIN BARRIER	RESISTANCE, RW (KIPS) NEAR BARRIER END
45" SINGLE SLOPE PARAPET (NORMAL CONCRETE)	MASH - 2009	TL - 5	124.0	218.6	126.5
45" SINGLE SLOPE PARAPET (UHPC)	MASH - 2009	TL - 5	124.0	487.9	300.6
45" SINGLE SLOPE PARAPET (HYBRID)	MASH - 2009	TL - 5	124.0	177.5	127.5

Table 3. 45-inch single slope parapet resistance summary.

Cost:

The cost of UHPC bridge parapet per linear foot way far exceeds the cost of bridge parapet with normal strength concrete in the U.S. It is expected that the cost difference between the two will diminish as the implementation of UHPC increases in the U.S. and when a non-proprietary UHPC mix is advanced. To minimize the cost of UHPC in a bridge project, this study recommends the usage of UHPC as facing only on the exposed faces of crash-tested conventional concrete bridge parapets.

8. Design Examples

8.1 General

This section of the report provides UHPC design examples. The first example illustrates the design of a 45-inch single slope UHPC parapet originally crash-tested by TXDOT as 36-inch tall and then modified to 42 inches through structural analysis. The parapet was further modified by CTDOT to 45-inch tall to account for 3-inch overlay. The second example illustrates the design of a hybrid parapet including UHPC as facing only on the said parapet.

8.2 45-inch UHPC Single Slope Parapet Design Example

This example illustrates the design of a 45-inch UHPC single slope parapet for TL-5.

The UHPC compressive strength is assumed to be 18 ksi under air-cured condition.

The tensile strength of the vertical bars is determined based on the ratio of the embedment depth that can be provided to a 8.5-inch deck slab to the required development length.

Parapet top width is considered as 6 inches for any appurtenance attachment.

DESIGN INPUT

H_1	=	15	in
H_2	=	15	in
H_3	=	15	in
H_{top}	=	30	in
H_{bottom}	=	15	in
$H_{overall}$	=	45	in
W_{top}	=	6	in
W_{center}	=	11.5	in
W_{bottom}	=	14	in
$L_{joint-to-joint}$	=	50	ft

Rebar Quantity

Horizontal Bars:						
	Top portion:	2	bars	Rebar	# 3	Area	Diameter
	Center portion:	1	bars			0.11	0.375
	Bottom portion:	2	bars	f_y	=	60	ksi

Vertical Bars:	Bar spacing =	24	in	Rebar	# 3	Area	Diameter
						0.11	0.375

Yield Strength: *Adjust fy to account for inadequate embedment in deck* f_y = 56.25 ksi

UHPC 28-day Compressive Strength		f_{CU}	=	18.0	ksi
Modulus of Elasticity	$1{,}460\sqrt{f_{cu}}\ (ksi)$	E_{UHPC}	=	6194.3	ksi
28-day Tensile Strength		f_{TU}	=	1.2	ksi
28-day Tensile Strain			=	0.007	
Cover - inside face			=	1.0	in
phi factor	*Extreme Event II (AASHTO 1.3.2.1)*		=	1.0	

Choose Test Level

Select the designed Test Level (TL) and see the result of the barrier analysis in the next section.

Test Level	F_t (Kips)	F_L (Kips)	F_v (Kips)	L_t and L_L (ft)	L_v (ft)	H_e (in)	H_{min} (in)
5 ⇕	124	41	80	8	40	42	42

Analysis Results

The nominal railing resistance, Rw, of the barrier is computed and compared to the transverse force Ft specified for the selected Test Level. (Detailed calculations are shown in the next section - "Calculations").

I. Impact within wall segment: R_w = 487.9 kips   > F_t = 124.0 kips   OK

II. Impact near wall end: R_w = 300.6 kips   > F_t = 124.0 kips   OK

PASS

CALCULATIONS

I. Calculate Mc

$$As_{VERT} = Rebar\ Area * \frac{12}{Rebar\ Spacing} \qquad\qquad = \quad \mathbf{0.055} \quad \text{in}^2/\text{ft}$$

Section I :

$$\rho_{STEEL} = \frac{As_{VERT}}{12W_{top}} \qquad\qquad = \quad \mathbf{0.000764}$$

$$d = W_{top} - cover - \frac{1}{2}Dia_{Vert_{bar}} \qquad\qquad = \quad \mathbf{4.81} \quad \text{in}$$

Determine controlling limit state:

$$\left(\frac{f_{TU} + \rho_{STEEL}f_y}{0.5f_{CU} + f_{TU}}\right) \ < \ 0.314 \quad \textit{Tension-Controlled} \qquad = \quad \mathbf{0.122}$$

Determine c : $\qquad\qquad = \quad \mathbf{1.16} \quad \text{in}$

For Compression-Controlled

$$c = \left(\frac{f_{TU} + \rho_{STEEL}f_y}{0.5f_{CU} + f_{TU}}\right)W_{Top} \qquad\qquad = \quad 0.73 \quad \text{in}$$

For Tension-Controlled $\qquad\qquad\qquad\qquad$ *GOVERNS* $\quad$ | Run Solver |

$$c = \left(\frac{f_{TU} + \rho_{STEEL}f_y}{\frac{1}{2}\varepsilon_{TU}E_{UHPC}\left(\frac{c}{W_{Top} - c}\right) + f_{TU}}\right)W_{Top} \qquad \boxed{0.00} \ \Longleftarrow \qquad = \quad 1.16 \quad \text{in}$$

Determine Factored Flexural Capacity:

$$\Phi M_{C1} = f_{TU}12(W_{Top} - c)\left(\frac{3W_{Top} + c}{6}\right) + \rho_{STEEL}f_y12W_{Top}\left(d - \frac{c}{3}\right) \qquad = \quad \mathbf{19.68} \quad \text{k-ft/ft}$$

Section II :

$$\rho_{STEEL} = \frac{As_{VERT}}{12W_{center}} \qquad\qquad = \quad \mathbf{0.000399}$$

$$d = W_{center} - cover - \frac{1}{2}Dia_{Vert_{bar}} \qquad\qquad = \quad \mathbf{10.31} \quad \text{in}$$

Determine controlling limit state:

$$\left(\frac{f_{TU} + \rho_{STEEL}f_y}{0.5f_{CU} + f_{TU}}\right) \ < \ 0.314 \quad \textit{Tension-Controlled} \qquad = \quad \mathbf{0.120}$$

Determine c : $\qquad\qquad = \quad \mathbf{2.21} \quad \text{in}$

For Compression-Controlled

$$c = \left(\frac{f_{TU} + \rho_{STEEL}f_y}{0.5f_{CU} + f_{TU}}\right)W_{Center} \qquad\qquad = \quad 1.38 \quad \text{in}$$

For Tension-Controlled $\qquad\qquad\qquad\qquad$ *GOVERNS* $\quad$ | Run Solver |

$$c = \left(\frac{f_{TU} + \rho_{STEEL}f_y}{\frac{1}{2}\varepsilon_{TU}E_{UHPC}\left(\frac{c}{W_{Center} - c}\right) + f_{TU}}\right)W_{Center} \qquad \boxed{0.00} \ \Longleftarrow \qquad = \quad 2.21 \quad \text{in}$$

Determine Factored Flexural Capacity

$$\Phi M_{C2} = f_{TU}12(W_{Center} - c)\left(\frac{3W_{Center} + c}{6}\right) + \rho_{STEEL}f_y12W_{Center}\left(d - \frac{c}{3}\right) \qquad = \quad \mathbf{70.67} \quad \text{k-ft/ft}$$

Section III :

$$\rho_{STEEL} = \frac{As_{VERT}}{12W_{bottom}} \qquad\qquad = \quad \mathbf{0.000327}$$

$$d = W_{bottom} - cover - \frac{1}{2}Dia_{Vert_{bar}} \qquad\qquad = \quad \mathbf{12.81} \quad \text{in}$$

Determine controlling limit state:

$$\left(\frac{f_{TU} + \rho_{STEEL}f_y}{0.5f_{CU} + f_{TU}}\right) \ < \ 0.314 \quad \textit{Tension-Controlled} \qquad = \quad \mathbf{0.119}$$

$$c = \left(\frac{f_{TU} + \rho_{STEEL}f_y}{0.5f_{CU} + f_{TU}}\right)W_{Bottom}$$

$$\left(\frac{f_{TU} + \rho_{STEEL}f_y}{0.5f_{CU} + f_{TU}}\right) > 0.314$$

Determine c : = **2.69** in

For Compression-Controlled

$$c = \left(\frac{f_{TU} + \rho_{STEEL}f_y}{0.5f_{CU} + f_{TU}}\right)W_{Bottom}$$ = 1.67 in

For Tension-Controlled *GOVERNS*

Run Solver

$$c = \left(\frac{f_{TU} + \rho_{STEEL}f_y}{\frac{1}{2}\varepsilon_{TU}E_{UHPC}\left(\frac{c}{W_{Bottom} - c}\right) + f_{TU}}\right)W_{Bottom}$$ `0.00` = 2.69 in

Determine Factored Flexural Capacity:

$$\Phi M_{C3} = f_{TU}12(W_{Bottom} - c)\left(\frac{3W_{Bottom} + c}{6}\right) + \rho_{STEEL}f_y12W_{Bottom}\left(d - \frac{c}{3}\right)$$ = **104.18** k-ft/ft

Determine Mc :

$$\Phi M_c = \frac{\left(\frac{\Phi M_{c1} + \Phi M_{c2}}{2}H_{Top} + \frac{\Phi M_{c2} + \Phi M_{c3}}{2}H_{Bottom}\right)}{H_{Overall}}$$ = **59.26** k-ft/ft

---

II. Calculate Mw

Top Portion :

$$W_{Top_{Ave}} = (\frac{W_{top} + W_{center}}{2} + W_{top})/2$$ = **7.38** in

As_{Horz} = Sectional steel area of ___2 Bars___ = **0.22** in²/ft
$As_{Horz} =$

$$\rho_{STEEL} = \frac{As_{HOR}}{H_1\left(\frac{\frac{W_{top} + W_{center}}{2} + W_{top}}{2}\right)}$$ = **0.001989**

$$d = \left(\frac{\frac{W_{top} + W_{center}}{2} + W_{top}}{2}\right) - cover - Dia_{Vert_{bar}} - \frac{1}{2}Dia_{Horz_{bar}}$$ = **5.81** in

Determine controlling limit state:

$$\left(\frac{f_{TU} + \rho_{STEEL}f_y}{0.5f_{CU} + f_{TU}}\right) < 0.314 \quad \textit{Tension-Controlled}$$ = **0.129**

Determine c : = **1.47** in

For Compression-Controlled

$$c = \left(\frac{f_{TU} + \rho_{STEEL}f_y}{0.5f_{CU} + f_{TU}}\right)W_{Top_{Ave}}$$ = 0.95 in

For Tension-Controlled *GOVERNS*

Run Solver

$$c = \left(\frac{f_{TU} + \rho_{STEEL}f_y}{\frac{1}{2}\varepsilon_{TU}E_{UHPC}\left(\frac{c}{W_{Top_{Ave}} - c}\right) + f_{TU}}\right)W_{Top_{Ave}}$$ `0.00` = 1.47 in

Determine Factored Flexural Capacity:

$$\Phi M_{W1} = f_{TU}H_1\left(W_{Top_{Ave}} - c\right)\left(\frac{3W_{Top_{Ave}} + c}{6}\right) + \rho_{STEEL}f_yH_1W_{Top_{Ave}}\left(d - \frac{c}{3}\right)$$ = **40.68** k-ft/ft

Center Portion :

$$W_{Center_{Ave}} = (\frac{W_{top} + W_{center}}{2} + W_{center})/2$$ = **10.13** in

As_{Horz} = Sectional steel area of ___1 Bars___ = **0.11** in²/ft

$$\rho_{STEEL} = \frac{As_{HOR}}{H_2\left(\frac{\frac{W_{top} + W_{center}}{2} + W_{center}}{2}\right)}$$ = **0.000724**

$$d = \left(\frac{\frac{W_{top} + W_{center}}{2} + W_{center}}{2}\right) - cover - Dia_{Vert_{bar}} - \frac{1}{2}Dia_{Horz_{bar}}$$ = **8.56** in

$$\left(\frac{f_{TU} + \rho_{STEEL}f_y}{0.5f_{CU} + f_{TU}}\right) > 0.314$$

Determine controlling limit state:

$$\left(\frac{f_{TU} + \rho_{STEEL}f_y}{0.5f_{CU} + f_{TU}}\right) \quad < \quad 0.314 \quad \textit{Tension-Controlled} \qquad = \qquad \mathbf{0.122}$$

Determine c : $\qquad = \qquad \mathbf{1.96} \quad$ in

For Compression-Controlled

$$c = \left(\frac{f_{TU} + \rho_{STEEL}f_y}{0.5f_{CU} + f_{TU}}\right)W_{Center\_Ave} \qquad = \qquad 1.23 \quad \text{in}$$

For Tension-Controlled $\qquad\qquad\qquad\qquad\qquad\qquad$ *GOVERNS* $\qquad$ Run Solver

$$c = \left(\frac{f_{TU} + \rho_{STEEL}f_y}{\frac{1}{2}\varepsilon_{TU}E_{UHPC}\left(\frac{c}{W_{Center_{Ave}} - c}\right) + f_{TU}}\right)W_{Center_{Ave}} \quad \boxed{0.00} \qquad = \qquad 1.96 \quad \text{in}$$

Determine Factored Flexural Capacity:

$$\Phi M_{W2} = f_{TU}H_2\left(W_{Center_{Ave}} - c\right)\left(\frac{3W_{Center_{Ave}} + c}{6}\right) + \rho_{STEEL}f_yH_2W_{Center_{Ave}}\left(d - \frac{c}{3}\right) = \qquad \mathbf{70.34} \quad \text{k-ft/ft}$$

Bottom Portion :

$$W_{Bottom_{Ave}} = (W_{center} + W_{bottom})/2 \qquad = \qquad \mathbf{12.75} \quad \text{in}$$

$$As_{Horz} = \text{Sectional steel area of} \qquad \underline{\text{2 Bars}} \qquad = \qquad \mathbf{0.22} \quad \text{in}^2/\text{ft}$$

$$\rho_{STEEL} = \frac{As_{HOR}}{H_3\left(\frac{W_{center} + W_{bottom}}{2}\right)} \qquad = \qquad \mathbf{0.00115}$$

$$d = \left(\frac{W_{center} + W_{bottom}}{2}\right) - cover - Dia_{Vert\,bar} - \frac{1}{2}Dia_{Horz\,bar} \qquad = \qquad \mathbf{11.19} \quad \text{in}$$

Determine controlling limit state:

$$\left(\frac{f_{TU} + \rho_{STEEL}f_y}{0.5f_{CU} + f_{TU}}\right) \quad < \quad 0.314 \quad \textit{Tension-Controlled} \qquad = \qquad \mathbf{0.124}$$

Determine c : $\qquad = \qquad \mathbf{2.50} \quad$ in

For Compression-Controlled

$$c = \left(\frac{f_{TU} + \rho_{STEEL}f_y}{0.5f_{CU} + f_{TU}}\right)W_{Bottom} \qquad = \qquad 1.59 \quad \text{in}$$

For Tension-Controlled $\qquad\qquad\qquad\qquad\qquad\qquad$ *GOVERNS* $\qquad$ Run Solver

$$c = \left(\frac{f_{TU} + \rho_{STEEL}f_y}{\frac{1}{2}\varepsilon_{TU}E_{UHPC}\left(\frac{c}{W_{Bottom} - c}\right) + f_{TU}}\right)W_{Bottom} \quad \boxed{0.00} \qquad = \qquad 2.50 \quad \text{in}$$

Determine Factored Flexural Capacity:

$$\Phi M_{W3} = f_{TU}H_3\left(W_{Bottom_{Ave}} - c\right)\left(\frac{3W_{Bottom_{Ave}} + c}{6}\right) + \rho_{STEEL}f_yH_3W_{Bottom_{Ave}}\left(d - \frac{c}{3}\right) = \qquad \mathbf{115.84} \quad \text{k-ft/ft}$$

Determine Mw :

$$\Phi M_W = \Phi M_{W_1} + \Phi M_{W_2} + \Phi M_{W_3} \qquad = \qquad \mathbf{226.85} \quad \text{k-ft/ft}$$

III. Calculate M_b

$$M_b = M_{b,\,Assumed} \qquad = \qquad \boxed{0.00} \quad \text{k-ft/ft}$$

IV. Calculate L_C, R_W

a. Impact within parapet segment

Determine Critical Length:

$$L_c = \frac{L_t}{2} + \sqrt{\left(\frac{L_t}{2}\right)^2 + \frac{8H(M_b + M_w)}{M_c}} \qquad \textbf{AASHTO LRFD Eq. A13.3.1-2} \qquad = \qquad \mathbf{15.44} \quad \text{ft}$$

Parapet Resistance to Transverse Impact:

$$R_w = \left(\frac{2}{2L_c - L_t}\right)\left(8M_b + 8M_w + \frac{M_cL_c^2}{H}\right) \qquad \textbf{AASHTO LRFD Eq. A13.3.1-1} \qquad = \qquad \mathbf{487.9} \quad \text{kips}$$

$$R_w = \left(\frac{2}{2L_c - L_t}\right)\left(8M_b + 8M_w + \frac{M_c L_c^2}{H}\right)$$ **AASHTO LRFD Eq. A13.3.1-1**

---

b. Impact near parapet end:

Determine Critical Length:

$$L_c = \frac{L_t}{2} + \sqrt{\left(\frac{L_t}{2}\right)^2 + H\left(\frac{M_b + M_w}{M_c}\right)}$$ **AASHTO LRFD Eq. A13.3.1-4**   =   **9.51**   ft

Parapet Resistance to Transverse Impact:

$$R_w = \left(\frac{2}{2L_c - L_t}\right)\left(M_b + M_w + \frac{M_c L_c^2}{H}\right)$$ **AASHTO LRFD Eq. A13.3.1-3**   =   **300.6**   kips

---

b. Impact near parapet end:

Determine Critical Length:

$$L_c = \frac{L_t}{2} + \sqrt{\left(\frac{L_t}{2}\right)^2 + H\left(\frac{M_b + M_w}{M_c}\right)}$$ **AASHTO LRFD Eq. A13.3.1-4**   =   **9.51**   ft

8.3 45-inch Hybrid Single Slope Parapet Design Example

This example illustrates the design of a 45-inch hybrid single slope parapet for TL-5.

The UHPC compressive strength is assumed to be 18 ksi under air-cured condition.

The tensile strength of the vertical bars is determined based on the ratio of the embedment depth that can be provided to a 8.5-inch deck slab to the required development length.

For conservatism, assume UHPC facing provides resistance from one parapet side only (either front or rear face).

DESIGN INPUT

t_{UHPC} =	**3**	*in*
H_1 =	**15**	*in*
H_2 =	**15**	*in*
H_3 =	**15**	*in*
H_{top} =	**30**	*in*
H_{bottom} =	**15**	*in*
$H_{overall}$ =	**45**	*in*
W_{top} =	**12**	*in*
W_{center} =	**17.33**	*in*
W_{bottom} =	**20**	*in*

UHPC Reinforcement

Horizontal Rebar$_{UHPC}$	# 3	Area	Diameter
		0.11	**0.375**
f_y =		**60**	*ksi*
Vertical Rebar$_{UHPC}$	# 3	Area	Diameter
		0.11	**0.375**

Adjust fy to account for inadequate embedment in deck f_y = **56.25** *ksi*

Cover - inside face = **0.75** *in*

Normal Concrete Reinforcement

UHPC / Normal Conc.

Horizontal Rebar Quantity

	UHPC	Normal Conc.	
Top portion:	**2**	**2**	*bars*
Center portion:	**1**	**1**	*bars*
Bottom portion:	**2**	**2**	*bars*

Horizontal Rebar	# 6	Area	Diameter
		0.44	**0.75**
f_y =		**60**	*ksi*

Vertical Rebar Spacing

	UHPC	Normal Conc.	
Bar spacing =	**12**	**6**	*in*

Vertical Rebar	# 5	Area	Diameter
		0.31	**0.625**

Yield Strength: Adjust fy to account for inadequate embedment in deck f_y = **37.5** *ksi*

Cover - inside face = **1.0** *in*

UHPC	28-day Compressive Strength	f_{CU} =	**18.0**	*ksi*
Normal Conc.	28-day Compressive Strength	f_C' =	**4.0**	*ksi*
	Modulus of Elasticity $1,460\sqrt{f_{cu}}$ (ksi)	E_{UHPC} =	**6194.3**	*ksi*
	28-day Tensile Strength	f_{TU} =	**1.2**	*ksi*
	28-day Tensile Strain	=	**0.007**	
	phi factor Extreme Event II *(AASHTO 1.3.2.1)*	=	**1.0**	

Choose Test Level

Select the designed Test Level (TL) and see the result of the barrier analysis in the next section.

Test Level	F_t (Kips)	F_L (Kips)	F_v (Kips)	L_t and L_L (ft)	L_v (ft)	H_e (in)	H_{min} (in)
5 ⇕	*124*	*41*	*80*	*8*	*40*	*42*	*42*

Analysis Results

The nominal railing resistance, Rw, of the barrier is computed and compared to the transverse force Ft specified for the selected Test Level. (Detailed calculations are shown in the next section - "Calculations").

I. Impact within wall segment:	R_w =	**177.5**	kips	>	F_t =	124.0 kips OK
II. Impact near wall end:	R_w =	**127.5**	kips	>	F_t =	124.0 kips OK

PASS

CALCULATIONS

I. Calculate Mc

Normal Concrete

A_s = Sectional steel area of vertical rebar / foot $\qquad$ = **0.62** in^2

$a = A_s f_y / (0.85\ f'c \times 12")$ $\qquad$ = **0.57** in

Section I :

$d = W_{top} - t_{UHPC}$ - Concrete cover - 0.5 bar dia. $\qquad$ = **4.69** in

$Mc_1 = \phi A_s f_y (d - a/2)$ $\qquad$ = **8.53** k-ft / ft

Section II :

$d = W_{center} - t_{UHPC}$ - Concrete cover - 0.5 bar dia. $\qquad$ = **10.02** in

$Mc_2 = \phi A_s f_y (d - a/2)$ $\qquad$ = **18.86** k-ft / ft

Section III :

$d = W_{bottom} - t_{UHPC}$ - Concrete cover - 0.5 bar dia. $\qquad$ = **12.69** in

$Mc_3 = \phi A_s f_y (d - a/2)$ $\qquad$ = **24.03** k-ft / ft

$$M_c = \frac{\left(\frac{M_{c1} + M_{c2}}{2} H_{Top} + \frac{M_{c2} + M_{c3}}{2} H_{Bottom}\right)}{H_{Overall}}$$ $\qquad$ = **16.28** k-ft / ft

Ultra-High-Performance Concrete

$$As_{VERT} = Rebar\ Area * \frac{12}{Rebar\ Spacing}$$ $\qquad$ = **0.11** in^2/ft

Section I :

$$\rho_{STEEL} = \frac{As_{VERT}}{12W_{top}}$$ $\qquad$ = **0.003056**

$$d = t_{UHPC} - cover - \frac{1}{2}Dia_{Vert\,bar}$$ $\qquad$ = **2.06** in

Determine controlling limit state:

$$\left(\frac{f_{TU} + \rho_{STEEL}f_y}{0.5f_{CU} + f_{TU}}\right) \quad < \quad 0.314 \quad \textit{Tension-Controlled}$$ $\qquad$ = **0.134**

Determine c : $\qquad$ = **0.61** in

For Compression-Controlled

$$c = \left(\frac{f_{TU} + \rho_{STEEL}f_y}{0.5f_{CU} + f_{TU}}\right)t_{UHPC}$$ $\qquad$ = 0.40 in

For Tension-Controlled $\qquad\qquad$ *GOVERNS* $\qquad$ Run Solver

$$c = \left(\frac{f_{TU} + \rho_{STEEL}f_y}{\frac{1}{2}\varepsilon_{TU}E_{UHPC}\left(\frac{c}{t_{UHPC} - c}\right) + f_{TU}}\right)t_{UHPC}$$ $\boxed{0.00}$ $\leftarrow$ = 0.61 in

Determine Factored Flexural Capacity:

$$\Phi M_{C1} = f_{TU}12(t_{UHPC} - c)\left(\frac{3t_{UHPC} + c}{6}\right) + \rho_{STEEL}f_y 12t_{UHPC}\left(d - \frac{c}{3}\right)$$ $\qquad$ = **5.55** k-ft/ft

Section II :

$$\rho_{STEEL} = \frac{As_{VERT}}{12W_{center}}$$ $\qquad$ = **0.003056**

$$d = t_{UHPC} - cover - \frac{1}{2}Dia_{Vert\,bar}$$ $\qquad$ = **2.06** in

Determine controlling limit state:

$$\left(\frac{f_{TU} + \rho_{STEEL}f_y}{0.5f_{CU} + f_{TU}}\right) \quad < \quad 0.314 \quad \textit{Tension-Controlled}$$ $\qquad$ = **0.134**

Determine c : $\qquad$ = **0.61** in

For Compression-Controlled

$$c = \left(\frac{f_{TU} + \rho_{STEEL}f_y}{0.5f_{CU} + f_{TU}}\right)t_{UHPC}$$ $\qquad$ = 0.40 in

GOVERNS

$$c = \left(\frac{f_{TU} + \rho_{STEEL}f_y}{\frac{1}{2}\varepsilon_{TU}E_{UHPC}\left(\frac{c}{\ }\right) + f_{TU}}\right)t_{UHPC}$$

$$c = \left(\frac{f_{TU} + \rho_{STEEL}f_y}{0.5f_{CU} + f_{TU}}\right) t_{UHPC}$$

For Tension-Controlled   *GOVERNS* | Run Solver |

$$c = \left(\frac{f_{TU} + \rho_{STEEL}f_y}{\frac{1}{2}\varepsilon_{TU}E_{UHPC}\left(\frac{c}{t_{UHPC} - c}\right) + f_{TU}}\right) t_{UHPC}$$ 0.00   =   0.61   in

Determine Factored Flexural Capacity:

$$\Phi M_{C2} = f_{TU}12(t_{UHPC} - c)\left(\frac{3t_{UHPC} + c}{6}\right) + \rho_{STEEL}f_y12t_{UHPC}\left(d - \frac{c}{3}\right)$$ =   **5.55**   k-ft/ft

Section III :

$$\rho_{STEEL} = \frac{As_{VERT}}{12W_{bottom}}$$ =   **0.003056**

$$d = t_{UHPC} - cover - \frac{1}{2}Dia_{Vert\,bar}$$ =   **2.06**   in

Determine controlling limit state:

$$\left(\frac{f_{TU} + \rho_{STEEL}f_y}{0.5f_{CU} + f_{TU}}\right) \quad < \quad 0.314 \quad \text{*Tension-Controlled*}$$ =   **0.134**

Determine c :   =   **0.61**   in

For Compression-Controlled

$$c = \left(\frac{f_{TU} + \rho_{STEEL}f_y}{0.5f_{CU} + f_{TU}}\right) t_{UHPC}$$ =   0.40   in

For Tension-Controlled   *GOVERNS* | Run Solver |

$$c = \left(\frac{f_{TU} + \rho_{STEEL}f_y}{\frac{1}{2}\varepsilon_{TU}E_{UHPC}\left(\frac{c}{t_{UHPC} - c}\right) + f_{TU}}\right) t_{UHPC}$$ 0.00   =   0.61   in

Determine Factored Flexural Capacity:

$$\Phi M_{C3} = f_{TU}12(t_{UHPC} - c)\left(\frac{3t_{UHPC} + c}{6}\right) + \rho_{STEEL}f_y12t_{UHPC}\left(d - \frac{c}{3}\right)$$ =   **5.55**   k-ft/ft

Determine Mc :

$$\Phi M_c = \frac{\left(\frac{\Phi M_{c1} + \Phi M_{c2}}{2}H_{Top} + \frac{\Phi M_{c2} + \Phi M_{c3}}{2}H_{Bottom}\right)}{H_{Overall}}$$ =   **5.55**   k-ft/ft

Determine Hybrid Mc :

$$\Phi M_{C,Hybrid} = \Phi M_{c\,Normal\,Concrete} + \Phi M_{c\,UHPC}$$ =   **21.83**   k-ft/ft

---

II. Calculate Mw

Normal Concrete

Top Portion

A_s = Sectional steel area of   <u>2</u>   bars   =   **0.88**   in²

$a = As\,f_y / (0.85\,f'c \times (H_1 - t_{UHPC})$ =   **1.29**   in

$d = 0.5\,[0.5(W_{top} + W_{center}) + W_{top}] - t_{UHPC} - Cover - Dia_{Vert.\,bar} - 0.5(Dia_{Hor.\,Bar})$ =   **5.33**   in

$Mw_1 = \Phi A_s\,f_y\,(d - a/2)$ =   **20.62**   k-ft / ft

Center Portion

A_s = Sectional steel area of   <u>1</u>   bar   =   **0.44**   in²

$a = As\,f_y / (0.85\,f'c \times H_2)$ =   **0.52**   in

$d = 0.5\,[0.5(W_{top} + W_{center}) + W_{center}] - t_{UHPC} - Cover - Dia_{Vert.\,bar} - 0.5(Dia_{Hor.\,Bar})$ =   **8.00**   in

$Mw_2 = \Phi A_s\,f_y\,(d - a/2)$ =   **10.64**   k-ft / ft

Bottom Portion

A_s = Sectional steel area of   <u>2</u>   bars   =   **0.88**   in²

$a = As\,f_y / (0.85\,f'c \times H_3)$ =   **1.04**   in

$d = 0.5(W_{center} + W_{bottom}) - t_{UHPC} - Cover - Dia_{Vert.\,bar} - 0.5(Dia_{Hor.\,Bar})$ =   **10.67**   in

$Mw_3 = \Phi A_s\,f_y\,(d - a/2)$ =   **27.91**   k-ft / ft

$$\Phi M_W = \Phi M_{W_1} + \Phi M_{W_2} + \Phi M_{W_3}$$ =   **59.16**   k-ft / ft

$0.5(W_{center}+W_{bottom}) - t_{UHPC}$ - Cover - $Dia_{Vert.\,bar}$ - $0.5(Dia_{Hor.\,Bar})$			=	**10.67** in
$Mw_3 = \phi A_s\, f_y\, (d - a/2)$			=	**27.91** k-ft / ft

$$\Phi M_W = \Phi M_{W_1} + \Phi M_{W_2} + \Phi M_{W_3}$$

Ultra-High-Performance Concrete

Top Portion

As_{Horz} = Sectional steel area of $\quad$ <u>2 Bars</u> $\qquad$ = **0.22** in²/ft

$\rho_{STEEL} = \dfrac{As_{Horz}}{H_1 t_{UHPC}}$ $\qquad$ = **0.004889**

$d = t_{UHPC} - cover - Dia_{vert\,bar} - \dfrac{1}{2}Dia_{Horz\,bar}$ $\qquad$ = **1.69** in

Determine controlling limit state:

$\left(\dfrac{f_{TU} + \rho_{STEEL}f_y}{0.5f_{CU} + f_{TU}}\right) \; < \; 0.314 \quad$ *Tension-Controlled* $\qquad$ = **0.146**

Determine c : $\qquad$ = **0.64** in

For Compression-Controlled

$c = \left(\dfrac{f_{TU} + \rho_{STEEL}f_y}{0.5f_{CU} + f_{TU}}\right) t_{UHPC}$ $\qquad$ = 0.44 in

For Tension-Controlled $\qquad$ *GOVERNS* [Run Solver]

$c = \left(\dfrac{f_{TU} + \rho_{STEEL}f_y}{\frac{1}{2}\varepsilon_{TU}E_{UHPC}\left(\dfrac{c}{t_{UHPC} - c}\right) + f_{TU}}\right) t_{UHPC}$ $\quad$ [0.00] $\qquad$ = 0.64 in

Determine Factored Flexural Capacity:

$\Phi M_{W1} = f_{TU}H_1(t_{UHPC} - c)\left(\dfrac{3t_{UHPC} + c}{6}\right) + \rho_{STEEL}f_y H_1 t_{UHPC}\left(d - \dfrac{c}{3}\right)$ $\qquad$ = **7.32** k-ft/ft

Center Portion

As_{Horz} = Sectional steel area of $\quad$ <u>1 Bars</u> $\qquad$ = **0.11** in²/ft

$\rho_{STEEL} = \dfrac{As_{Horz}}{H_2 t_{UHPC}}$ $\qquad$ = **0.002444**

$d = t_{UHPC} - cover - Dia_{vert\,bar} - \dfrac{1}{2}Dia_{Horz\,bar}$ $\qquad$ = **1.69** in

Determine controlling limit state:

$\left(\dfrac{f_{TU} + \rho_{STEEL}f_y}{0.5f_{CU} + f_{TU}}\right) \; < \; 0.314 \quad$ *Tension-Controlled* $\qquad$ = **0.132**

Determine c : $\qquad$ = **0.61** in

For Compression-Controlled

$c = \left(\dfrac{f_{TU} + \rho_{STEEL}f_y}{0.5f_{CU} + f_{TU}}\right) t_{UHPC}$ $\qquad$ = 0.40 in

For Tension-Controlled $\qquad$ *GOVERNS* [Run Solver]

$c = \left(\dfrac{f_{TU} + \rho_{STEEL}f_y}{\frac{1}{2}\varepsilon_{TU}E_{UHPC}\left(\dfrac{c}{t_{UHPC} - c}\right) + f_{TU}}\right) t_{UHPC}$ $\quad$ [0.00] $\qquad$ = 0.61 in

Determine Factored Flexural Capacity:

$\Phi M_{W2} = f_{TU}H_2(t_{UHPC} - c)\left(\dfrac{3t_{UHPC} + c}{6}\right) + \rho_{STEEL}f_y H_2 t_{UHPC}\left(d - \dfrac{c}{3}\right)$ $\qquad$ = **6.57** k-ft/ft

Bottom Portion

As_{Horz} = Sectional steel area of $\quad$ <u>2 Bars</u> $\qquad$ = **0.22** in²/ft

$\rho_{STEEL} = \dfrac{As_{Horz}}{H_3 t_{UHPC}}$ $\qquad$ = **0.004889**

$d = t_{UHPC} - cover - Dia_{vert\,bar} - \dfrac{1}{2}Dia_{Horz\,bar}$ $\qquad$ = **1.69** in

$\left(\dfrac{f_{TU} + \rho_{STEEL}f_y}{0.5f_{CU} + f_{TU}}\right) > 0.314$

$$\rho_{STEEL} = \frac{As_{Horz}}{H_3 t_{UHPC}}$$

$$d = t_{UHPC} - cover - Dia_{Vert\,bar} - \frac{1}{2}Dia_{Horz\,bar}$$

Determine controlling limit state:

$$\left(\frac{f_{TU} + \rho_{STEEL}f_y}{0.5f_{CU} + f_{TU}}\right) < 0.314 \quad \textit{Tension-Controlled} \qquad = \quad \mathbf{0.146}$$

Determine c : $\qquad\qquad\qquad\qquad = \quad \mathbf{0.64} \quad$ in

For Compression-Controlled

$$c = \left(\frac{f_{TU} + \rho_{STEEL}f_y}{0.5f_{CU} + f_{TU}}\right) t_{UHPC} \qquad = \quad 0.44 \quad \text{in}$$

For Tension-Controlled $\qquad\qquad\qquad\qquad$ *GOVERNS* $\qquad$ | Run Solver |

$$c = \left(\frac{f_{TU} + \rho_{STEEL}f_y}{\frac{1}{2}\varepsilon_{TU}E_{UHPC}\left(\frac{c}{t_{UHPC} - c}\right) + f_{TU}}\right) t_{UHPC} \qquad \boxed{0.00} \leftarrow \quad = \quad 0.64 \quad \text{in}$$

Determine Factored Flexural Capacity:

$$\Phi M_{W3} = f_{TU}H_3(t_{UHPC} - c)\left(\frac{3t_{UHPC} + c}{6}\right) + \rho_{STEEL}f_y H_3 t_{UHPC}\left(d - \frac{c}{3}\right) \qquad = \quad \mathbf{7.32} \quad \text{k-ft/ft}$$

Determine Mw :

$$\Phi M_W = \Phi M_{W_1} + \Phi M_{W_2} + \Phi M_{W_3} \qquad = \quad \mathbf{21.20} \quad \text{k-ft/ft}$$

Determine Hybrid Mw :

$$\Phi M_{W,Hybrid} = \Phi M_{W_{Normal\,Concrete}} + \Phi M_{W_{UHPC}} \qquad = \quad 80.36 \quad \text{k-ft/ft}$$

III. Calculate M_b

$$M_b = M_{b,\,Assumed} \qquad\qquad = \quad \boxed{0.00} \quad \text{k-ft/ft}$$

IV. Calculate L_C, R_W

a. Impact within parapet segment

Determine Critical Length:

$$L_c = \frac{L_t}{2} + \sqrt{\left(\frac{L_t}{2}\right)^2 + \frac{8H(M_b + M_w)}{M_c}} \qquad \textbf{AASHTO LRFD Eq. A13.3.1-2} \quad = \quad \mathbf{15.25} \quad \text{ft}$$

Parapet Resistance to Transverse Impact:

$$R_w = \left(\frac{2}{2L_c - L_t}\right)\left(8M_b + 8M_w + \frac{M_c L_c^2}{H}\right) \qquad \textbf{AASHTO LRFD Eq. A13.3.1-1} \quad = \quad \mathbf{177.5} \quad \text{kips}$$

b. Impact near parapet end:

Determine Critical Length:

$$L_c = \frac{L_t}{2} + \sqrt{\left(\frac{L_t}{2}\right)^2 + H\left(\frac{M_b + M_w}{M_c}\right)} \qquad \textbf{AASHTO LRFD Eq. A13.3.1-4} \quad = \quad \mathbf{9.46} \quad \text{ft}$$

Parapet Resistance to Transverse Impact:

$$R_w = \left(\frac{2}{2L_c - L_t}\right)\left(M_b + M_w + \frac{M_c L_c^2}{H}\right) \qquad \textbf{AASHTO LRFD Eq. A13.3.1-3} \quad = \quad \mathbf{127.5} \quad \text{kips}$$

Appendix

This example illustrates the design of a 45-inch normal concrete Texas single slope parapet for TL-5.

SPECIFICATIONS
1. AASHTO LRFD - Eight Edition 2017
2. CTDOT - Bridge Design Manual (2003)

DESIGN INPUT

I. Geometry:

H_{top}	=	30	in
H_{bottom}	=	15	in
$H_{overall}$	=	45	in
W_{top}	=	12	in
W_{center}	=	17.25	in
W_{bottom}	=	20	in
$L_{joint-to-joint}$	=	96	ft

II. Reinforcement

Horizontal Bars:
- Top portion: 4 bars
- Center portion: 2 bars
- Bottom portion: 4 bars

Bar size: # 6
f_y = 60 ksi

Vertical Bars: Bar spacing = 6 in
Bar size: # 5
Yield Strength: f_y = 37.5 ksi

Adjust fy to account for inadequate embedment in deck

III. Concrete

28-day Compressive Strength	f'_c	=	4.0	ksi
Cover - inside face		=	3.0	in
ϕ factor		=	1.0	

TEST LEVEL

Select the designed Test Level (TL) and see the result of the barrier analysis in the next section.

Test Level	F_t kips	F_L kips	F_v kips	L_t and L_L ft	L_v ft	H_e in	Minimum Height, H_{min} in
5	124	41	80	8	40	42	42

ANALYSIS RESULT

The **nominal railing resistance, R_w**, of the barrier is computed and compared to the transverse force F_t specified for the selected Test Level. (Detailed calculations are shown in the next section - "Calculations").

I. Impact within wall segment: R_w = **218.63** kips   > F_t = 124.0 kips   **OK**

II. Impact near wall end: R_w = **126.53** kips   > F_t = 124.0 kips   **OK**

PASS

CALCULATIONS

I. CALCULATE M_c:

A_s	= Sectional steel area of vertical rebar / foot	=	0.61	sq-in
a	= $A_s f_y$ / (0.85 f'c x 12")	=	0.56	in

Section I:
d1	= W_{top} - Concrete cover - 0.5 bar dia.	=	8.69	in
M_{c_1}	= $\phi A_s f_y$ (d1 - a/2)	=	16.12	k-ft / ft

Section II:
d2	= W_{center} - Concrete cover - 0.5 bar dia.	=	13.94	in
M_{c_2}	= $\phi A_s f_y$ (d2 - a/2)	=	26.18	k-ft / ft

Section III:
d3	= W_{bottom} - Concrete cover - 0.5 bar dia.	=	16.69	in
M_{c_3}	= $\phi A_s f_y$ (d3 - a/2)	=	31.46	k-ft / ft

Assume the failure mechanism includes the entire height of the barrier, then the Moment Capacity M_c is computed by averaging the above components over their respective heights:

c

$$M_c = \frac{\left[\left(\dfrac{M_{c\_1} + M_{c\_2}}{2}\right) \times H_{top} + \left(\dfrac{M_{c\_2} + M_{c\_3}}{2}\right) \times H_{bottom}\right]}{H_{overall}}$$

| | = | 23.71 | k-ft / ft |

II. CALCULATE M_w:
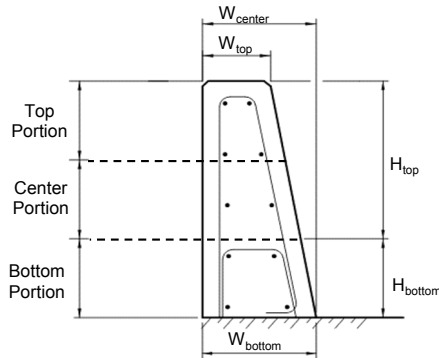
a. Top portion:

A_s	= Sectional steel area of 2 bars	=	0.88	sq-in
a	= $A_s f_y / (0.85\, f'c \times (0.5 \times H_{top}))$	=	1.04	in
d	= $0.5 [0.5(W_{top}+W_{center})+W_{top}]$ - Cover - $\varnothing_{Vert.\,bar}$ - $0.5(\varnothing_{Hor.\,Bar})$	=	9.31	in
M_{w_top}	= $\phi\, A_s f_y (d - a/2)$	=	38.85	k-ft / ft

b. Center portion:

A_s	= Sectional steel area of 1 $\varnothing$bar $\varnothing$	=	0.44	sq-in
a	= $A_s f_y / (0.85\, f'c \times (0.5 \times H_{top}))$	=	0.52	in
d	= $0.5 [0.5(W_{top}+W_{center})+W_{center}]$ - Cover - $\varnothing_{Vert.bar}$ - $0.5(\varnothing_{Hor.Bar})$	=	11.94	in
M_{w_center}	= $\phi\, A_s f_y (d - a/2)$	=	25.80	k-ft / ft

b. Bottom portion:

A_s	= Sectional steel area of 2$\varnothing$ bars	=	0.88	sq-in
a	= $A_s f_y / (0.85\, f'c \times (H_{bottom}))$	=	1.04	in
d	= $0.5(W_{center} + W_{bottom})$ - Cover - $\varnothing_{Vert.bar}$ - $0.5(\varnothing_{Hor.Bar})$	=	14.63	in
M_{w_bottom}	= $\phi\, A_s f_y (d - a/2)$	=	62.32	k-ft / ft

Positive and Negative Moments should be computed and the average should be used. However, in the case of collision near the end of the wall, which is the controlling case, the only yield line is caused by a moment causing tension along the inside face. Therefore only the flexural resistance for negative moment should be used. Assume the failure mechanism includes the entire height of the barrier, the ultimate flexural resistance barrier about its vertical axis, M_w, is computed by adding each of the three components:

| M_w | = | 38.85 | + | 25.80 | + | 62.32 | = | 126.96 | k-ft / ft |

III. CALCULATE M_B:

| $M_{b,assumed}$ | = | 0.00 | k-ft |

IV. CALCULATE Lc, Rw:

a. Impact within the Wall segment:

Critical Length Lc: L_c =

$$\frac{L_t}{2} + \sqrt{\left(\frac{L_t}{2}\right)^2 + \frac{8H(M_b + M_w)}{M_c}}$$

| | = | 17.29 | ft |

AASHTO LRFD Equation A13.3.1-2

Railing Resistance to Transverse Impact, R_w:

$$R_w = \left(\frac{2}{2L_c - L_t}\right)\left(8M_b + 8M_w + \frac{M_c L_c^2}{H}\right)$$

| | = | 218.63 | kips |

AASHTO LRFD Equation A13.3.1-1

b. Impact near wall end:

Critical Length Lc: L_c =

$$\frac{L_t}{2} + \sqrt{\left(\frac{L_t}{2}\right)^2 + \frac{H(M_b + M_w)}{M_c}}$$

| | = | 10.01 | ft |

AASHTO LRFD Equation A13.3.1-4

Railing Resistance to Transverse Impact, R_w:

$$R_w = \left(\frac{2}{2L_c - L_t}\right)\left(M_b + M_w + \frac{M_c L_c^2}{H}\right)$$

| | = | 126.53 | kips |

AASHTO LRFD Equation A13.3.1-3

References

1) AASHTO, "AASHTO LRFD Bridge Design Specifications." *American Association of State Highway and Transportation Officials, Eight Edition, 2017.*

2) Ahlborn, M., T., Peuse, J., E., Misson, L., D. Ultra-High-Performance-Concrete for Michigan Bridges Material Performance – Phase I. Research report RC-1525, Michigan Department of Transportation Construction and Technology Division, Lansing, MI. 2008.

3) Baby, F. and Graybeal, B., "Development of Direct Tension Test Method for Ultra-High-Performance Fiber-Reinforced Concrete." ACI Materials Journal, V. 110, No. 2, March-April 2013. Pp. 177-186.

4) Baby, F. and Graybeal, B., "Tension Testing of Ultra-High Performance Fiber Concrete." Federal Highway Administration, Report No. FHWA-HRT-17-053.

5) Graybeal, B., Haber, Z., Helou, R., Nakashoji, B., Varga, I., "Properties and Behavior of UHPC-Class Materials." Federal Highway Administration, Report No. FHWA-HRT-18-036.

6) Graybeal, B., "Material Property Characterization of Ultra-High Performance Concrete." Federal Highway Administration, Report No. FHWA-HRT-06-103.

7) Graybeal, B., "Structural Behavior of Ultra-High Performance Concrete Prestress I-Girders." Federal Highway Administration, Report No. FHWA-HRT-06-115.

8) Graybeal, B., "Development of Non-Proprietary Ultra-High Performance Concrete for Use in the Highway Bridge Sector." Federal Highway Administration, Report No. FHWA-HRT-13-100.

9) Japan Society of Civil Engineers, "Recommendations for Design and Construction of High Performance Fiber Reinforced Cement Composites with Multiple Fine Cracks (HPFRCC)." Concrete Engineering Series 82, March 2008.

10) Sriram, A., Peterson, B., Sritharan, S., "Design Guide for Precast UHPC Waffle Deck Panel System, Including Connections." Federal Highway Administration, Report No. FHWA-HIF-13-032.

11) Tadros, M. K., Sevenker, A., and Berry, R., "Ultra-High-Performance Concrete, A Game Changer." Structure Magazine, April 2019. Pp. 8-11.

12) Voort, T., Suleiman, M., Sritharan, S., "Design and Performance Verification of UHPC Piles